Supporting Information

Illuminating apoptosis: Visible light-activated chloride carrier for chloride transport and cell death

Manzoor Ahmad,[a] Naveen J. Roy,[a] Debashis Mondal,[a] Thangavel Vijayakanth,[c] Mayurika Lahiri,[b] and Pinaki Talukdar*[a]

[a] Department of Chemistry, Indian Institute of Science Education and Research Pune, Dr. Homi Bhabha Road, Pashan, Pune 411008, Maharashtra, India. E-mail: ptalukdar@iiserpune.ac.in

[b] Department of Biology, Indian Institute of Science Education and Research Pune, Dr. Homi Bhabha Road, Pashan, Pune 411008, Maharashtra, India.

[c] The Shmunis School of Biomedicine and Cancer Research, George S. Wise Faculty of Life Sciences, Tel Aviv University, Tel Aviv 6997801, Israel.

Table of contents

No.	Topic	Page No.
I	General methods	2
II	Physical Measurements	2
III	Synthesis	3
IV	Anion Binding Studies by ^{1}H NMR	14
V	Ion Transport Studies	18
VI	Photoresponsive studies	31
VII	Phototriggered ion transport across EYPC-LUVs⊃HPTS	38
VIII	Biological Studies	41
IX	Single Crystal X-ray Diffraction Studies	45
X	Geometry optimization and binding energy calculations	68
XI	NMR Spectra	77
XII	References	111

I. General Methods

All chemical reactions were carried out under a nitrogen atmosphere. All reagents and solvents for synthesis were purchased from commercial sources (Sigma-Aldrich and Spectrochem) and used without further purification. Column chromatography was carried out using Merck silica gel (100-200 mesh size). Thin layer chromatography (TLC) was performed on Merck silica gel 60-F254 plates. Egg yolk phosphatidylcholine (EYPC) as a solution of chloroform (25 mg/mL), mini extruder, and polycarbonate membrane of 100 nm and 200 nm were purchased from Avanti Polar Lipids (Merck). HEPES, HPTS, lucigenin, NaOH, Sephadex G-50, Triton X-100, valinomycin, and all inorganic salts were of molecular biology grade purchased from Sigma Aldrich (Merck).

II. Physical Measurements

All the NMR spectra were recorded on Bruker Avance III HD 400 MHz and JEOL JNM-ECS 400 MHz NMR spectrophotometers. The residual solvent signals were considered as the internal reference (δ_H = 7.26 ppm for $CDCl_3$, δ_H = 2.50 for DMSO-d_6, and δ_H = 1.94 for CD_3CN) to calibrate spectra. The chemical shifts were reported in ppm. The following abbreviations were used to indicate multiplicity patterns m: multiplet, s: singlet, d: doublet, t: triplet, q: triplet, dd: doublet of doublets, td: triplet of doublets, ddd: doublet of doublet of doublets. The coupling constants were measured in Hz. Infra-red (IR) spectra were measured using a Bruker ALPHA-E FT–IR spectrometer and reported in cm^{-1}. High-resolution mass spectra (HRMS) were recorded on a Waters SYNAPT G2 mass spectrometer equipped with a Waters Z-Spray electrospray ionization (ESI) source and a time-of-flight (TOF) detector. Fluorescence experiments were recorded on a Fluoromax-4 spectrofluorometer from HORIBA Jobin Yvon equipped with an injector port and a magnetic stirrer. The pH adjustment of buffer solutions was conducted using a HI98107 pH meter from Hanna Instruments. UV-Vis spectra were recorded on a Shimadzu UV-2600 UV-Vis spectrophotometer. Chloride ion efflux measurements were performed using Thermo Scientific Orion Chloride ionplus Sure-Flow Combination ISE connected to a Fisherbrand accumet AB 250 benchtop pH/ISE meter for recording chloride concentration in ppm. The single-crystal X-ray diffraction (SCXRD) measurements were performed on a Bruker KAPPA APEX diffractometer using Mo Kα radiation (λ = 0.71073Å). The crystal structures were solved using intrinsic methods and then refined by full-matrix least-squares against F^2 using all data by using SHELXL-2014/7 built in the Apex-3 package. ChemDraw 22.2.0 software was used for drawing structures and

processing figures and schemes. The LEDs for photoactivation experiments and the associated components were procured from Mouser Electronics India or sourced locally.

III. Synthesis

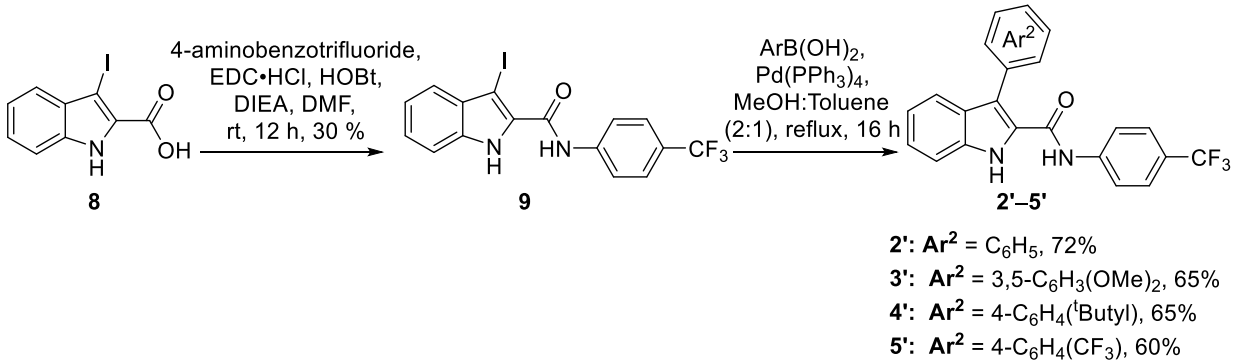

Scheme S1. Chemical synthesis of the desired compounds **2´–5´**.

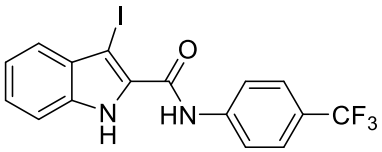

$C_{16}H_{10}F_3IN_2O$
Mol. Wt.: 430.16

3-Iodo-*N*-(4-(trifluoromethyl)phenyl)-1*H*-indole-2-carboxamide (9): In a 25 mL round bottom flask, 3-iodo-1*H*-indole-2-carboxylic acid **8** (1.0 g, 1 eq) EDC·HCl (998 mg, 1.5 eq) and HOBt (611 mg, 1.3 eq) were dissolved in DMF (10 mL). The resulting solution was stirred at room temperature for 30 min. After 30 min, 4-(trifluoromethyl)aniline (841 mg, 1.5 eq) and *N*,*N*-diisopropylethylamine (585 mg, 1.3 eq.) were added. The reaction mixture was stirred at room temperature for an additional 12 h. After completion of the reaction, the reaction mixture was quenched with water (10 mL), extracted with EtOAc (3 × 20 mL), washed with brine (2 × 20 mL), the organic layer was dried over Na_2SO_4 and concentrated under reduced pressure. The crude product was purified by column chromatography over 100-200 mesh silica gel (*Eluent* - EtOAc : petroleum ether 1:10 v/v) to furnish **9** as white solid (450 mg, 30%). **^{1}H NMR (400 MHz, Chloroform-*d*):** δ 9.80 (s, 1H), 9.21 (s, 1H), 7.87 (d, *J* = 8.4 Hz, 2H), 7.67 (d, *J* = 8.5 Hz, 2H), 7.52 (d, *J* = 8.1 Hz, 1H), 7.46 – 7.37 (m, 2H), 7.31 – 7.26 (m, 1H); **^{13}C NMR (101 MHz, Chloroform-*d*):** δ 172.66, 140.93, 127.27, 125.36, 124.51, 119.69, 118.36, 30.16, 10.07; **IR (Neat, ν/cm^{-1}):** 3732, 3391, 3322, 3020, 2931, 1739, 1638, 1522, 1494, 1364, 1216; **HRMS (ESI):** Calc. for $C_9H_{12}N_2OH^+$ $[M+H]^+$: 165.1022, found 165.1028.

i. General procedure for synthesizing the compounds 2´-5´:

General method A: In a 25 mL round bottom flask, 3-iodo-*N*-(4-(trifluoromethyl)phenyl)-1H-indole-2-carboxamide **9** (100 mg, 1.0 eq), and an appropriate aromatic boronic anhydride

(1.0 eq) were degassed using nitrogen in a mixture of ethanol and toluene (2:1, 30mL) for 30 min. After that, tetrakis(triphenylphosphine)palladium(0) (13 mg, 0.05 eq) and aqueous sodium nitrate solution (1 mL of 2 N solution) were added, and the reaction mixture was refluxed using an oil bath for 16 h. After the completion of the reaction, monitored through TLC, the reaction mixture was filtered through celite, and volatiles were evaporated under a high vacuum using a rotary evaporator. The crude mixture was extracted with EtOAc (3 × 20 mL), washed with brine (2 × 20 mL), dried on anhydrous Na_2SO_4, and purified through column chromatography using 100-200 mesh silica gel to furnish the desired compounds **2´–5´**.

3-Phenyl-*N*-(4-(trifluoromethyl)phenyl)-1*H*-indole-2-carboxamide (2´): Synthesized by reacting 3-iodo-*N*-(4-(trifluoromethyl)phenyl)-1*H*-indole-2-carboxamide **9** (100 mg, 1.0 eq) with phenylboronic acid (42 mg, 1.5 eq). The crude product was purified by column chromatography over 100-200 mesh silica gel (*Eluent*: EtOAc : petroleum ether 1:9 v/v) to furnish **2´** as white solid (63 mg, 72%); **^{1}H NMR (400 MHz, $CDCl_3$):** δ 9.52 (s, 1H), 7.88 (s, 1H), 7.68 – 7.60 (m, 5H), 7.51 (d, *J* = 7.6 Hz, 4H), 7.41 – 7.35 (m, 1H), 7.33 (d, *J* = 8.5 Hz, 2H), 7.17 (t, *J* = 8.0 Hz, 1H); **^{13}C NMR (101 MHz, $CDCl_3$):** δ 159.8, 140.6, 135.4, 133.2, 130.9, 129.6, 128.9, 128.2, 126.0 (q, *J* = 272.2 Hz), 126.30 (q, *J* = 3.9 Hz), 126.2, 126-125 (q, *J* = 32.3 Hz), 125.7, 121.1, 118.8, 111.9; **IR (Neat, ν/cm^{-1}):** 3402, 3312, 1690, 1655, 1600, 1532, 1447, 1408, 1318, 1237, 1187, 1162, 1100, 1064; **HRMS (ESI):** Calc. for $C_{22}H_{16}F_3N_2O$ $[M+H]^+$: 381.1029 found 381.1029.

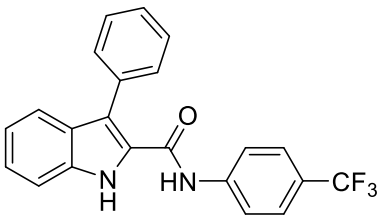

$C_{22}H_{15}F_3N_2O$
Mol. Wt.: 380.37

3-(3,5-Dimethoxyphenyl)-*N*-(4-(trifluoromethyl)phenyl)-1*H*-indole-2-carboxamide (3´): Synthesized by reacting 3-iodo-*N*-(4-(trifluoromethyl)phenyl)-1*H*-indole-2-carboxamide **9** (100 mg, 1.0 eq) with (3,5-dimethoxyphenyl)boronic acid (63 mg, 1.5 eq). The crude product was purified by column chromatography over 100-200 mesh silica gel (*Eluent*: EtOAc : petroleum ether 2:8 v/v) to furnish **3´** as white (66 mg, 65%); **^{1}H NMR (400 MHz, $CDCl_3$):** δ 9.71 (s, 1H), 8.16 (s, 1H), 7.58 – 7.47 (m, 4H), 7.44 – 7.34 (m, 3H), 7.22 – 7.08 (m, 4H), 4.03 (s, 3H), 3.90 (s, 3H); **^{13}C NMR (101 MHz, $CDCl_3$):** δ 159.8, 149.8, 149.5, 140.6, 135.4, 128.4, 126.4, 126.1, 126.3 (q, *J* = 3.9 Hz), 125.7 (q, *J* = 32.3 Hz), 125.6, 125.2, 123.15, 122.68 (q, *J* = 272 Hz), 121.1, 121.0, 119.3, 118.9, 113.6, 111.9, 111.9, 56.1; **IR (Neat, ν/cm^{-1}):** 3402, 3306, 1689, 1657, 1601,

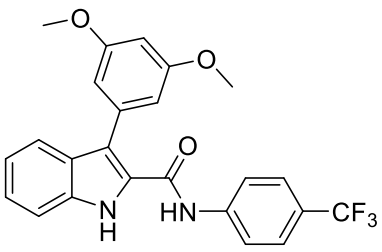

$C_{24}H_{19}F_3N_2O_3$
Mol. Wt.: 440.42

1531, 1449, 1407, 1320, 1235, 1186, 1162, 1097, 1064; **HRMS (ESI):** Calc. for $C_{24}H_{20}F_3N_2O_3$ $[M+H]^+$: 441.1420 found 441.1426.

3-(4-(tert-butyl)phenyl)-*N*-(4-(trifluoromethyl)phenyl)-1*H*-indole-2-carboxamide (4´):

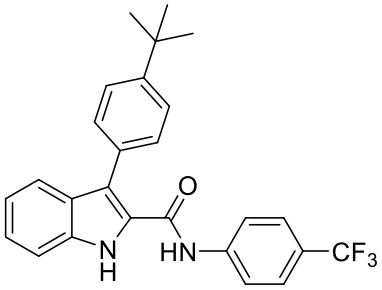

$C_{26}H_{23}F_3N_2O$
Mol. Wt.: 436.47

Synthesized by reacting 3-iodo-*N*-(4-(trifluoromethyl)phenyl)-1*H*-indole-2-carboxamide **9** (100 mg, 1.0 eq) with (4-(tert-butyl)phenyl)boronic acid (62 mg, 1.5 eq). The crude product was purified by column chromatography over 100-200 mesh silica gel (*Eluent*: EtOAc : petroleum ether 1:9 v/v) to furnish **4´** as white solid (65 mg, 65%). **^{1}H NMR (400 MHz, $CDCl_3$):** δ 9.41 (s, 1H), 7.91 (s, 1H), 7.68 (d, *J* = 8.3 Hz, 2H), 7.59 – 7.49 (m, 6H), 7.40 (t, *J* = 7.6 Hz, 1H), 7.30 (d, *J* = 7.6 Hz, 2H), 7.19 (t, *J* = 7.5 Hz, 1H), 1.49 (s, 9H); **^{13}C NMR (101 MHz, Chloroform-d):** δ 159.8, 152.4, 140.6, 135.4, 130.6, 130.0, 128.3, 126.5, 126.38, 126.24 (q, *J* = 3.9 Hz), 125.9 (q, *J* = 32.3 Hz), 125.6, 122.6 (q, *J* = 272 Hz), 121.3, 121.0, 119.6, 118.7, 111.8, 34.9, 31.3; **IR (Neat, ν/cm^{-1}):** 3405, 3310, 1688, 1657, 1599, 1533, 1447, 1409, 1318, 1235, 1189, 1162, 1099, 1068; **HRMS (ESI):** Calc. for $C_{26}H_{24}F_3N_2O$ $[M+H]^+$: 437.1835 found 437.1836.

***N*,3-bis(4-(trifluoromethyl)phenyl)-1*H*-indole-2-carboxamide (5´):** Synthesized by reacting 3-iodo-*N*-(4-(trifluoromethyl)phenyl)-1*H*-indole-2-carboxamide **9** (100 mg, 1.0 eq) with 4-trifluoromethyl phenylboronic acid (66 mg, 1.5 eq). The crude product was purified by column chromatography over 100-200 mesh silica gel (*Eluent*: EtOAc : petroleum ether 1:9 v/v) to furnish **5´** as white solid (62 mg, 60%). **^{1}H NMR (400 MHz, $CDCl_3$):** δ 9.79 (s, 1H), 7.91 (d, *J* = 8.0 Hz, 2H), 7.78 (d, *J* = 8.0 Hz, 2H), 7.63 (s, 1H), 7.57 – 7.47 (m, 4H), 7.40 (t, *J* = 7.6 Hz, 1H), 7.35 (d, *J* = 8.5 Hz, 2H), 7.20 (t, *J* = 7.5 Hz, 1H); **^{13}CNMR (101 MHz, Chloroform-d):** δ 140.3, 135.5, 131.4, 130.9 (q, *J* = 272.2 Hz), 127.9, 126.64, 126.61, 126.57, 126.53, 126.49, 126.47, 126.2 (q, *J* = 272.2 Hz), 126.1, 125.1 (q, *J* = 32.3 Hz), 122.5 (q, *J* = 32.3 Hz), 120.7, 119.1, 117.7; **IR (Neat, ν/cm^{-1}):** 3402, 3310, 1687, 1657, 1599, 1531, 1447, 1407, 1318, 1235, 1186, 1162, 1099, 1064; **HRMS (ESI):** Calc. for $C_{23}H_{15}F_6N_2O$ $[M+H]^+$: 449.1083 found 449.1078.

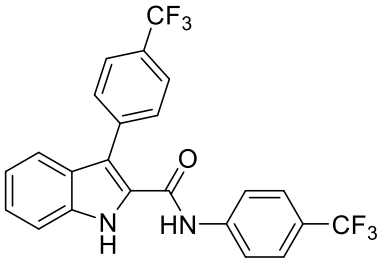

$C_{23}H_{14}F_6N_2O$
Mol. Wt.: 448.36

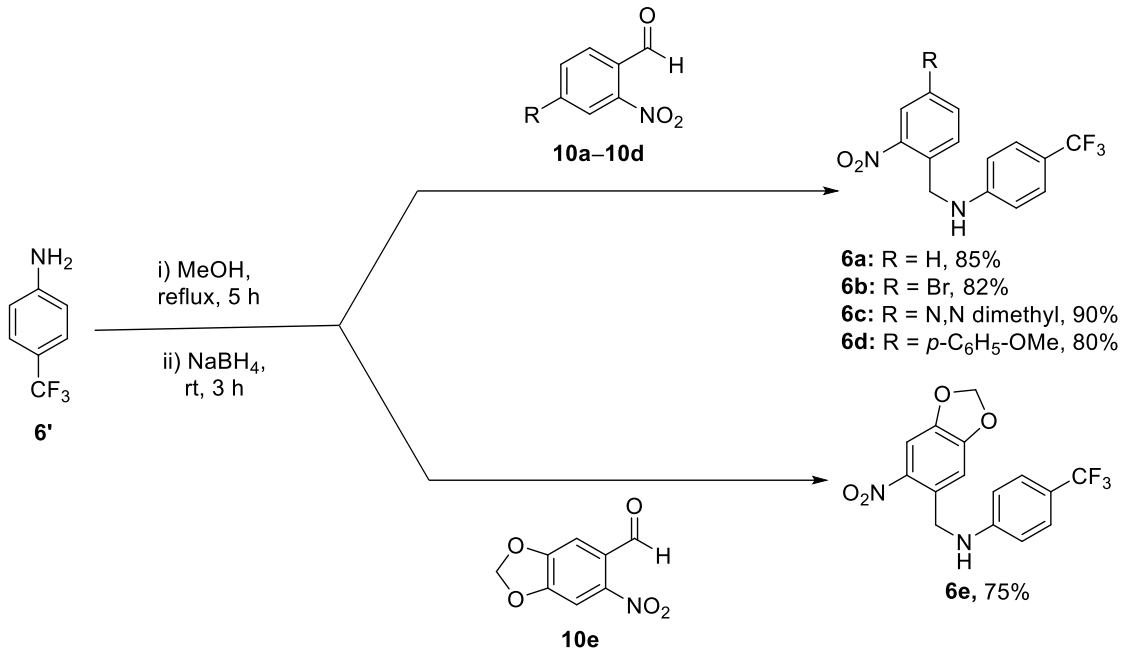

Scheme S2. Chemical synthesis of the protected amine compounds **6a–6e**.

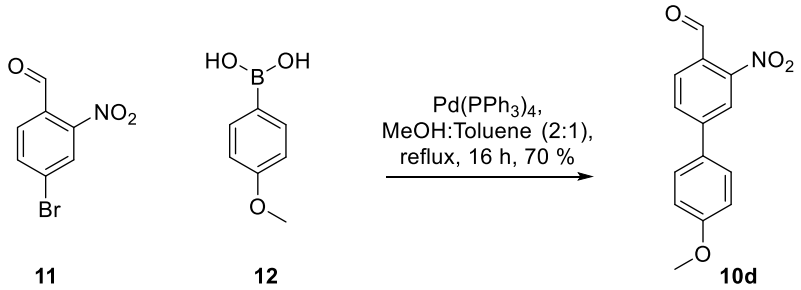

Scheme S3. Chemical synthesis for the compound **10d**.

ii. General procedure for synthesizing the compound 10d:

In a 25 mL round bottom flask, (4-methoxyphenyl)boronic acid **12** (264 mg, 2 eq), and 4-bromo-2-nitrobenzaldehyde **11** (200 mg, 1 eq) were degassed using nitrogen in a mixture of Methanol and toluene (2:1, 20 mL) for 30 min. After that tetrakis(triphenylphosphine)palladium(0) (50 mg, 0.5 eq) and aqueous sodium nitrate solution (2 mL of 2 N solution) were added, and the reaction mixture was refluxed using an oil bath for 16 h. After the completion of the reaction, monitored through TLC, the reaction mixture was filtered through celite, and volatiles were evaporated under the high vacuum using a rotary evaporator. The crude mixture was extracted with EtOAc (3 × 20 mL), washed with brine (2 × 20 mL), dried on anhydrous Na_2SO_4, and purified through column chromatography using 100-200 mesh silica gel to furnish the desired compound **10d** as white solid (156 mg, 70%). **^{1}H**

NMR (400 MHz, Chloroform-d): δ 10.41 (s, 1H), 8.23 (s, 1H), 8.01 (d, *J* = 8.1 Hz, 1H), 7.92 (d, *J* = 8.0 Hz, 1H), 7.60 (d, *J* = 8.7 Hz, 2H), 7.03 (d, *J* = 8.7 Hz, 2H); **^{13}C NMR (101 MHz, Chloroform-d):** δ 187.8,16.0, 150.5, 146.9, 131.2, 130.3, 128.6, 122.1, 114.9, 55.5; **IR (Neat, ν/cm^{-1}):** 2362, 1725, 1682, 1600, 1514, 1443, 1398, 1346, 1302, 1275, 1245; **HRMS (ESI):** Calc. for $C_{14}H_{12}NO_4$ $[M+H]^+$: 258.076 found 258.0775.

iii. General procedure for synthesizing the amine derivatives 6a-6e:

General method B: In a 25 mL round bottom flask, a solution of 4-(trifluoromethyl) aniline **6´** (100 mg, 1.0 eq), pyrrolidine (10 mg, 2 eq), molecular sieves 4 A˚ (1.0 gram), and the appropriate benzaldehyde **10a-10e** (1.0 eq) were refluxed in dry dichloromethane for 16 h. The reaction mixture was allowed to cool to room temperature, and the solvent was removed. Subsequently, the crude product was redissolved in dry methanol (20 mL), and $NaBH_4$ (4.0 eq) was added to the reaction mixture and stirred for an extra 3 h at room temperature. After the completion of the reaction, monitored through TLC, the solvent was evaporated under reduced pressure using a rotary evaporator. The residue was dissolved in ethyl acetate (30 mL), and water (15 mL) was added. The crude product was extracted in ethyl acetate (3 × 20 mL). The organic layer was washed with water (2 × 10 mL) and brine (2 × 10 mL), dried over Na_2SO_4, and filtered. The filtrate was concentrated under reduced pressure. The purification of the crude product was done using either 100-200 mesh silica gel or neutral aluminium oxide column chromatography to furnish the desired compounds **6a–6e**.

***N*-(2-nitrobenzyl)-4-(trifluoromethyl)aniline (6a):** Synthesized by reacting 4-trifluoromethyl aniline **6´** (100 mg, 1.0 eq) with *ortho*-nitrobenzaldehyde **10a** (94 mg, 1.0 eq). The crude product was purified by column chromatography over 100-200 mesh silica gel (*Eluent*: EtOAc : petroleum ether 1:9 v/v) to furnish **6a** as a yellow oil (155 mg, 85%). **^{1}H NMR (400 MHz, Chloroform-d**): δ 8.11 (d, *J* = 7.8 Hz, 1H), 7.63 – 7.57 (m, 2H), 7.46 (ddd, *J* = 6.4, 5.8, 3.1 Hz, 1H), 7.38 (d, *J* = 8.8 Hz, 2H), 6.58 (t, *J* = 5.7 Hz, 2H), 4.79 (d, *J* = 6.1 Hz, 2H), 4.71 (d, *J* = 5.7 Hz, 1H).

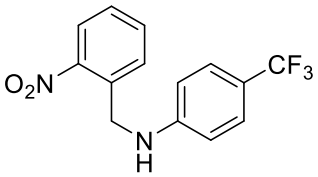

$C_{14}H_{11}F_3N_2O_2$
Mol. Wt.: 296.24

The ^{1}H NMR matched with the reported literature.[S1]

***N*-(4-bromo-2-nitrobenzyl)-4-(trifluoromethyl)aniline (6b):** Synthesized by reacting 4-trifluoromethyl aniline **6´** (100 mg, 1.0 eq) with *4*-bromo-*2*-nitrobenzaldehyde **10b** (142 mg, 1.0 eq). The crude product was purified by column chromatography over 100-200 mesh silica gel (*Eluent*: EtOAc : petroleum ether 2:8 v/v) to furnish **6b** as reddish solid (190 mg, 82%). **^{1}H NMR (400 MHz, Chloroform-*d*):** δ 8.25 (s, 1H), 7.70 (d, *J* = 8.3 Hz, 1H), 7.49 (d, *J* = 8.4 Hz, 1H), 7.39 (d, *J* = 8.7 Hz, 2H), 6.56 (d, *J* = 8.7 Hz, 2H), 4.74 (d, *J* = 5.8 Hz, 2H), 4.69 (s, 1H); **^{13}C NMR (101 MHz, Chloroform-*d*):** δ 149.5, 148.5, 136.9, 133.8, 131.0, 128.4, 126.8 (q, *J*= 3.9 Hz), 126.1 (q, *J* = 272 Hz)), 121.5,120.25 (q, *J* = 32.3), 112.20, 45.2; **IR (Neat, ν/cm^{-1}):** 3449, 2361, 1661, 1533, 1464, 1443, 1409, 1322, 1275, 1248; **HRMS (ESI):** Calc. for $C_{14}H_{11}BrF_3N_2O_2$ $[M+H]^+$: 374.9950 found 374.9938.

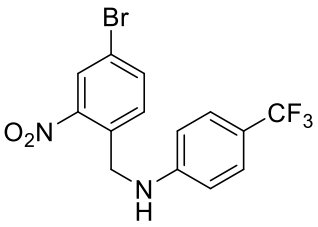

$C_{14}H_{10}BrF_3N_2O_2$
Mol. Wt.: 375.14

***N*,*N*-dimethyl-3-nitro-4-(((4-(trifluoromethyl)phenyl)amino)methyl)aniline (6c):** Synthesized by reacting 4-trifluoromethyl aniline **6´** (100 mg, 1.0 eq) with 4-(dimethylamino)-2-nitrobenzaldehyde **10c** (120 mg, 1.0 eq). The crude product was purified by column chromatography over neutral alumunium oxide (*Eluent*: EtOAc : petroleum ether 1:9 v/v) to furnish **6c** as red solid (189 mg, 90%). **^{1}H NMR (400 MHz, Chloroform-*d*):** δ 7.41 – 7.29 (m, 4H), 6.85 (dd, *J* = 8.7, 2.8 Hz, 1H), 6.68 – 6.51 (m, 2H), 4.62 (d, *J* = 15.0 Hz, 3H), 3.00 (s, 6H); **^{13}C NMR (101 MHz, Chloroform-*d*):** δ 150.2, 150.0, 130.8, 126.6 (q *J* = 3.9 Hz),126.2 (q, *J* = 272 Hz), 120.4, 119.3 (q, *J* = 32.3 Hz), 116.7, 112.1, 107.9, 44.9, 40.2; **IR (Neat, ν/cm^{-1}):** 3447, 2360, 1661, 1533, 1466, 1442, 1409, 1321, 1277, 1249; **HRMS (ESI):** Calc. for $C_{16}H_{17}F_3N_2O_2$ $[M+H]^+$: 340.1267 found 340.1235.

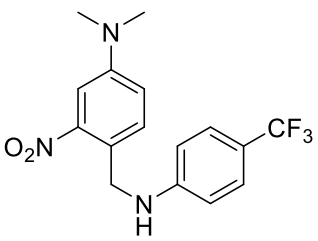

$C_{16}H_{16}F_3N_3O_2$
Mol. Wt.: 339.31

***N*-((4'-methoxy-3-nitro-[1,1'-biphenyl]-4-yl)methyl)-4-(trifluoromethyl)aniline (6d):** Synthesized by reacting 4-trifluoromethyl aniline **6´** (100 mg, 1.0 eq) with 4'-methoxy-3-nitro-[1,1'-biphenyl]-4-carbaldehyde **10d** (160 mg, 1.0 eq). The crude product was purified by column chromatography over 100-200 mesh silica gel (*Eluent*: EtOAc : petroleum ether 2:8 v/v) to furnish **6d** as white solid (199 mg, 80%). **^{1}H NMR (400 MHz, Chloroform-*d*):** δ 8.27 (s, 1H), 7.74 (dd, *J* = 8.1, 1.9 Hz, 1H), 7.60 (d, *J* = 8.1 Hz, 1H), 7.53 (d, *J* = 8.7 Hz, 2H), 7.38 (d, *J* = 8.5 Hz, 2H), 6.99 (d, *J* = 8.9 Hz, 2H), 6.60 (d, *J* = 8.5 Hz, 2H), 4.78 (s,

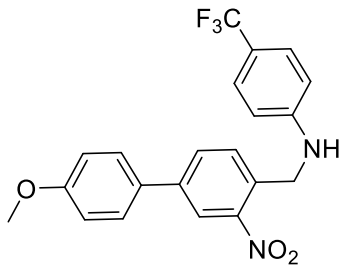

$C_{21}H_{17}F_3N_2O_3$
Mol. Wt.: 402.37

2H), 4.71 (s, 1H), 3.85 (s, 3H); **^{13}C NMR (101 MHz, Chloroform-*d*):** δ 160.1, 149.9, 141.5, 132.4, 131.6, 130.5, 130.1, 128.20, 126.8 (q, *J* = 3.9 Hz), 126.2 (q, *J* = 272 Hz), 123.3, 119.8 (q, *J* = 32.3 Hz), 114.6, 112.2, 55.5, 45.3; .**IR (Neat, ν/cm^{-1}):** 3449, 2359, 1660, 1533, 1464, 1445, 1407, 1322, 1277, 1248; **HRMS (ESI):** Calc. for $C_{21}H_{18}F_3N_2O_3$ $[M+H]^+$: 403.1264 found 403.1270.

***N*-((6-nitrobenzo[*d*][1,3]dioxol-5-yl)methyl)-4-(trifluoromethyl)aniline (6e):** Synthesized by reacting 4-trifluoromethyl aniline **6´** (100 mg, 1.0 eq) with 6-nitrobenzo[*d*][1,3]dioxole-5-carbaldehyde **10e** (121 mg, 1.0 eq). The crude product was purified by column chromatography over 100-200 mesh silica gel (*Eluent*: EtOAc : petroleum ether 2:8 v/v) to furnish **6e** as white solid (158 mg, 80%). **^{1}H NMR (400 MHz, Chloroform-*d*):** δ 7.65 (s, 1H), 7.39 (d, *J* = 8.4 Hz, 2H), 7.02 (s, 1H), 6.57 (d, *J* = 8.4 Hz, 2H), 6.10 (s, 2H), 4.73 (s, 3H); **^{13}C NMR (101 MHz, Chloroform-*d*):** δ 152.8, 149.8, 141.8, 132.7, 126.8 (q, *J* = 3.9 Hz), 123.5 (q, *J* = 272 Hz), 119.9 (q, *J* = 32.3 Hz), 112.2, 108.2, 106.3, 103.1, 46.0; **IR (Neat, ν/cm^{-1}):** 3449, 2363, 1659, 1531, 1464, 1443, 1410, 1322, 1277, 1246; **HRMS (ESI):** Calc. for $C_{15}H_{12}F_3N_2O_4$ $[M+H]^+$: 341.0743 found 341.0750.

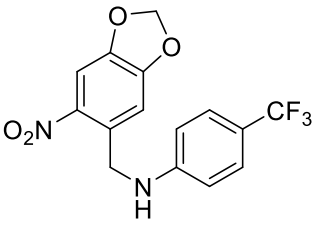

$C_{15}H_{11}F_3N_2O_4$
Mol. Wt.: 340.25

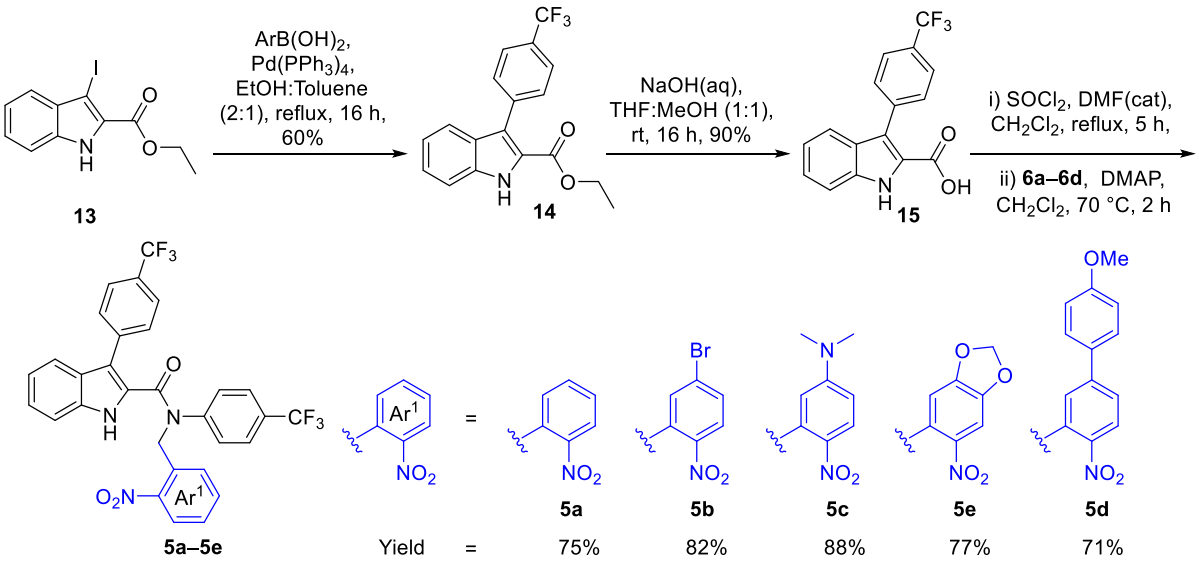

Scheme S4. Chemical synthesis of the protected indole compounds **5a–5e**.

Ethyl 3-(4-(trifluoromethyl)phenyl)-1*H*-indole-2-carboxylate (14): In a 25 mL round bottom flask, ethyl 3-iodo-1H-indole-2-carboxylate **13** (1 g, 1 eq), and 4-trifluoromethyl phenylboronic acid (1.5g, 1.0 eq) were degassed using nitrogen in a mixture of ethanol and toluene (2:1, 40 mL) for 30 min. After that, tetrakis(triphenylphosphine)palladium(0) (183 mg, 0.5 eq) and aqueous sodium nitrate solution (5 mL of 2 N solution) were added, and the reaction mixture was refluxed using an oil bath for 16 h. After the completion of the reaction, monitored through TLC, the reaction mixture was filtered through celite, and volatiles were evaporated under a high vacuum using a rotary evaporator. The crude mixture was extracted with EtOAc (3 × 30 mL), washed with brine (2 × 20 mL), dried on anhydrous Na_2SO_4 and purified through column chromatography using 100-200 mesh silica gel (*Eluent* : EtOAc : petroleum ether 1:10 v/v) to furnish the desired compound **14** as white solid (636 mg, 60%).**^{1}H NMR (400 MHz, Chloroform-d):** δ 9.11 (s, 1H), 7.74 – 7.65 (m, 4H), 7.58 (d, *J* = 8.2 Hz, 1H), 7.47 (d, *J* = 8.4 Hz, 1H), 7.42 – 7.35 (m, 1H), 7.22 – 7.13 (m, 1H), 4.30 (q, *J* = 7.1 Hz, 2H), 1.24 (t, *J* = 7.1 Hz, 3H); **^{13}C NMR (101 MHz, Chloroform-*d*):** δ 161.7, 137.5, 135.7, 131.05, 129.4 (q, *J* = 32.3 Hz), 127.6, 126.1, 125.8 (q, *J* = 272 Hz), 124.8 (q, *J* = 3.9 Hz), 123.1, 122.6, 121.4, 121.3, 111.9, 61.2, 14.1;.**IR (Neat, ν/cm^{-1}):** 3323, 1679, 165, 1549, 1502, 1450, 1303, 1318; **HRMS (ESI):** Calc. for $C_{18}H_{15}F_3NO_2$ $[M+H]^+$: 334.1049, found 334.1048

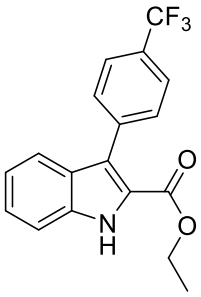

$C_{18}H_{14}F_3NO_2$
Mol. Wt.: 333.31

3-(4-(trifluoromethyl)phenyl)-1*H*-indole-2-carboxylic acid (15): A suspension of **14** (600 mg) in a solution of aqueous NaOH (10 mL, 2N), tetrahydrofuran (10 mL) and MeOH (10 mL) was stirred at rt for 24 h. After that, the solvent was removed under reduced pressure using a rotary evaporator. The pH of the solution was adjusted to 1 with concentrated HCl, and the crude product was then extracted with EtOAc (2 x 50 mL), and the combined organic phase was washed with brine (2 x 30 mL). It was then dried over Na_2SO_4, and the solvent was removed under vacuum using a rotary evaporator. The crude product was purified by column chromatography using 100-200 mesh silica gel (*Eluent*: 5% MeOH in $CHCl_3$) to get **15** as white solid (494 mg, 90%). **^{1}H NMR (400 MHz, DMSO-*d*$_6$):** δ 13.04 (s, 1H), 12.00 (s, 1H), 7.79 (d, *J* = 8.4 Hz, 2H), 7.73 (d, *J* = 8.2 Hz, 2H), 7.50 (t, *J* = 8.8 Hz, 2H), 7.31 (t, *J* = 7.2 Hz, 1H), 7.10 (t, *J* = 7.6 Hz, 1H); **^{13}C NMR (101 MHz, DMSO-*d*$_6$):** δ 163.0, 138.8, 136.4, 131.6, 127.6 (q, *J* = 32.4 Hz), 127.0, 126.3 (q, *J* = 32.4 Hz), 125.4, 125.08, 125.8, 124.58, 121.2, 120.6 (q, *J* = 3.9 Hz), 113.2; **IR (Neat, ν/cm^{-1}):** 3459, 1724,

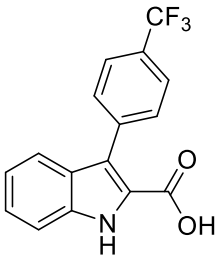

$C_{16}H_{10}F_3NO_2$
Mol. Wt.: 305.25

1662, 1615, 1553, 1532, 1512, 1463, 1402**. HRMS (ESI):** Calc. for $C_{16}H_{11}F_3NO_2$ $[M+H]^+$: 306.0736, found 306.0740.

iv. General procedure for synthesizing the protecting indole derivatives (5a-5e):

General method C: To a solution of 3-(4-(trifluoromethyl)phenyl)-1H-indole-2-carboxylic acid **15** (200 mg, 2.0 eq) in dichloromethane (15 mL), thionyl chloride (779 mg, 20.0 eq), and 2 drops of DMF were added. The reaction mixture was refluxed using an oil bath for 6 h. The excess of thionyl chloride and the solvent was then evaporated to dryness *in vacuo* to give 3-(4-(trifluoromethyl)phenyl)-1*H*-indole-2-carbonyl chloride. The residue was dissolved in dry dichloromethane (10 mL). To this solution, amine derivatives **7a–7e** (1.0 eq) in dichloromethane (5 mL) were added dropwise, followed by the addition of triethylamine (50 mg, 1.5 eq). The reaction mixture was heated at 70 °C and stirred for 2 h. After the completion of the reaction, monitored through TLC, the reaction was quenched with water and extracted with CH_2Cl_2 (3 × 10 mL). The organic phase was washed with water (2 × 10 mL), and brine (2 × 10 mL) and then dried over Na_2SO_4, filtered, and concentrated under reduced pressure. The crude product was purified by either 100-200 mesh silica gel or basic aluminium oxide column chromatography to give the desired protected compounds compound **5a**–**5e**.

***N*-(2-nitrobenzyl)-N,3-bis(4-(trifluoromethyl)phenyl)-1*H*-indole-2-carboxamide (5a):**

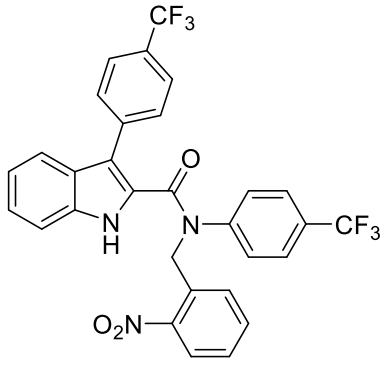

$C_{30}H_{19}F_6N_3O_3$
Mol. Wt.: 583.49

Synthesized by reacting 3-(4-(trifluoromethyl)phenyl)-1*H*-indole-2-carboxylic acid **15** (200 mg, 2.0 eq) with *N*-(2-nitrobenzyl)-4-(trifluoromethyl)aniline (97 mg, 1.0 eq). The crude product was purified by column chromatography over 100-200 mesh silica gel (*Eluent*: EtOAc : petroleum ether 3:7 v/v) to furnish **5a** as white solid (143 mg, 75%). **^{1}H NMR (400 MHz, Chloroform-*d*):** δ 9.29 (s, 1H), 7.98 (d, *J* = 8.2 Hz, 1H), 7.59 – 7.54 (m, 1H), 7.51 (d, *J* = 7.8 Hz, 3H), 7.41 (q, *J* = 7.5, 6.7 Hz, 3H), 7.35 – 7.29 (m, 1H), 7.13 (t, *J* = 8.0 Hz, 1H), 7.06 (dd, *J* = 12.6, 8.2 Hz, 4H), 6.52 (d, *J* = 8.4 Hz, 2H), 5.48 (s, 2H); **^{13}C NMR (101 MHz, Chloroform-*d*):** δ 165.0, 148.1, 144.5, 137.3, 135.9, 133.4, 129.8, 129.4 (q, *J* = 272 Hz), 129.1, 128.5, 128.1 (q, *J* = 32.3 Hz), 126.1, 126.1, 125.6, 125.5, 125.3, 125.3,124.8 (q, *J* = 272 Hz), 122.8 (q, *J* = 32.3 Hz), 121.5, 120.4, 111.9, 50.7; **IR (Neat, ν/cm^{-1}):** 3316, 2361, 1661, 1608, 1549, 1531, 1498, 1481; **HRMS (ESI):** Calc. for $C_{30}H_{20}F_6N_3O_3$ $[M+H]^+$: 584.1403 found 584.1406.

***N*-(4-bromo-2-nitrobenzyl)-*N*,3-bis(4-(trifluoromethyl)phenyl)-1*H*-indole-2-carboxamide (5b):** Synthesized by reacting 3-(4-(trifluoromethyl)phenyl)-1*H*-indole-2-carboxylic acid **15** (200 mg, 2.0 eq) with *N*-(4-bromo-2-nitrobenzyl)-4-(trifluoromethyl)aniline (122 mg, 1.0 eq). The crude product was purified by column chromatography over 100-200 silica gel (*Eluent*: EtOAc : petroleum ether 3:7 v/v) to furnish **5b** as reddish solid (177 mg, 82%). **^{1}H NMR (400 MHz, Chloroform-*d*):** δ 9.31 (s, 1H), 8.09 (d, *J* = 2.0 Hz, 1H), 7.65 (d, *J* = 8.4 Hz, 1H), 7.52 (d, *J* = 8.0 Hz, 2H), 7.45 – 7.30 (m, 4H), 7.13 (t, *J* = 7.6 Hz, 1H), 7.06 (d, *J* = 8.2 Hz, 4H), 6.51 (d, *J* = 8.4 Hz, 2H), 5.41 (s, 2H); **^{13}C NMR (101 MHz, Chloroform-*d*):** δ 164.9, 144.2, 137.2, 136.2, 135.8, 130.6, 130.6, 129.7, 129.4 (q, *J* = 32.3 Hz), 128.0, 127.9 (q, *J* = 32.5 Hz), 126.1, 125.8, 125.5, 125.5, 125.4, 125.4, 125.4, 124.7 (q, *J* = 272 Hz), 121.5, 120.4, 119.3 (q, *J* = 272 Hz), 111.8, 50.2; **IR (Neat, ν/cm^{-1}):** 3315, 2359, 1659, 1607, 1548, 1530, 1498, 1480; **HRMS (ESI):** Calc. for $C_{30}H_{19}BrF_6N_3O_3$ $[M+H]^+$: 662.0508 found 662.0505.

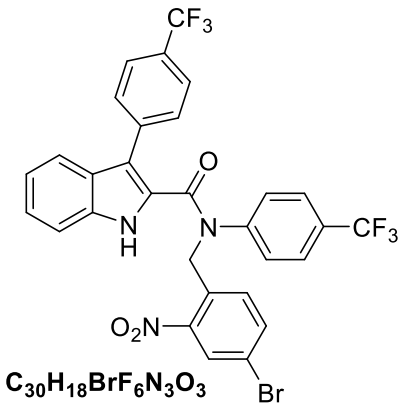

$C_{30}H_{18}BrF_6N_3O_3$
Mol. Wt.: 662.04

***N*-(4-(dimethylamino)-2-nitrobenzyl)-*N*,3-bis(4-(trifluoromethyl)phenyl)-1*H*-indole-2-carboxamide (5c):** Synthesized by reacting 3-(4-(trifluoromethyl)phenyl)-1H-indole-2-carboxylic acid **15** (200 mg, 2.0 eq) with *N*,*N*-dimethyl-3-nitro-4-(((4-(trifluoromethyl)phenyl)amino)methyl) aniline (111 mg, 1.0 eq). The crude product was purified by column chromatography over basic aluminium oxide (*Eluent*: EtOAc : petroleum ether 3:7 v/v) to furnish **5c** as red solid (180 mg, 88%). **^{1}H NMR (400 MHz, Chloroform-*d*):** δ 9.55 (s, 1H), 7.50 (d, *J* = 8.1 Hz, 2H), 7.39 (t, *J* = 8.2 Hz, 2H), 7.31 – 7.25 (m, 2H), 7.15 – 7.05 (m, 4H), 7.01 (d, *J* = 8.4 Hz, 2H), 6.73 (dd, *J* = 8.8, 2.8 Hz, 1H), 6.47 (d, *J* = 8.3 Hz, 2H), 5.37 (s, 2H), 2.93 (s, 6H); **^{13}C NMR (101 MHz, Chloroform-*d*):** δ 164.9, 149.8, 144.5, 137.4, 135.8, 130.5, 129.7, 129.1 (q, *J* = 272 Hz), 128.8 (q, *J* = 272 Hz), 126.7, 126.0, 125.5 (q, *J* = 32.3 Hz), 125.8, 125.3, 125.0, 122.8 (q, *J* = 323.3 Hz), 121.2, 120.2, 117.8, 117.1, 116.0, 111.9, 107.3, 49.8, 40.0; **IR (Neat, ν/cm^{-1}):** 3316, 2360, 1660, 1607, 1549, 1532, 1498, 1483; **HRMS (ESI):** Calc. for $C_{32}H_{25}F_6N_4O_3$ $[M+H]^+$: 627.1825 found 627.1826.

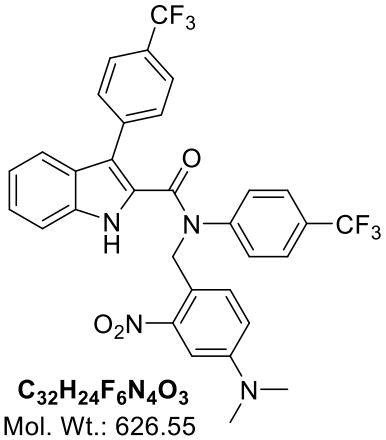

$C_{32}H_{24}F_6N_4O_3$
Mol. Wt.: 626.55

***N*-((4'-methoxy-3-nitro-[1,1'-biphenyl]-4-yl)methyl)-*N*,3-bis(4-(trifluoromethyl)phenyl)-1*H*-indole-2-carboxamide (5d)**: Synthesized by reacting 3-(4-(trifluoromethyl)phenyl)-1*H*-indole-2-carboxylic acid **15** (200 mg, 2.0 eq) with N-((4'-methoxy-3-nitro-[1,1'-biphenyl]-4-yl)methyl)-4-(trifluoromethyl)aniline (131 mg, 1.0 eq). The crude product was purified by column chromatography over 100-200 mesh silica gel (*Eluent*: EtOAc : petroleum ether 3:7 v/v) to furnish **5d** as white solid (160 mg, 71%). **^{1}H NMR (400 MHz, Chloroform-*d*):** δ 9.69 (s, 1H), 8.10 (s, 1H), 7.65 (d, *J* = 8.2 Hz, 1H), 7.51 (d, *J* = 8.1 Hz, 3H), 7.44 – 7.33 (m, 4H), 7.28 (d, *J* = 6.9 Hz, 1H), 7.07 (td, *J* = 14.6, 13.4, 8.1 Hz, 5H), 5.52 (s, 2H), 3.82 (s, 3H); **^{13}C NMR (101 MHz, Chloroform-*d*):** δ 165.2, 160.2, 148.7, 144.5, 137.3, 135.9, 131.0, 129.8, 129.4, 128.1, 126.21, 125.7, 125.5, 125.3, 122.9, 121.4, 120.4, 118.2, 114.6, 111.9, 55.4, 50.7; **IR (Neat, ν/cm^{-1}):** 3315, 2359, 1659, 1604, 1549, 1530, 1497, 1481; **HRMS (ESI):** Calc. for $C_{37}H_{26}F_6N_3O_4$ $[M+H]^+$: 690.1822 found 690.1816.

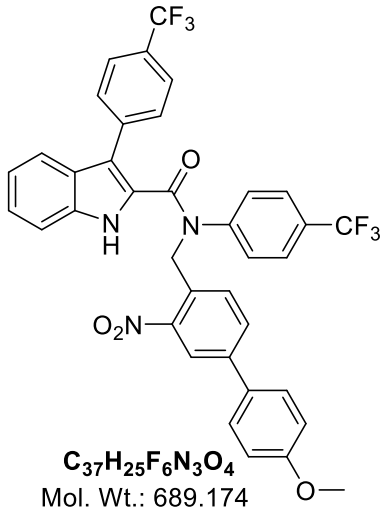

***N*-((6-nitrobenzo[*d*][1,3]dioxol-5-yl)methyl)-N,3-bis(4-(trifluoromethyl)phenyl)-1*H*-indole-2-carboxamide (5e):** Synthesized by reacting 3-(4-(trifluoromethyl)phenyl)-1*H*-indole-2-carboxylic acid **15** (200 mg, 2.0 eq) with *N*-((6-nitrobenzo[*d*][1,3]dioxol-5-yl)methyl)-4-(trifluoromethyl)aniline (111 mg, 1.0 eq). The crude product was purified by column chromatography over 100-200 mesh silica gel (*Eluent*: EtOAc : petroleum ether 3:7 v/v) to furnish **5e** as white solid (157 mg, 77%). **^{1}H NMR (400 MHz, Chloroform-*d*):** δ 9.60 (s, 1H), 7.53 (d, *J* = 8.0 Hz, 2H), 7.48 (s, 1H), 7.39 (dd, *J* = 15.9, 8.2 Hz, 2H), 7.32 – 7.27 (m, 1H), 7.14 – 7.03 (m, 5H), 6.95 (s, 1H), 6.53 (d, *J* = 8.3 Hz, 2H), 6.02 (s, 2H), 5.48 (s, 2H); **^{13}C NMR (101 MHz, Chloroform-*d*):** δ 165.2, 152.3, 147.2, 144.4, 137.2, 135.8, 129.7,129.4 (q, *J* = 32.3 Hz), 129.2, 128.1 (q, *J* = 323 Hz) , 126.1, 126.0, 125.5, 125.4, 125.3, 124.7 (q, *J* = 272 Hz), 122.0 (q, *J* = 272 Hz), 121.4, 120.3, 111.8, 107.4, 106.0, 103.1, 51.1; **.IR (Neat, ν/cm^{-1}):** 3316, 2361, 1660, 1606, 1551, 1531, 1497, 1481; **HRMS (ESI):** Calc. for $C_{31}H_{20}F_6N_3O_5$ $[M+H]^+$: 628.1301 found 628.1323.

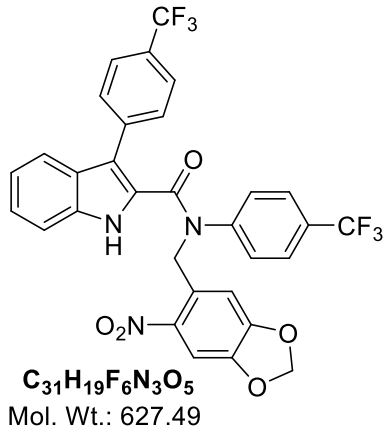

IV. Anion Binding Studies by ^{1}H NMR:

^{1}H NMR titration was carried out at room temperature on a Bruker AVANCE III HD 400 MHz spectrometer. The residual solvent signal (CD_3CN, δ_H = 1.94 ppm) was considered as an internal reference to calibrate spectra. Both the TBACl salt and receptor were dried under vacuum before use. The titrations were performed by the addition of aliquots from the tetrabutylammonium chloride (TBACl) solution (1 M in CD_3CN) to the solution of either **2´**, **3´**, **4´**, or **5´** (0.0025 M in CD_3CN). All NMR data were processed using MestReNova 6.0, and the collected data were fitted into different binding modes using *BindFit* 0.5.[S2]

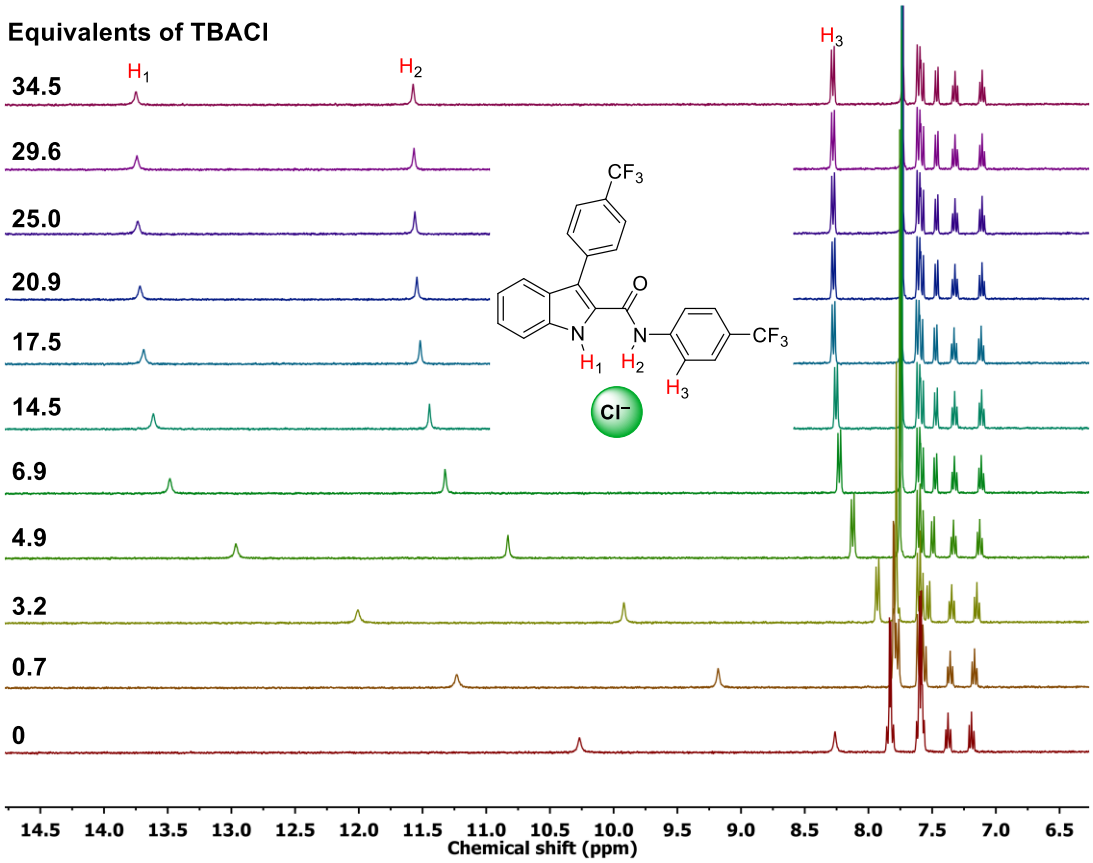

Fig. S1 ^{1}H NMR titration spectra for **5´** (0.0025 M) with stepwise addition of TBACl in CD_3CN. The equivalents of added TBACl are shown on the stack spectra.

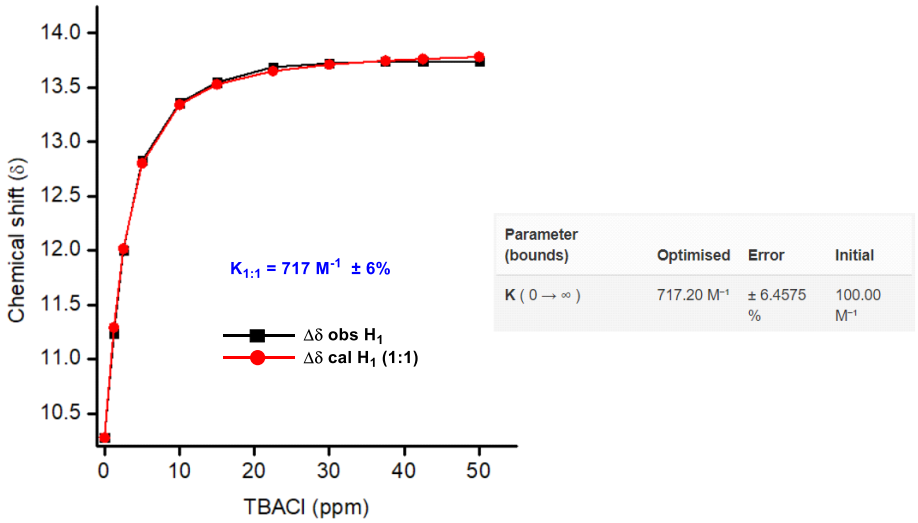

Fig. S2 The plot of chemical shift (δ) of H_1 protons *vs* concentration of TBACl added, fitted to 1:1 binding model of *BindFit* 0.5.

http://app.supramolecular.org/bindfit/view/ce336a99-7e4b-4920-84c3-82c3a793b9d5-(**5´** with TBACl).

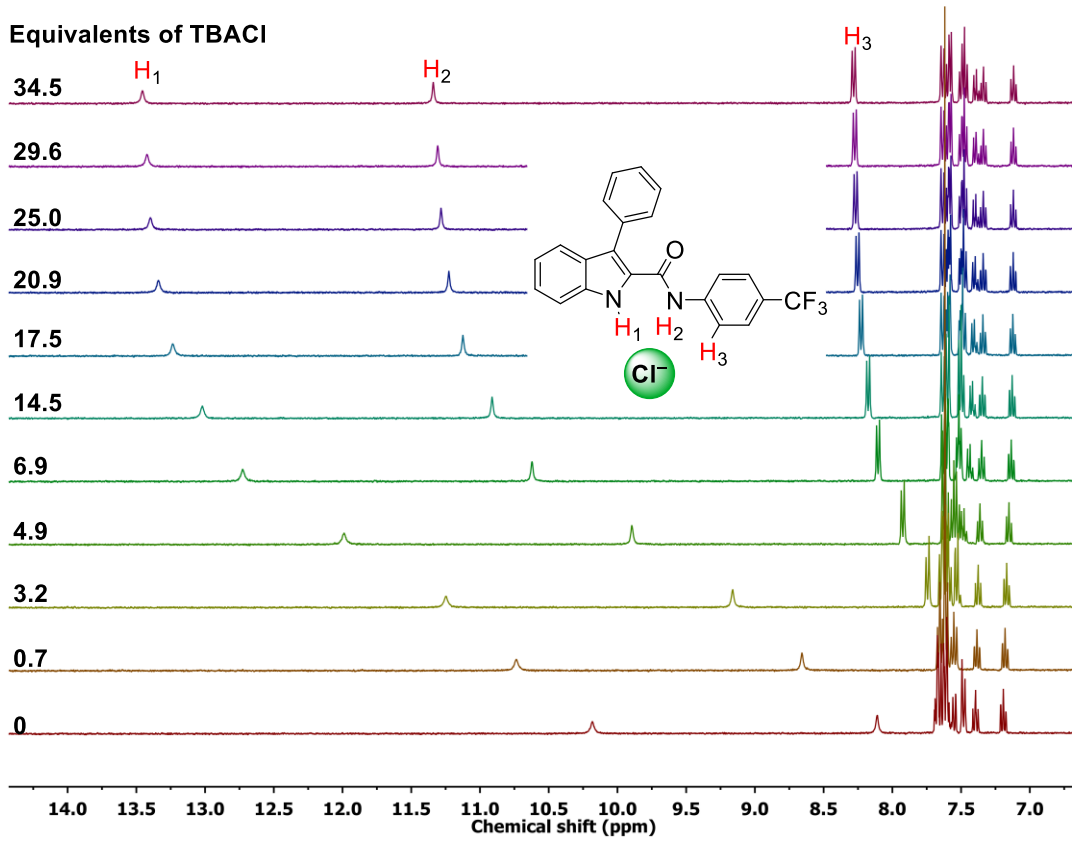

Fig. S3 ^{1}H NMR titration spectra for **2´** (0.0025 M) with stepwise addition of TBACl in CD_3CN. The equivalents of added TBACl are shown on the stack spectra.

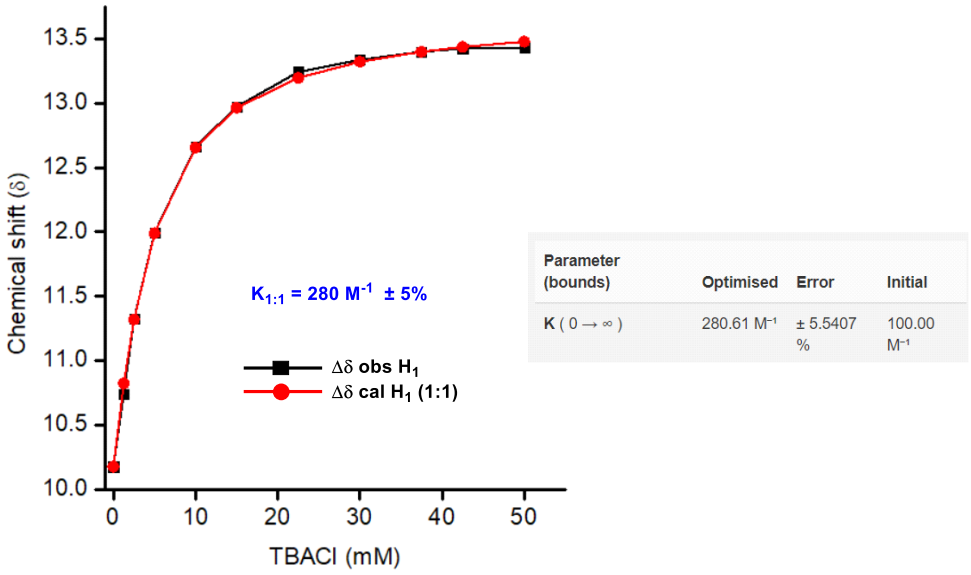

Fig. S4 The plot of chemical shift (δ) of H_1 protons *vs* concentration of TBACl added, fitted to 1:1 binding model of *BindFit* 0.5.

http://app.supramolecular.org/bindfit/view/d7a4d498-42d8-471b-aaa5-b9c45bcc017c-(**2´** with TBACl).

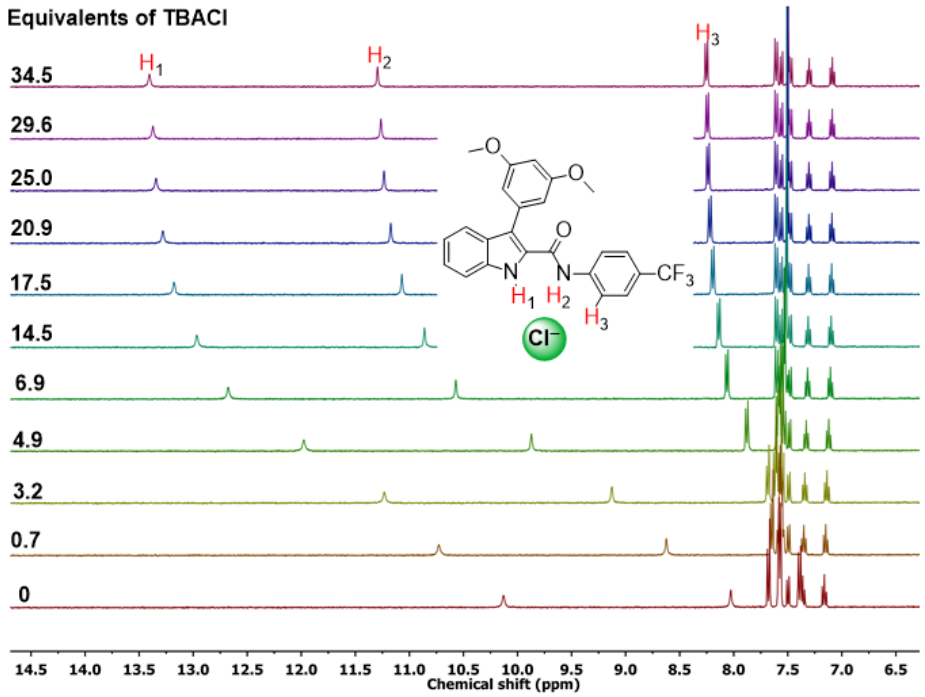

Fig. S5 ^{1}H NMR titration spectra for **3´** (0.0025 M) with stepwise addition of TBACl in CD_3CN. The equivalents of added TBACl are shown on the stack spectra.

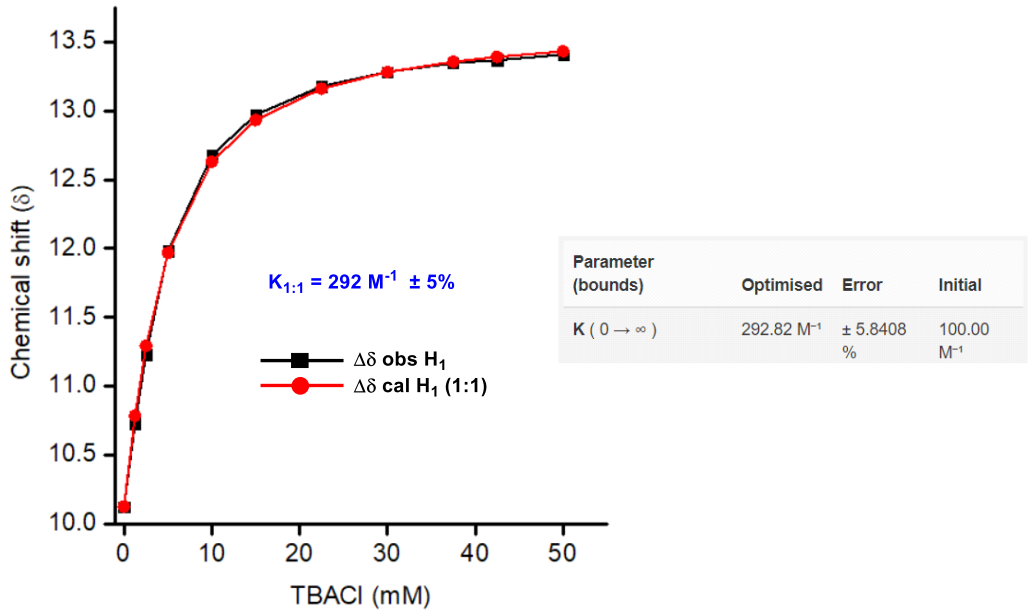

Fig. S6 The plot of chemical shift (δ) of H_1 protons *vs* concentration of TBACl added, fitted to 1:1 binding model of *BindFit* 0.5.

http://app.supramolecular.org/bindfit/view/9ac3650e-7e13-40c1-806a-7dfc79e66a9e-(**3´** with TBACl).

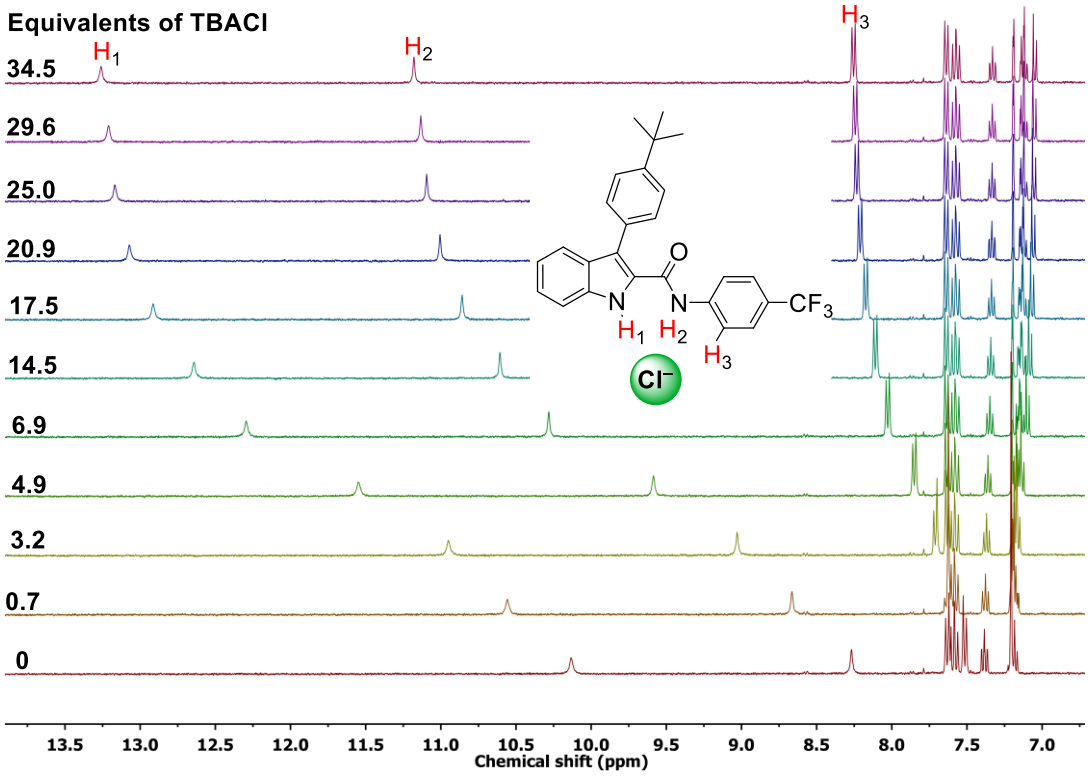

Fig. S7 ^{1}H NMR titration spectra for **4´** (0.0025 M) with stepwise addition of TBACl in CD_3CN. The equivalents of added TBACl are shown on the stack spectra.

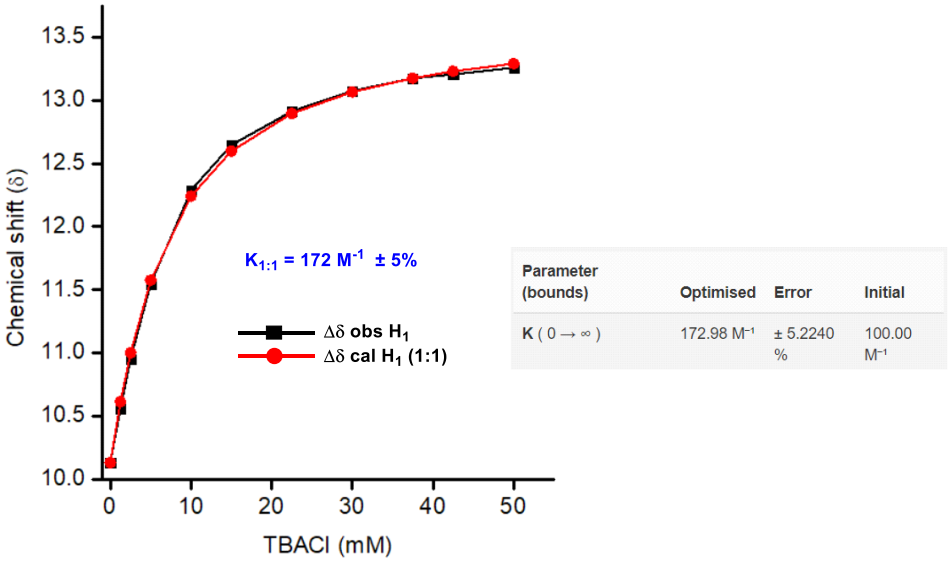

Fig. S8 The plot of chemical shift (δ) of H_1 protons *vs* concentration of TBACl added, fitted to 1:1 binding model of *BindFit* 0.5.

http://app.supramolecular.org/bindfit/view/e2dc3df0-df1a-4bd9-8d38-55abce32c6e0-(**4´** with TBACl).

V. Ion Transport Studies[S3]

Ion transporting activity studies across EYPC-LUVs⊃HPTS:

Preparation of HEPES buffer and stock solutions: The HEPES buffer of pH = 7.0 was prepared by dissolving an appropriate amount of solid HEPES (10 mM) and NaCl (100 mM) in autoclaved water. The pH was adjusted to 7.0 by the addition of aliquots from 0.5 M NaOH solution. The stock solution of all carriers was prepared using HPLC grade DMSO.

Preparation of EYPC-LUVs⊃HPTS in NaCl: In a 10 mL clean and dry round bottom flask, a thin transparent film of egg yolk phosphatidylcholine (EYPC) was formed using a 1 mL EYPC lipid (25 mg/mL in $CHCl_3$) by providing continuous rotation and purging nitrogen gas. The transparent thin film was completely dried under a high vacuum for 4-5 h. After that, the transparent thin film was hydrated with 1 mL HEPES buffer (1 mM HPTS, 10 mM HEPES, 100 mM NaCl, pH = 7.0), and the resulting suspension was vortexed at 10 min intervals for 1 h. This hydrated suspension was subjected to 15 cycles of freeze-thaw (liquid N_2, 55 °C) followed by extrusion through a 100 nm (pore size) polycarbonate membrane 21 times to obtain vesicles of average 100 nm diameter. The unentrapped HPTS dye was removed by size exclusion chromatography using Sephadex G-50 (Sigma-Aldrich) with eluting of HEPES buffer (10 mM HEPES, 100 mM NaCl, pH = 7.0). Finally, collected vesicles were diluted to 6

mL to get EYPC-LUVs⊃HPTS. *Final conditions:* ~ 5 mM EYPC, Inside: 1 mM HPTS, 10 mM HEPES, 100 mM NaCl, pH = 7.0, Outside: 10 mM HEPES, 100 mM NaCl, pH = 7.0.

Ion transport activity by HPTS assay: In clean and dry fluorescence cuvette, 1975 µL of HEPES buffer (10 mM HEPES, 100 mM NaCl, pH =7.0) and 25 µL of EYPC–LUVs⊃HPTS vesicle was added. The cuvette was placed under slow stirring conditions using a magnetic stirrer equipped with the fluorescence instrument (t = 0 s). The time-dependent HPTS emission intensity was monitored at λ_{em} = 510 nm (λ_{ex} = 450 nm) by creating a pH gradient between the intra- and extra-vesicular system by the addition of 0.5 M NaOH (20 µL) at t = 20 s. Then, different concentrations of carrier molecules in DMSO were added at t = 100 s. Finally, the vesicles were lysed by the addition of 10% Triton X-100 (25 µL) at t = 300 s to disrupt the pH gradient.

The time axis was normalized according to Equation S1:

$$t = t - 100 \qquad \text{Equation S1}$$

The time-dependent data were normalized to percent change in fluorescence intensity using Equation S2:

$$I_F = [(I_t - I_0) / (I_\infty - I_0)] \times 100 \qquad \text{Equation S2}$$

where, I_0 is the initial intensity, I_t is the intensity at time t, and I_∞ is the final intensity after the addition of Triton X-100.

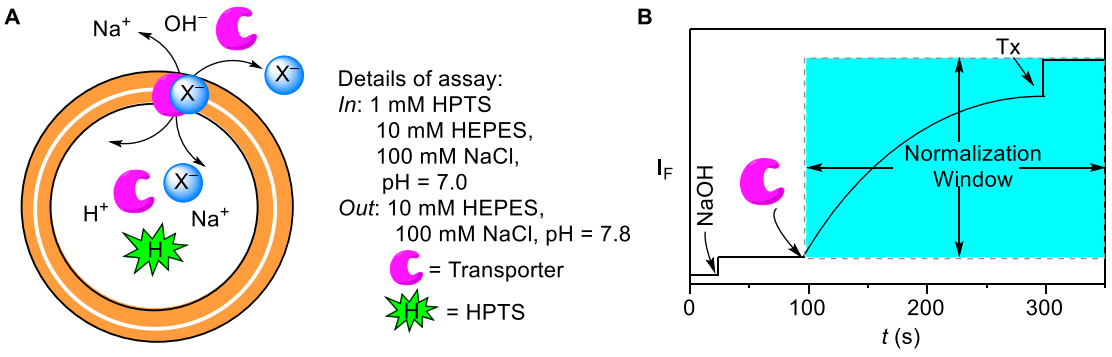

Fig. S9 Representation of fluorescence-based ion transport activity assay using EYPC-LUVs⊃HPTS (**A**), and illustration of ion transport kinetics showing normalization window (**B**).

Dose-response activity: The fluorescence kinetics of each carrier at different concentrations were studied over the course of time. The concentration profile data were evaluated at t = 290 s to get effective concentration, EC_{50} (i.e., the concentration of carrier needed to achieve 50% chloride efflux)[S4] using the Hill equation (Equation S3):

$$Y = Y_\infty + (Y_0 - Y_\infty) / [1 + (c/EC_{50})^n] \qquad \text{Equation S3}$$

where, Y_0 = fluorescence intensity just before the carrier addition (at t = 0 s), Y_∞ = fluorescence intensity with excess carrier concentration, c = concentration of carrier compound, and n = Hill coefficient (i.e., indicative for the number of monomers needed to form an active supramolecule).[S5]

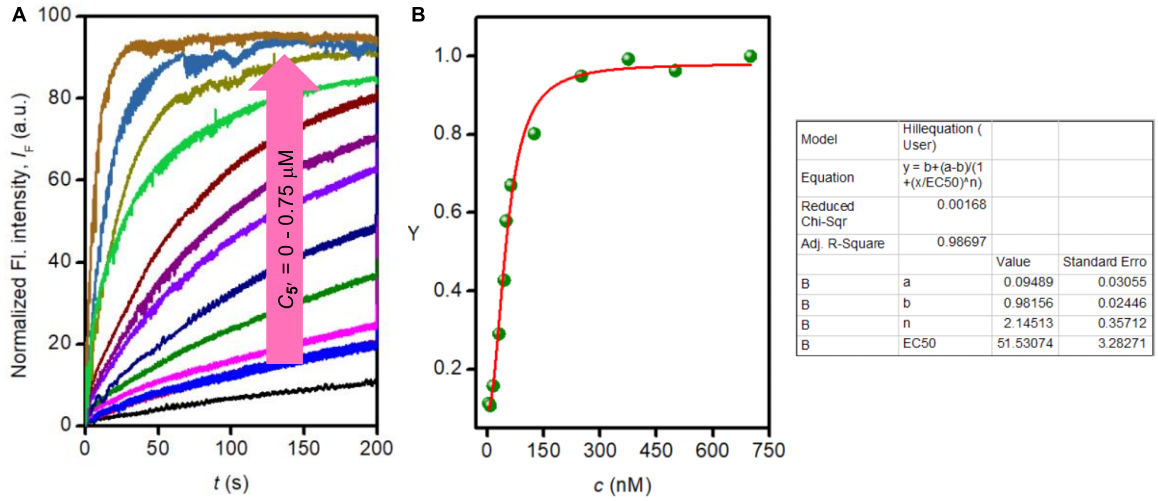

Model	Hillequation (User)		
Equation	y = b+(a-b)/(1 +(x/EC50)^n)		
Reduced Chi-Sqr	0.00168		
Adj. R-Square	0.98697		
		Value	Standard Erro
B	a	0.09489	0.03055
B	b	0.98156	0.02446
B	n	2.14513	0.35712
B	EC50	51.53074	3.28271

Fig. S10 Concentration-dependent activity of **5´** across EYPC-LUVs⊃HPTS (**A**). The dose-response plot of **5´** at 280 s after the addition of compound (**B**).

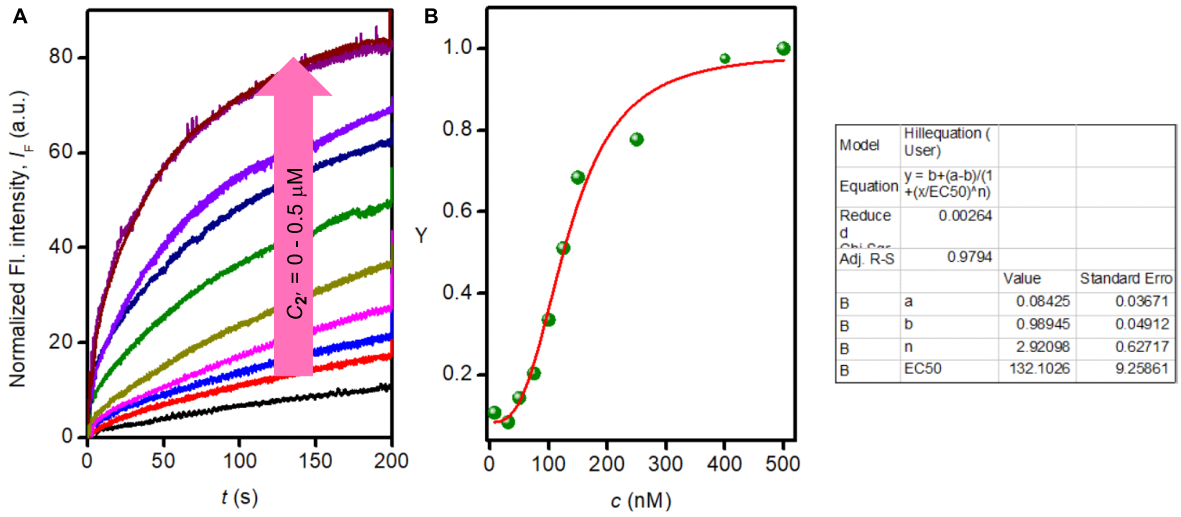

Model	Hillequation (User)		
Equation	y = b+(a-b)/(1 +(x/EC50)^n)		
Reduced	0.00264		
Adj. R-S	0.9794		
		Value	Standard Erro
B	a	0.08425	0.03671
B	b	0.98945	0.04912
B	n	2.92098	0.62717
B	EC50	132.1026	9.25861

Fig. S11 Concentration-dependent activity of **2´** across EYPC-LUVs⊃HPTS (**A**). The dose-response plot of **2´** at 280 s after the addition of compound (**B**).

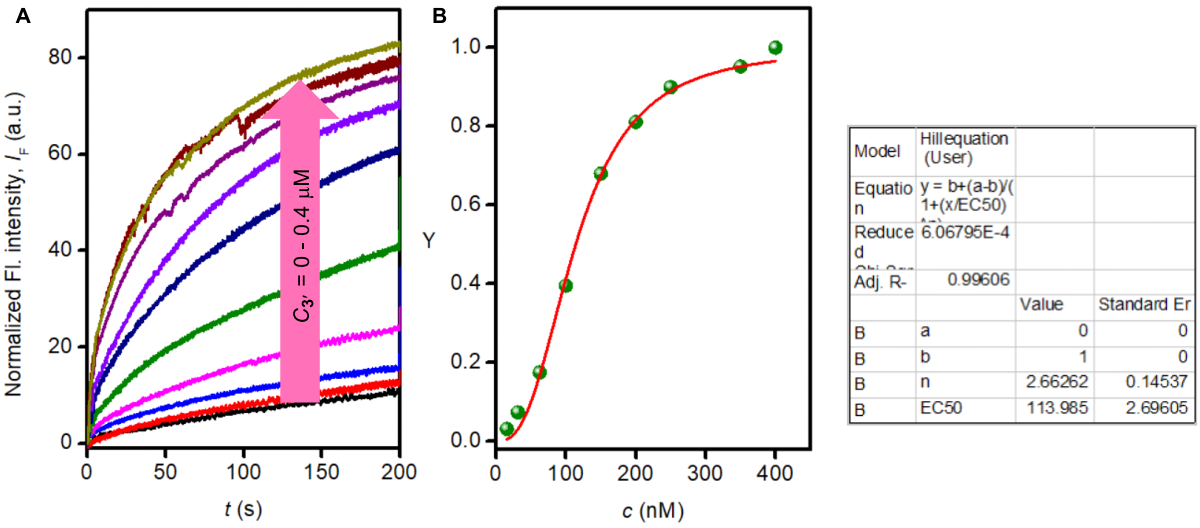

Model	Hillequation (User)		
Equation	y = b+(a-b)/(1+(x/EC50)		
Reduced	6.06795E-4		
Adj. R-	0.99606		
		Value	Standard Er
B	a	0	0
B	b	1	0
B	n	2.66262	0.14537
B	EC50	113.985	2.69605

Fig. S12 Concentration-dependent activity of **3´** across EYPC-LUVs⊃HPTS (**A**). The dose-response plot of **3´** at 280 s after the addition of compound (**B**).

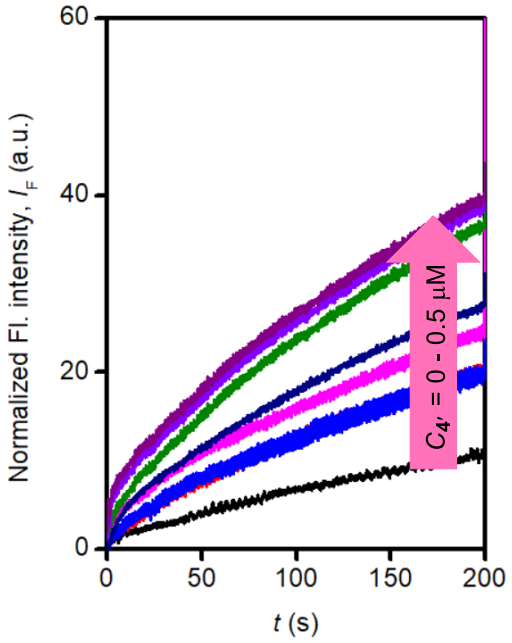

Fig. S13 Concentration-dependent activity of **4´** across EYPC-LUVs⊃HPTS (**A**). The dose-response plot of **4´** at 280 s after the addition of compound (**B**).

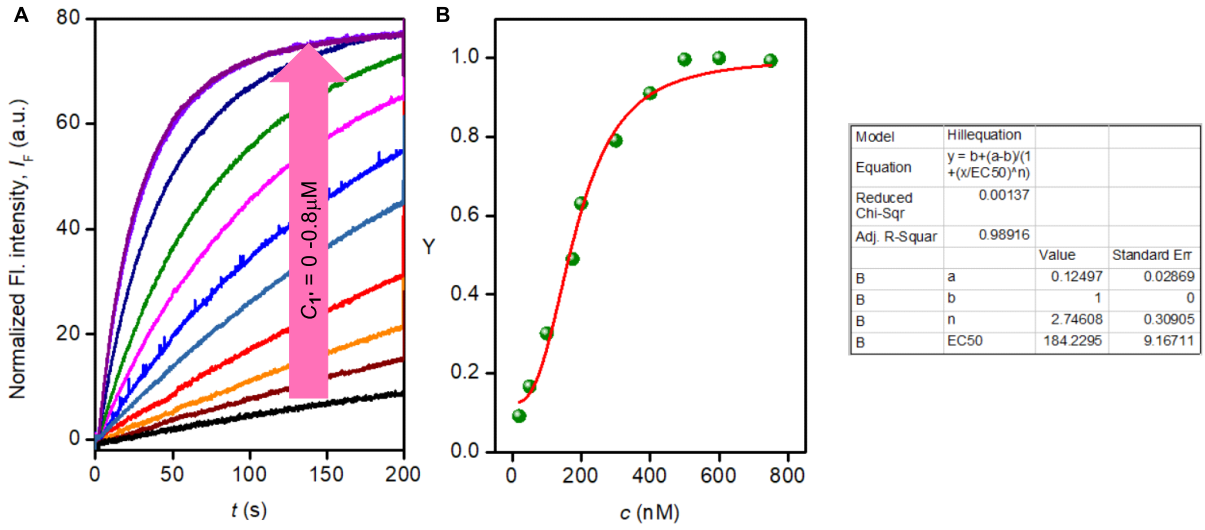

Model	Hillequation		
Equation	y = b+(a-b)/(1+(x/EC50)^n)		
Reduced Chi-Sqr	0.00137		
Adj. R-Squar	0.98916		
		Value	Standard Err
B	a	0.12497	0.02869
B	b	1	0
B	n	2.74608	0.30905
B	EC50	184.2295	9.16711

Fig. S14 Concentration-dependent activity of **1´** across EYPC-LUVs⊃HPTS (**A**). The dose-response plot of **1´** at 280 s after the addition of compound (**B**).

Anion selectivity studies:

Preparation of EYPC-LUVs⊃HPTS for anion selectivity: EYPC-LUVs⊃HPTS (~ 5.0 mM EYPC, inside: 1 mM HPTS, 10 mM HEPES, 100 mM NaCl, pH = 7.0 and outside: 10 mM HEPES, 100 mM NaX, pH = 7.0; where, (X^- = Cl^-, Br^-, SCN^-, NO_3^-, OAc^-, and I^-) were prepared following reported protocol.

Anion Selectivity Assay: In a clean fluorescence cuvette, 1975 µL of HEPES buffer (10 mM HEPES, 100 mM NaX, at pH = 7.0; where X^- = Cl^-, Br^-, SCN^-, NO_3^-, OAc^-, and I^-) was added followed by 25 µL of EYPC-LUVs⊃HPTS vesicle in slow stirring condition by a magnetic stirrer equipped within the fluorescence instrument (at t = 0 s). HPTS fluorescence emission intensity (F_t) was monitored with time at λ_{em} = 510 nm (λ_{ex} = 450 nm). 20 µL of 0.5 M NaOH was added to the cuvette at t = 20 s to make the pH gradient between the intra and extra vesicular system. The compound **5´** was added at t = 100 s, and at t = 300 s, 25 µL of 10% Triton X-100 was added to lyse all vesicles for the complete destruction of the pH gradient. For data analysis and comparison, time (X-axis) was normalized between the point of carrier addition (i.e., t = 100 s was normalized to t = 0 s) and the end point of the experiment (i.e., t = 300 s was normalized to t = 200 s) using Equation S1. Fluorescence intensities (F_t) were normalized to fractional emission intensity I_F using Equation S2.

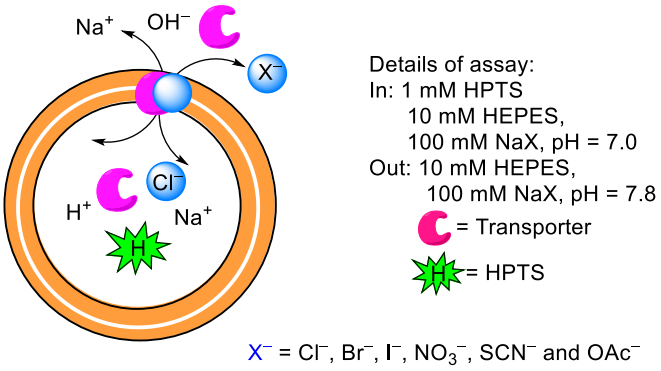

Fig. S15 Schematic representation of fluorescence-based anion assay by changing intravesicular as well as extravesicular anions.

Cation selectivity assay: Similarly, the cation selectivity of carrier **5´** (as a DMSO solution) was explored by changing extravesicular HEPES buffer solution (10 mM HEPES, 100 mM MCl, where M = Li^+, Na^+, K^+, Rb^+, and Cs^+). The time axis was normalized according to Equation S1. The fluorescence data were normalized to percent change in intensity as a function of time using Equation S2.

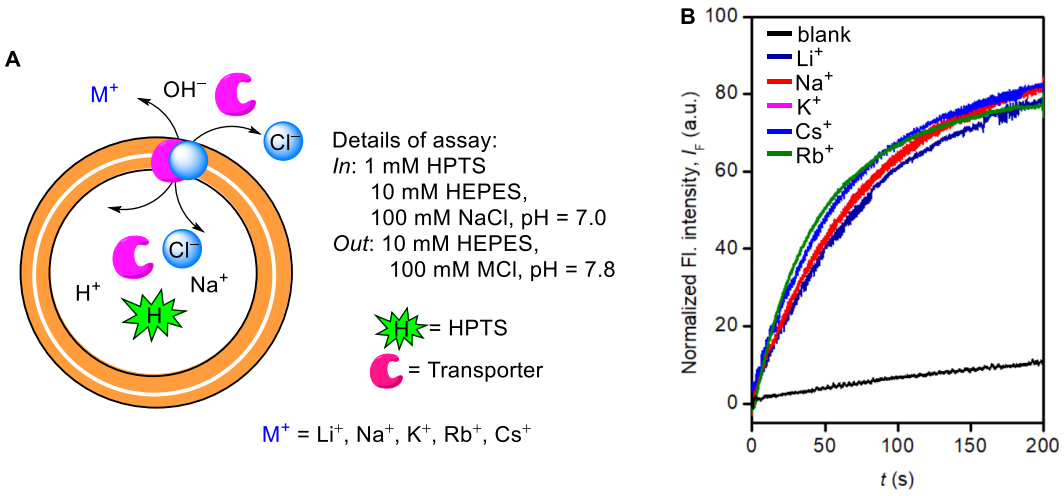

Fig. S16 Schematic representation of fluorescence-based cation selectivity assay (**A**). Cation selectivity of **5´** (340 nM) measured by varying external cations (M^+ = Li^+, Na^+, K^+, Rb^+, Cs^+) (**B**) across EYPC-LUVs⊃HPTS.

Chloride transport activity across EYPC-LUVs⊃lucigenin vesicles:

Preparation of EYPC-LUVs⊃lucigenin vesicles: In a 10 mL clean and dry round bottom flask, the thin transparent film of egg yolk phosphatidylcholine (EYPC) was formed by drying 1.0 mL egg yolk phosphatidylcholine (EYPC, 25 mg/mL in $CHCl_3$) with providing continuous

rotation and purging nitrogen. The transparent thin film was kept on a high vacuum for 4 hours to remove all traces of $CHCl_3$. Then, the transparent thin film was hydrated with 1 mL aqueous $NaNO_3$ (200 mM, 1 mM Lucigenin) with occasional vortexing at 10 min intervals for 1 h. The resulting suspension was subjected to freeze and thaw cycles (≥ 15, liquid nitrogen, 55 °C water bath) and 21 times extrusion through a 200 nm pore size polycarbonate membrane. Then, size exclusion chromatography (using Sephadex G-50) was performed to remove extravesicular dye using 200 mM $NaNO_3$ solution as an eluent. The collected vesicle suspension was diluted to 4 mL. Final conditions: ~ 5 mM EYPC; inside: 200 mM $NaNO_3$, 1 mM lucigenin, pH 7.0; outside: 200 mM $NaNO_3$.

Ion transport activity by Lucigenin assay:

In a clean and dry fluorescence cuvette, 200 mM $NaNO_3$ (1975 µL) and EYPC-LUVs⊃lucigenin (25 µL) were taken. This suspension was placed in a slow stirring condition in a fluorescence instrument equipped with a magnetic stirrer (at t = 0 s). The fluorescence intensity of lucigenin was monitored at λ_{em} = 535 nm (λ_{ex} = 455 nm) over time. A chloride gradient was created by the addition of 2.0 M NaCl (33.3 µL) at t = 20 s between intra- and extravesicular system, followed by the addition of carrier at t = 100 s. Finally, vesicles were lysed by the addition of 10% Triton X-100 (25 µL) at t = 300 s for the complete destruction of the chloride gradient.

The time-dependent data were normalized to percent change in fluorescence intensity using Equation S4:

$$I_F = [(I_t - I_0) / (I_\infty - I_0)] \times (-100) \qquad \text{Equation S4}$$

where, I_0 is the initial intensity, I_t is the intensity at time t, and I_∞ is the final intensity after the addition of Triton X-100.

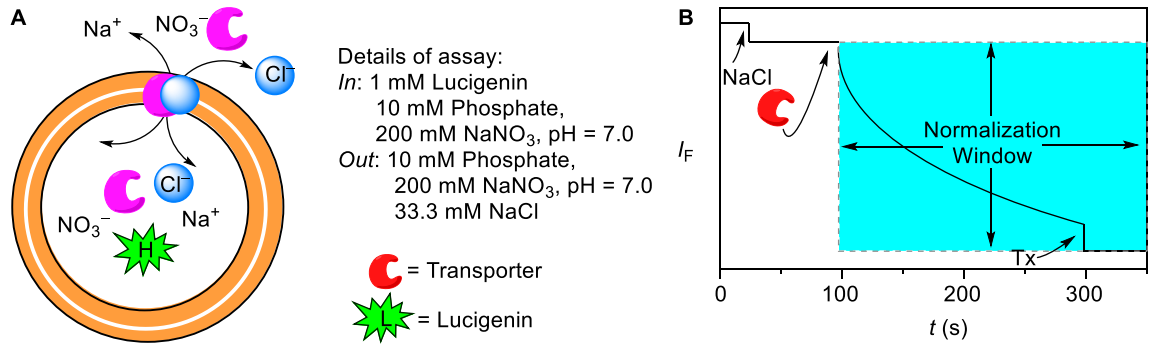

Fig. S17 Representations of fluorescence-based ion transport activity assay using EYPC-LUVs⊃Lucigenin (**A**), and illustration of ion transport kinetics showing normalization window (**B**).

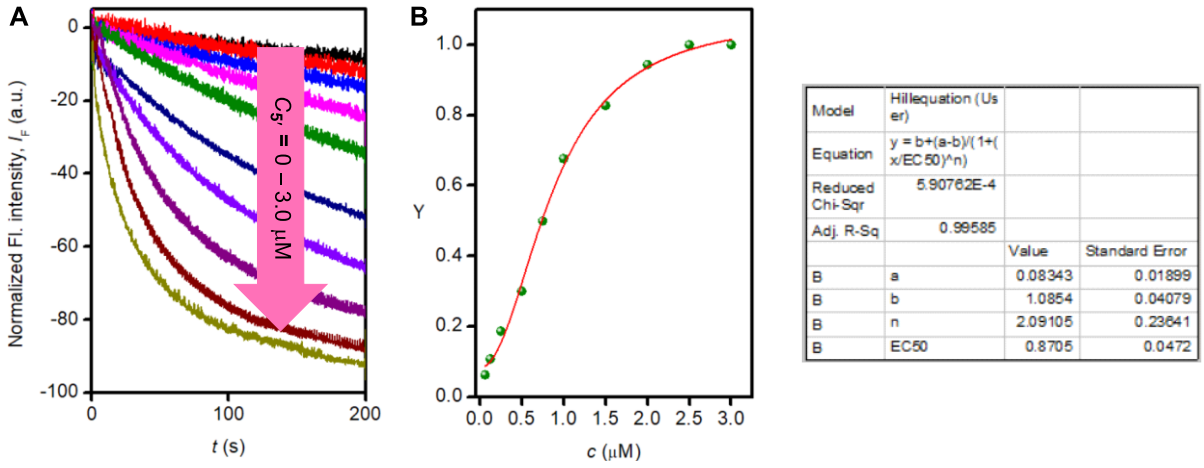

Model	Hillequation (User)		
Equation	y = b+(a-b)/(1+(x/EC50)^n)		
Reduced Chi-Sqr	5.90762E-4		
Adj. R-Sq	0.99585		
		Value	Standard Error
B	a	0.08343	0.01899
B	b	1.0854	0.04079
B	n	2.09105	0.23641
B	EC50	0.8705	0.0472

Fig. S18 Concentration-dependent activity of **5′** across EYPC-LUVs⊃Lucigenin (**A**). The dose-response plot of **5′** at 280 s after the addition of compound (**B**).

Cation selectivity assay across EYPC-LUVs⊃lucigenin vesicles:

The vesicles were prepared by following the same protocol as stated above. In a clean and dry fluorescence cuvette, 200 mM $NaNO_3$ (1975 μL) and EYPC-LUVs⊃lucigenin (25 μL) were taken. The suspension was kept under slow stirring conditions in a fluorescence instrument equipped with a magnetic stirrer at t = 0 s. The quenching of fluorescence intensity of lucigenin was monitored as a course of time at λ_{em} = 535 nm (λ_{ex} = 455 nm). At t = 20 s, the chloride gradient was created by the addition of 2 M chloride salts (33.3 μL) of different cations MCl (M = Li^+, Na^+, K^+, Rb^+, and Cs^+), followed by the addition of carrier **5′** at t = 100 s. Finally, vesicles were lysed by the addition of 10% Triton X-100 (25 μL) at t = 300 s to disrupt the

applied chloride gradient completely. The time-dependent data were normalized to percent change in fluorescence intensity using Equation S4.

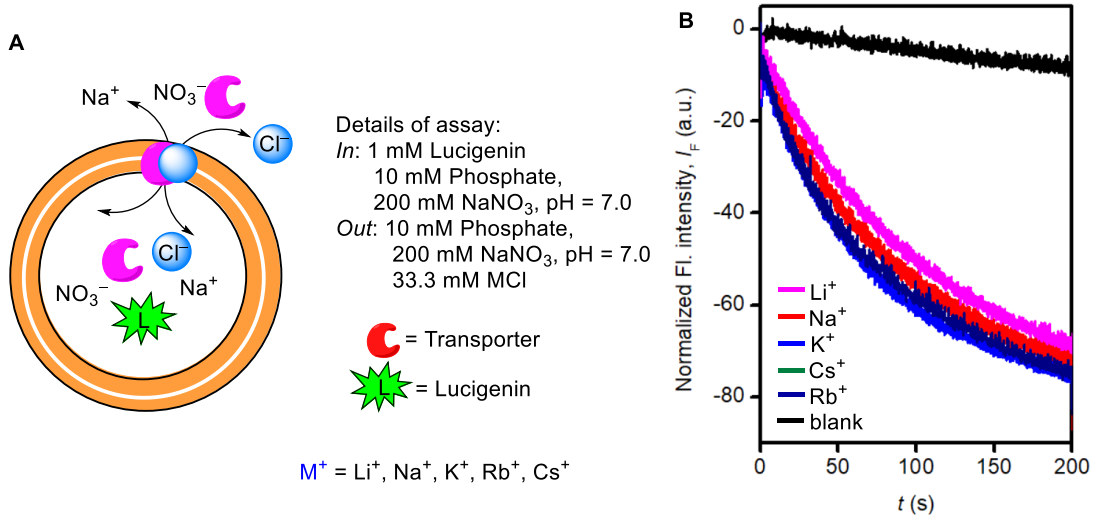

Fig. S19 Schematic representations of fluorescence-based cation selectivity assay (**A**) Cation selectivity of **5´** (1.25 μM) measured by varying external cations (M^+ = Li^+, Na^+, K^+, Rb^+, and Cs^+) across EYPC-LUVs⊃Lucigenin (**B**).

Ion transport activity across EYPC-LUVs⊃lucigenin in the presence of valinomycin

The antiport mechanism (i.e., simultaneous transport of two different ions, in opposite directions, across the membrane)[S6] of **5´** was experimentally confirmed by lucigenin assay in the presence of valinomycin. The ion transport activity of **5´** was monitored across vesicles entrapped with lucigenin (1 mM) and $NaNO_3$ (200 nM) suspended in KCl (2 M) solution with and without valinomycin. The remarkable enhancement in ion transport activity of **5´** in the presence of valinomycin gave a direct experimental insight into the antiport mechanism of ion transport.

Preparation of EYPC-LUVs⊃lucigenin: The vesicles were prepared by the following protocol as stated above.

Antiport mechanism: In clean and dry fluorescence cuvette, 1975 μL 200 mM $NaNO_3$ solution and 25 μL EYPC-LUVs⊃lucigenin vesicles were taken and slowly stirred in a fluorescence instrument equipped with a magnetic stirrer (at t = 0 s). The time-dependent fluorescence intensity of lucigenin was monitored at λ_{em} = 535 nm (λ_{ex} = 455 nm). A solution of 2 M KCl (33.3 μL) was added at t = 20 s to create a chloride gradient between intra- and

extra-vesicular system, followed by the addition of valinomycin (1.25 μM) at t = 50 s and carrier **5´** (3.0 μM) at t = 100 s. Finally, the destruction of the chloride gradient was done by the addition of 10 % Triton X-100 (25 μL) at t = 300 s. The time axis was normalized according to Equation S1, and the time-dependent data were normalized to percent change in fluorescence intensity using Equation S4.

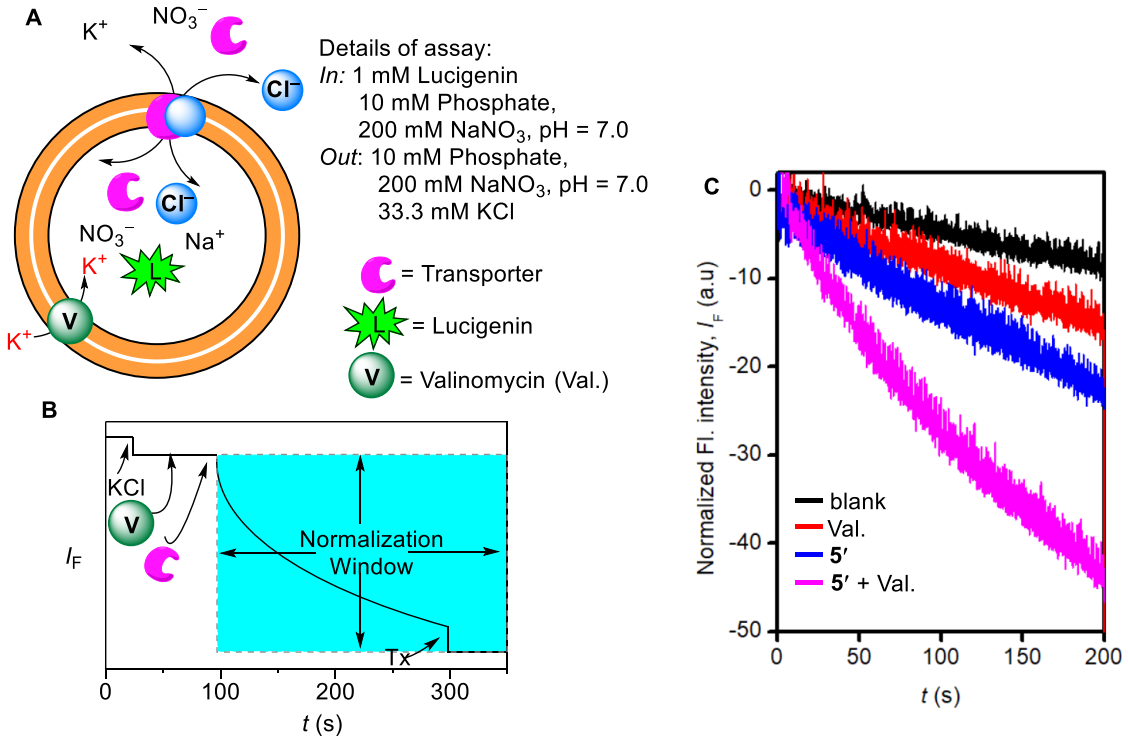

Fig. S20 Schematic representations of fluorescence-based cation selectivity assay (**A**), and illustration of ion transport kinetics showing normalization window (**B**). Comparison of Cl^- influx activity of **5´** (3 μM) in the absence and in the presence of valinomycin (1.25 μM) (**C**).

Proof of Antiport mechanism by lucigenin assay in the presence of external SO_4^{2-} and NO_3^- anions:

Preparation of EYPC-LUVs⊃lucigenin vesicles: In a 10 mL clean and dry round bottom flask, the thin transparent film of egg yolk phosphatidylcholine (EYPC) was formed by drying 1 mL egg yolk phosphatidylcholine (EYPC, 25 mg/mL in $CHCl_3$) with providing continuous rotation and purging nitrogen. The transparent thin film was kept on a high vacuum for 4 hours to remove all traces of $CHCl_3$. Then, the transparent thin film was hydrated with 1 mL aqueous NaCl (200 mM, 1.0 mM Lucigenin) with occasional vortexing at 10 min intervals for 1 h. The resulting suspension was subjected to freeze and thaw cycles (≥ 15, liquid nitrogen, 55 °C water

bath) and 21 times extrusion through a 200 nm pore size polycarbonate membrane. The size exclusion chromatography (using Sephadex G-50) was performed to remove extravesicular dye using 200 mM NaCl solution as eluent. The collected vesicle suspension was diluted to 4 mL. Final conditions: ~ 5 mM EYPC; inside: 200 mM NaCl, 1 mM lucigenin, pH 7.0; outside: either 200 mM $NaNO_3$ or 200 mM Na_2SO_4.

Ion transport assay:

In a clean and dry fluorescence cuvette, either 200 mM or 200 mM Na_2SO_4 (1975 µL) and EYPC-LUVs⊃lucigenin (25 µL) were taken. This suspension was placed in a slow stirring condition in a fluorescence instrument equipped with a magnetic stirrer (at t = 0 s). The fluorescence intensity of lucigenin was monitored at λ_{em} = 535 nm (λ_{ex} = 455 nm) over the course of time. The carrier molecule **5´** was added at t = 100 s. Finally, vesicles were lysed by the addition of 10% Triton X-100 (25 µL) at t = 300 s for the complete destruction of the chloride gradient.

The time axis was normalized according to Equation S1:

$$t = t - 100 \quad \text{`} \qquad \text{Equation S1}$$

The time-dependent data were normalized to percent change in fluorescence intensity using Equation S2:

$$I_F = [(I_t - I_0) / (I_\infty - I_0)] \times 100 \qquad \text{Equation S2}$$

where, I_0 is the initial intensity, I_t is the intensity at time t, and I_∞ is the final intensity after the addition of Triton X-100.

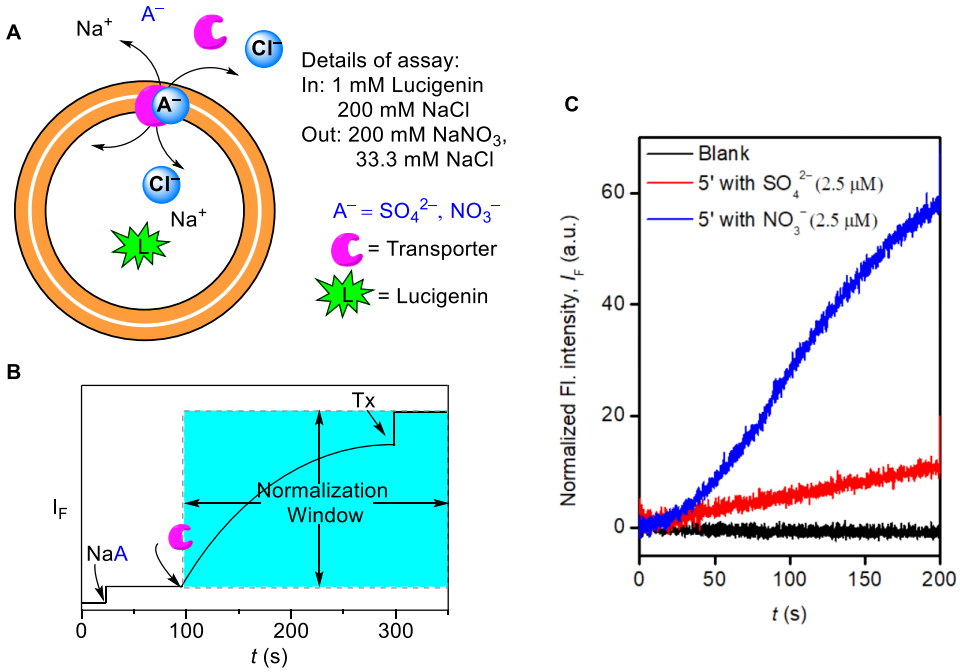

Fig. S21 Representation of fluorescence-based antiport assay using EYPC-LUVs⊃lucigenin (**A**) Representation of ion transport kinetics showing normalization window (**B**) Efflux of Cl^- ion by **5´** (5.0 μM) in the presence of either extravesicular SO_4^{2-} or extravesicular NO_3^- ion with iso-osmolar intravesicular Cl^- (**C**).

Ion transport mechanism by ISE studies:

Preparation of ISE vesicles: A chloroform solution (1 mL) of 1-palmitoyl-2-oleoylphosphatidylcholine (EYPC) (25 mg) was evaporated under reduced pressure to give a thin film. The lipid film was dried under a high vacuum for 4 hours. The thin film was rehydrated by vortexing with a sodium chloride solution (300 mM KCl, 5 mM phosphate buffer at pH = 7.2). The lipid suspension was then subjected to fifteen freeze-thaw cycles and was allowed to age for 1 h at room temperature. The suspension was extruded twenty-three times through a 200 nm polycarbonate membrane using an extruder (Avanti, The Mini-Extruder set) to obtain unilamellar vesicles containing KCl (300 mM in 5 mM phosphate buffer at pH = 7.2). Non-encapsulated KCl salts were removed by dialyzing the vesicles three times in a potassium gluconate solution (300 mM, 5 mM phosphate buffer at pH = 7.2).

Ion transport activity in the presence of Valinomycin and Monensin:

In a clean and dry glass vial, 50 μL of the above lipid solution and 1950 μL of 300 mM potassium gluconate of respective pH buffer solutions were taken and kept in slowly stirring condition by a magnetic stirrer (at t = 0 s), and chloride efflux was monitored with time. Carrier

molecule **5´** as DMSO solution was added at *t* = 50 s, Monensin and Valinomycin as DMSO solutions were added at *t* = 10 s, and finally, at *t* = 300 s, 25 µL of 10% Triton X-100 was added to lyse those vesicles for 100% chloride influx. The chloride efflux for **5´** was monitored in the presence and absence of Monensin and Valinomycin following the above sequence of addition of components. The reading at 50 seconds was set at 0% chloride efflux, and the final chloride reading at 300 s was set as 100% chloride efflux.

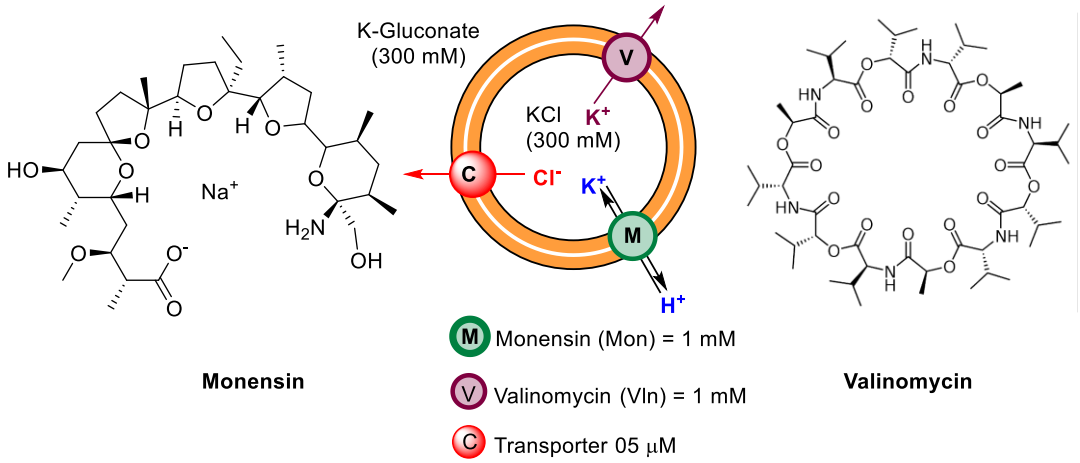

Fig. S22 Schematic representation of ISE-based Valinomycin and Monensin assay.

U-tube experiments for checking Cl^- transport:

In this experiment, we checked whether the chloride ion was transported via a mobile carrier mechanism or through ion channel formation by a carrier molecule. For that, we have set up an experiment using a U-tube where the left arm (Source arm) of the tube was filled with 7.5 mL of 500 mM NaCl solution buffered to pH 7.0 using 5mM phosphate buffer and the right arm (receiver arm) of the tube was filled with 7.5 mL of 500 mM $NaNO_3$ solution buffered to pH 7.0 using 5mM phosphate buffer. Two different salt solutions in the two arms were separated by a 15 mL solution of compound **5´** in $CHCl_3$ (1 mM compound **1f**, 1 mM tetrabutylammonium hexafluorophosphate) in such a way that the two salt solutions never come into contact with each other. Here, the transport of chloride ions is only possible via the mobile carrier mechanism due to the great length of the $CHCl_3$ layer, which does not allow the formation of an ion channel. Chloride ion concentration in the receiver arm was measured by chloride ISE to check transport activity via the carrier mechanism. The gradual increase of chloride ion concentration (Fig. S23) was measured in a fixed time interval for the time period of 7 days, evidence in support of the mobile carrier mechanism. In a control experiment, no increase in chloride ion concentration was observed when we omitted carrier molecule 5´, keeping other conditions the same.

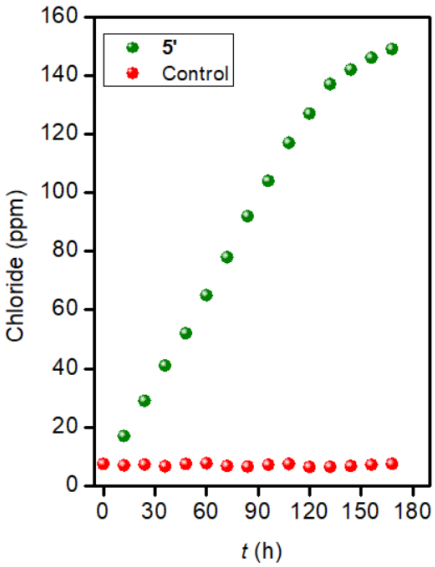

Fig. S23 The chloride transport in the U-tube experiment in the presence and absence of carrier molecule **5´**.

VI. Photoresponse studies

UV-Vis absorbance studies:

Photoisomerization studies of compounds **5a-5e**, were carried out in CH_3CN. Initially, stock solutions of these compounds (2 mM in CH_3CN) were prepared in different vials and covered with aluminium foil.

In a 2 mL UV cuvette, was placed 1900 µL of CH_3CN, and 100 µL of procarrier (**5a**, **5b**, **5c**, **5d** or **5e**) solution was added to get a final concentration of 100 µM. The cuvette was placed in a UV-Vis spectrophotometer, and the UV-Vis spectrum was recorded.

We also recorded pH-dependent UV-Visible absorption spectra of compound **5c**. Phosphate buffer (10 mM) was used to make solutions of different pH. Absorption was found to be constant at pH values of 7 and 8.

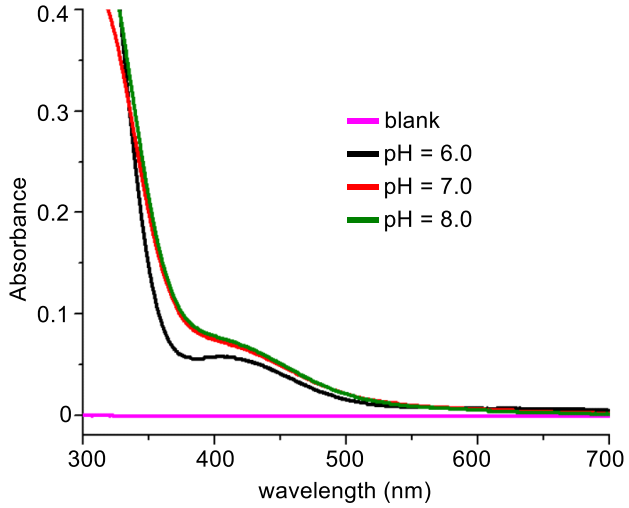

Fig. S24 UV-vis absorption spectra of **5c** at different pH values.

Photolytic Studies.

Assessment of photolysis of procarriers 5a-5e using ^{1}H NMR spectroscopy by irradiation at 400 nm: In a clean and dry NMR tube, a solution of procarrier **5a-5e** was taken in DMSO-d_6 (2 mM in 0.5 mL). The ^{1}H NMR spectrum of each sample was recorded first (t = 0 min). Then, the NMR tubes were kept in the photoreactor and irradiated with 400 nm visible light (1 × 12 Watt LED) for different time intervals, and ^{1}H NMR spectrum of the irradiated samples was recorded at the end of each irradiation. All ^{1}H NMR spectra were processed using MestReNova 6.0 by considering the residual solvent peak as an internal reference. Upon photoirradiation, the appearance and disappearance of the different proton peak signals were monitored by stacking all calibrated spectra. The photolytic conversion of procarriers **5a-5e** to carrier **5´** was confirmed by comparing the ^{1}H NMR spectra with that of the synthesized **5´**.

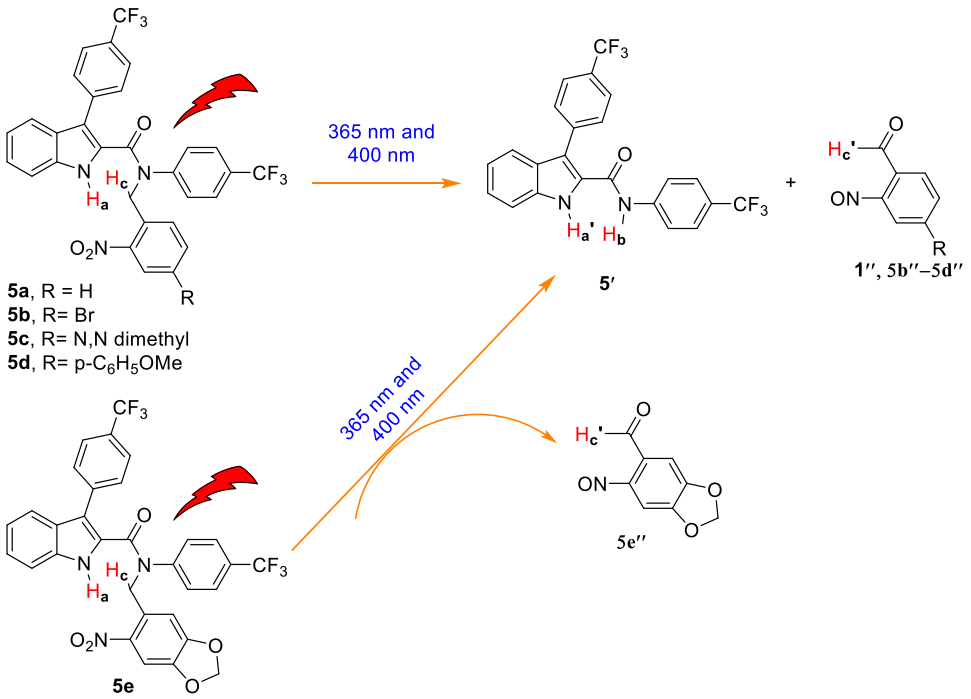

Scheme S5. Schematic representation of the photocleavage of procarriers **5a–5e**.

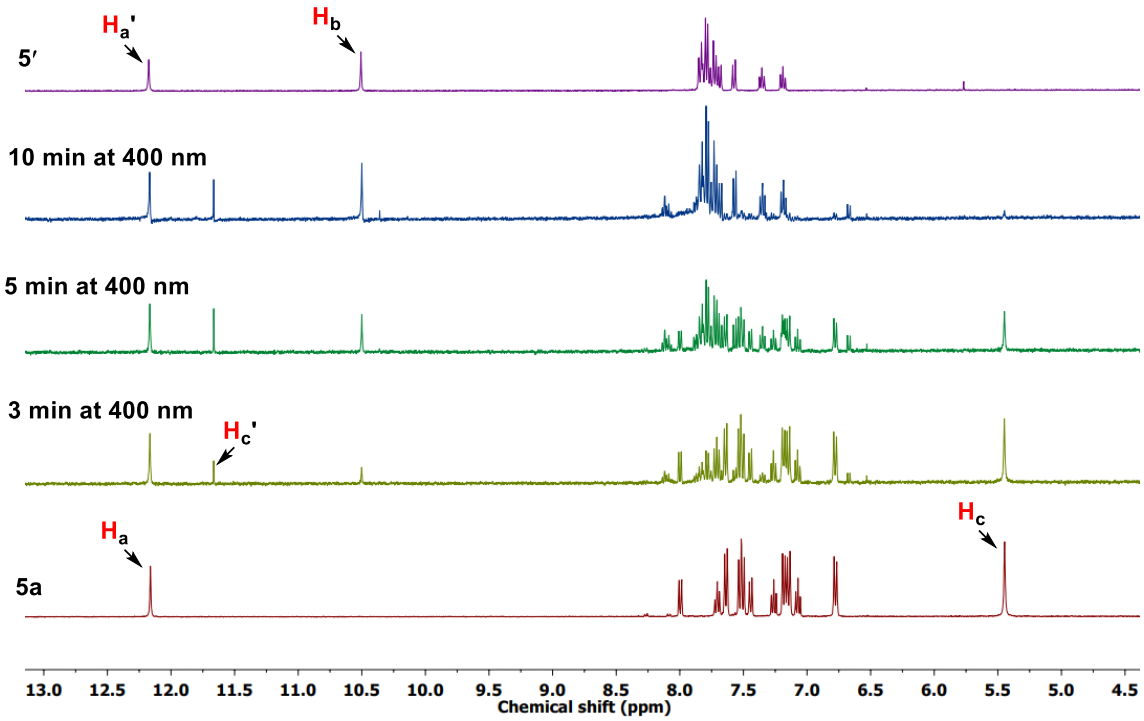

Fig. S25 Phototriggered release of indole carboxamide **5'** from procarrier **5a** monitored by ^{1}H NMR in DMSO-d_6 recorded at different time intervals upon irradiation at 400 nm of electromagnetic radiations.

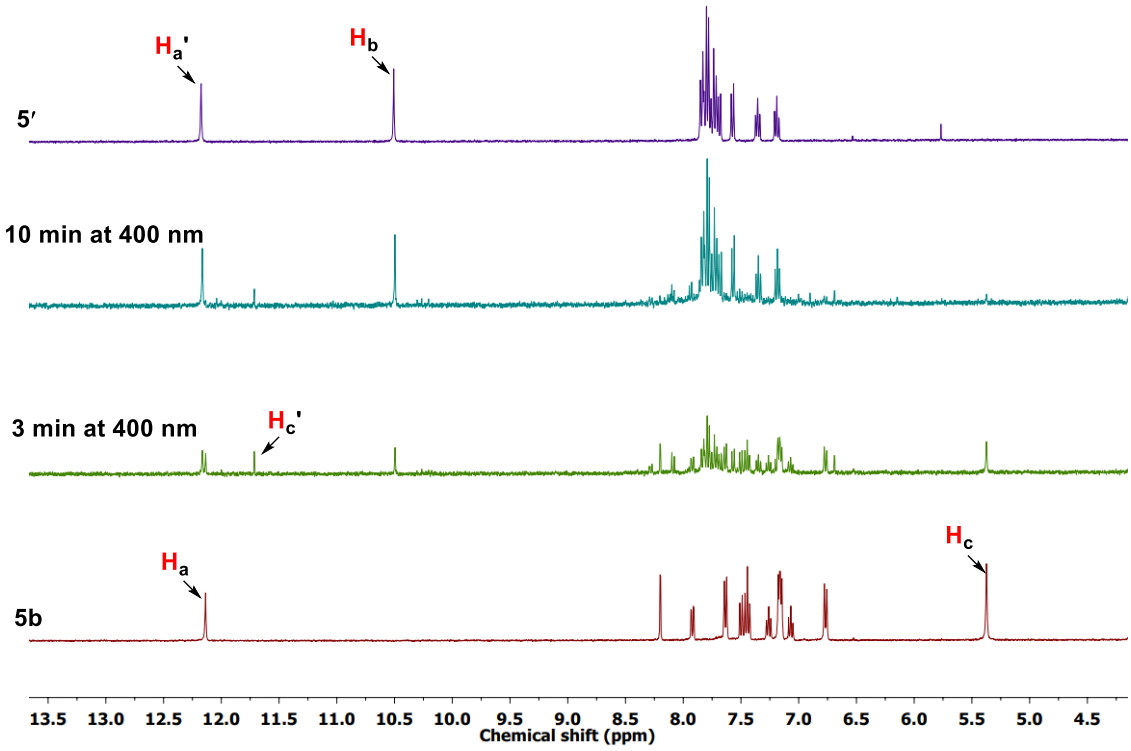

Fig. S26 Phototriggered release of indole carboxamide **5'** from procarrier **5b** monitored by ^{1}H NMR in DMSO-d_6 recorded at different time intervals upon irradiation at 400 nm of electromagnetic radiations.

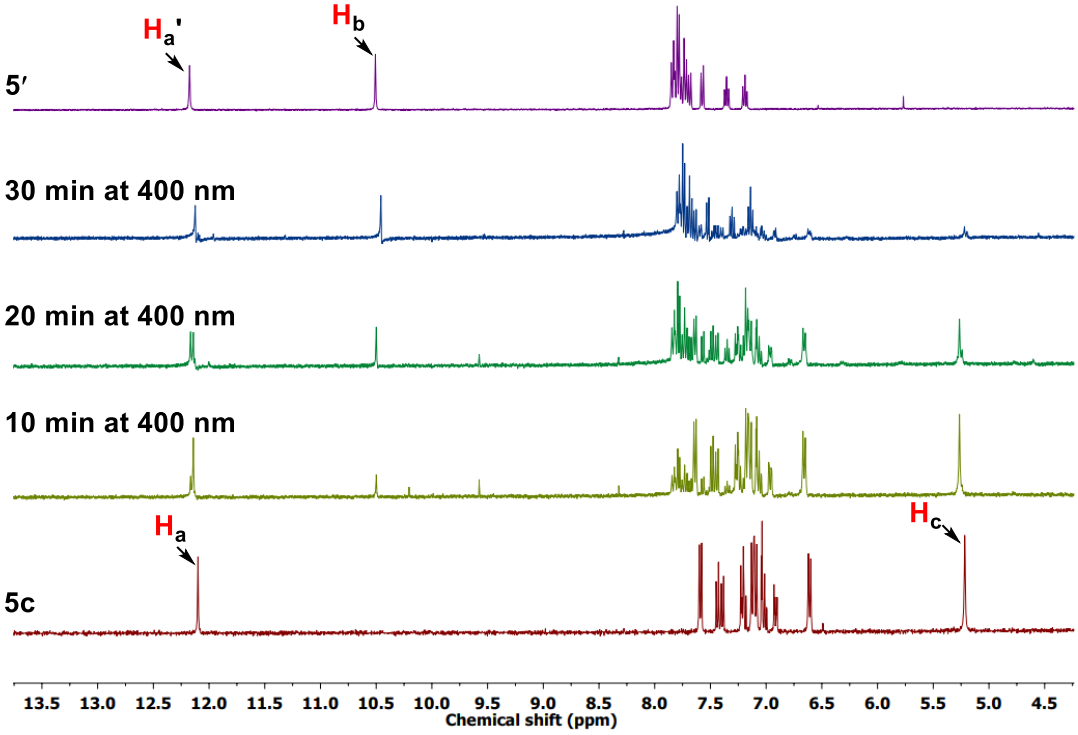

Fig. S27 Phototriggered release of indole carboxamide **5'** from procarrier **5c** monitored by ^{1}H NMR in DMSO-d_6 recorded at different time intervals upon irradiation at 400 nm of electromagnetic radiations.

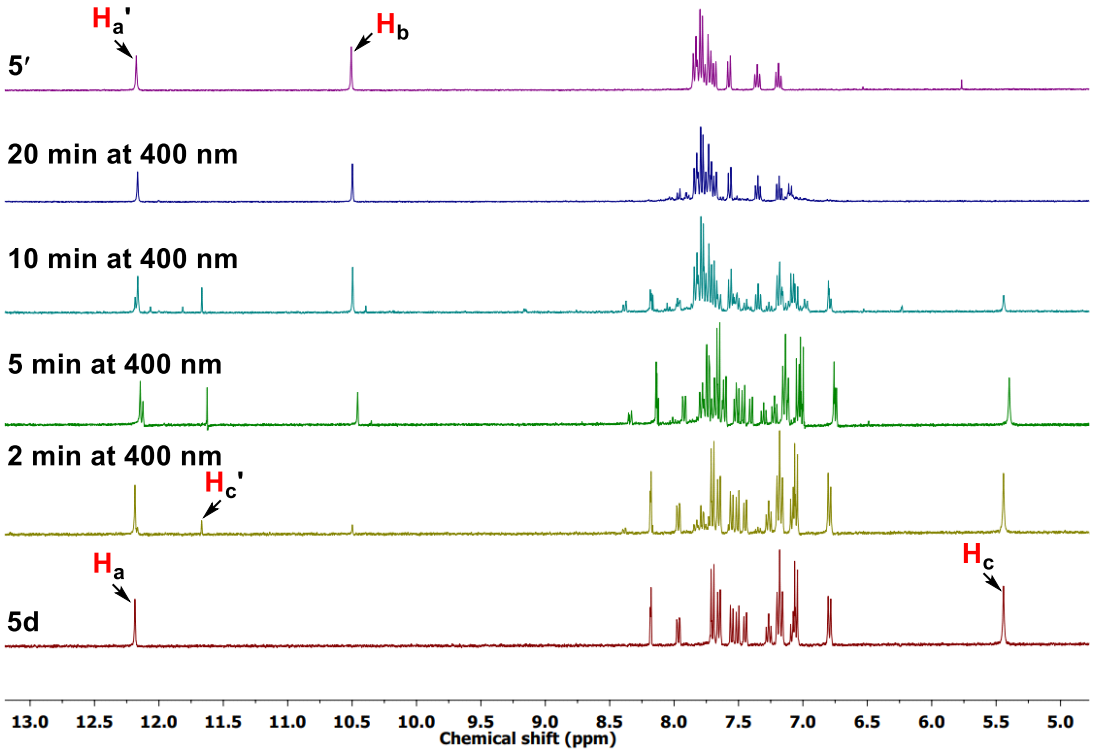

Fig. S28 Phototriggered release of indole carboxamide **5'** from procarrier **5d** monitored by ^{1}H NMR in DMSO-d_6 recorded at different time intervals upon irradiation at 400 nm of electromagnetic radiations.

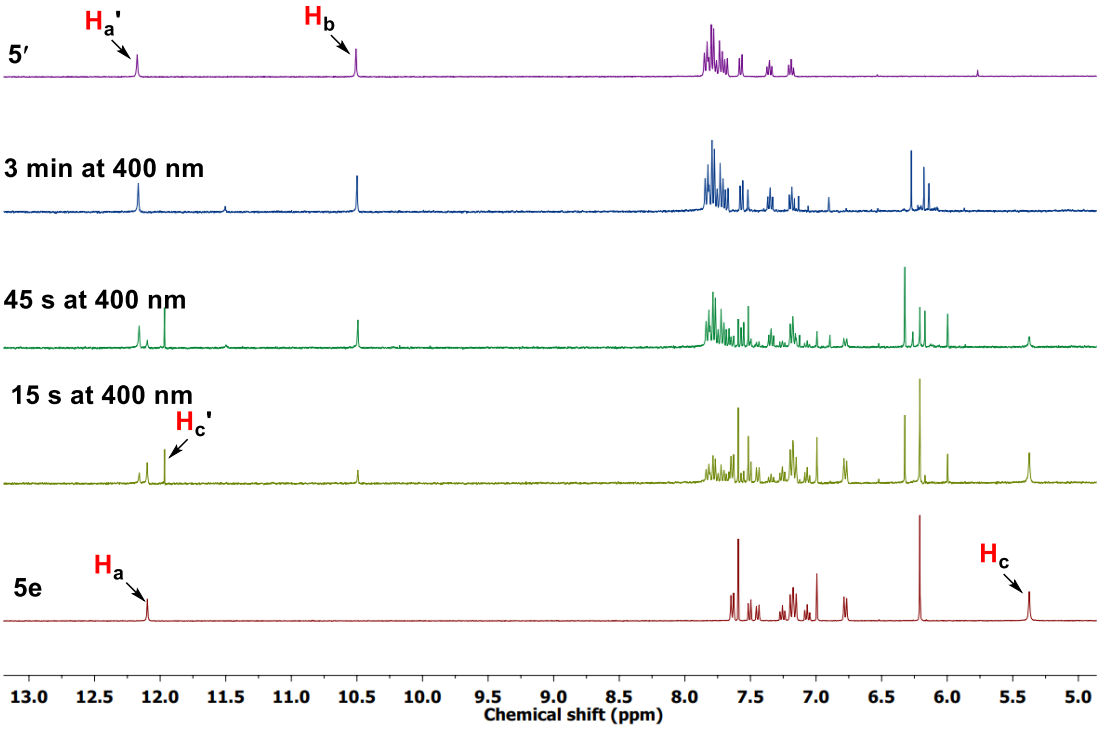

Fig. S29 Phototriggered release of indole carboxamide **5'** from procarrier **5e** monitored by ^{1}H NMR in DMSO-d_6 recorded at different time intervals upon irradiation at 400 nm of electromagnetic radiations.

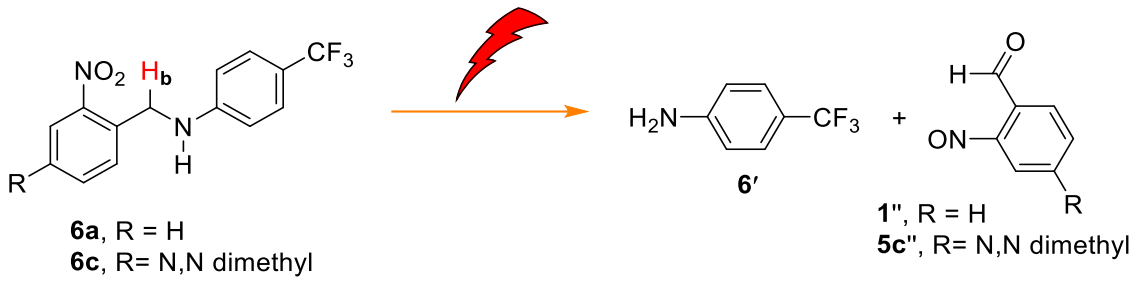

Scheme S6. Schematic representation of the photocleavage of intermediates **6a** and **6c**.

The photocleavable studies of intermediates **6a** and **6c** were carried out by ^{1}H NMR studies. In a clean and dry NMR tube, the solution of compounds **6a** or **6c** was taken in DMSO-d_6 (2 mM in 0.5 mL). The ^{1}H NMR spectrum was recorded first (at t = 0 min). Then, the sample **6a** was photoirradiated with 400 nm light (1 × 12 Watt LED) and **6c** with 450 nm light (3 × 1 Watt LEDs) for different time intervals, and ^{1}H NMR spectrum of the irradiated samples were recorded at the end of each irradiation. All ^{1}H NMR spectra were processed using MestReNova 6.0 by considering the residual solvent peak as an internal reference. Upon photoirradiation, the appearance and disappearance of the different proton peak signals were monitored by stacking all calibrated spectra. The photolytic conversion of compounds **6a** and **6c** to the corresponding 4-trifluoromethylaniline was confirmed by comparing the ^{1}H NMR spectra with the standard pure 4-trifluoromethylaniline (**6'**).

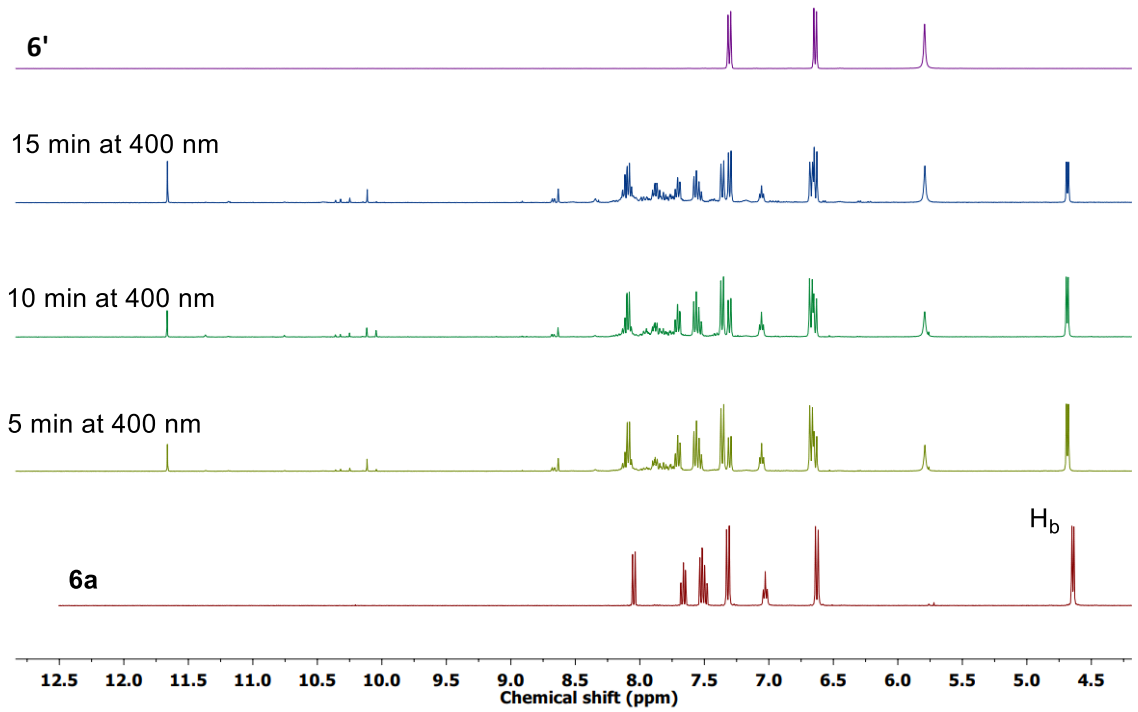

Fig. S30 Photocleavage of compound **6a** by 400 nm UV light.

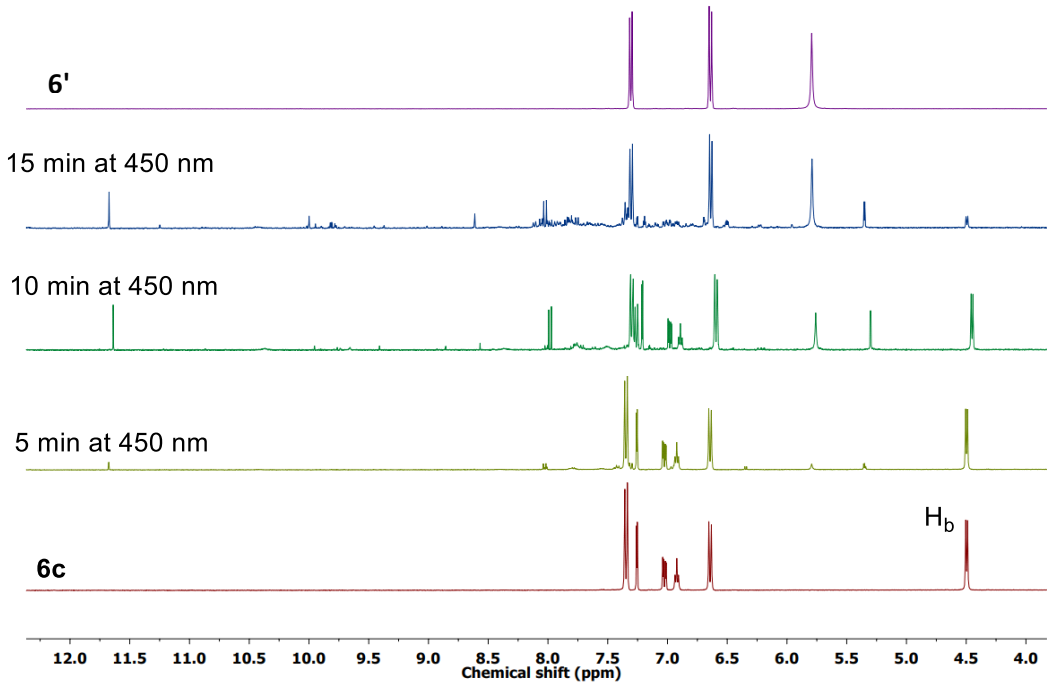

Fig. S31 Photocleavage of compound **6c** by 450 nm UV light.

Assessment of photolysis of procarrier 5c using mass spectrometric studies by irradiation at 450 nm: The solution of **5c** (10 μM, 2 mL in MeOH:CH_3CN:H_2O (2:2:1)) was photoirradiated at 450 nm using (3 × 1 Watt LEDs) for 2 h in a 4 mL cuvette. After photoirradiation, the sample was subjected to ESI-MS studies. The ESI-MS data confirms the photocleavage of protected compound **5c** into the active carrier **5'** and corresponding *N*,*N* dimethyl nitrosobenzaldehye byproduct.

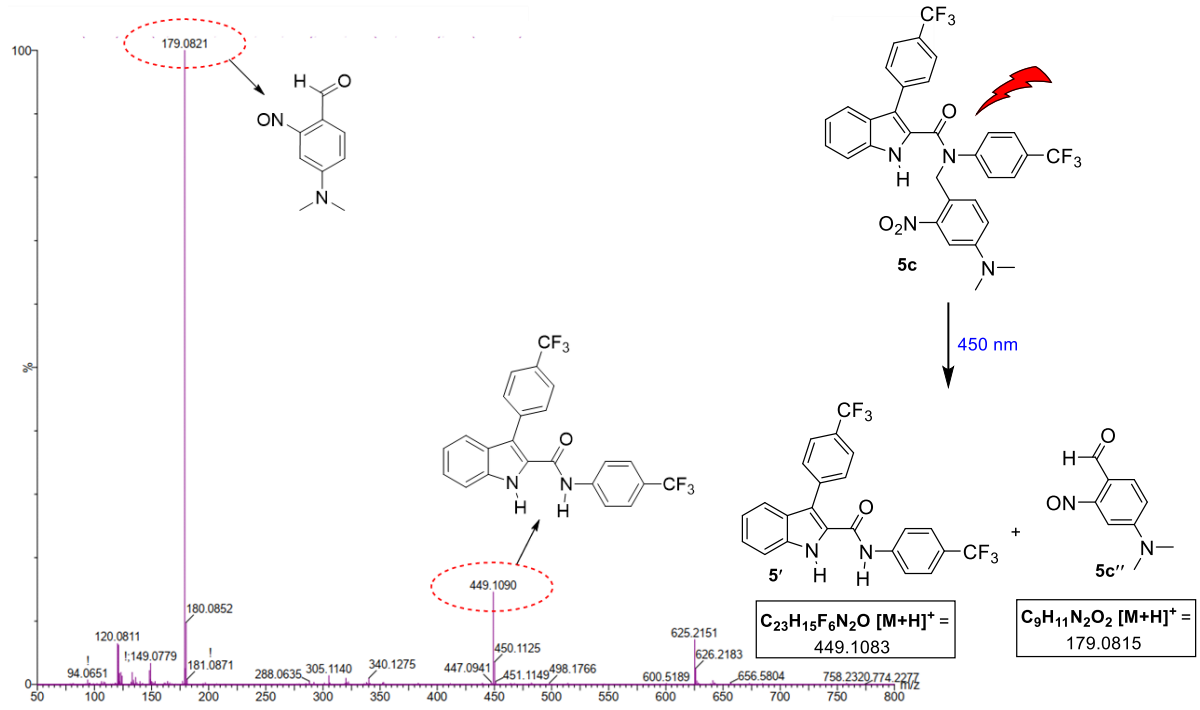

Fig. S32 ESI-MS spectrum of **5c** recorded after irradiation at 450 nm using (3 × 1 Watt LEDs) for 2 h in a mixture of MeOH:CH_3CN:H_2O (2:2:1).

VII. Phototriggered ion transport across EYPC-LUVs⊃HPTS

Preparation of HEPES buffer and stock solutions: The HEPES buffer of pH = 7.0 was prepared by dissolving an appropriate amount of solid HEPES (10 mM) and NaCl (100 mM) in autoclaved water. The pH was adjusted to 7.0 by the addition of aliquots from 0.5 M NaOH solution using pH meter. The stock solutions of carrier **5′** and procarriers **5a–5e** were prepared using HPLC grade DMSO.

Preparation of EYPC-LUVs⊃HPTS: The vesicles were prepared by the following protocol as stated above.

Phototriggered activation and ion transport assay in LUVs: In clean and dry fluorescence cuvette, 1975 μL HEPES buffer (10 mM HEPES, 100 mM NaCl, pH = 7.0) and 25 μL EYPC-LUVs⊃HPTS vesicles were placed. To this suspension, procarriers **5a–5e** (20 μL as DMSO solution) were added to get the final concentration of 300 nM. The suspension with either of the procarriers **5a–5e** was then photoirradiated with either 400 nm (using one 12 W LED) or 450 nm (using three 1 W LEDs) light for different time intervals. Each irradiated sample was then placed in the fluorescence instrument equipped with a magnetic stirrer. The fluorescence intensity of HPTS at λ_{em} = 510 nm (λ_{ex} = 450 nm) of each sample was monitored as a course

of time *t*. At *t* = 100 s, a pH gradient was created by the addition of 20 µL NaOH (0.5 M). Finally, at *t* = 300 s vesicles were lysed by the addition of 10% Triton X-100 (25 µL) to get the complete destruction of the applied pH gradient. Each time-dependent fluorescence data was normalized using Equation S2. A sample containing 1975 µL HEPES buffer (10 mM HEPES, 100 mM NaCl, pH = 7.0), 25 µL EYPC-LUVs⊃HPTS, and 20 µL DMSO was also subjected to 5 min irradiation with the same LEDs. The ion transport activity of this sample was measured by adding 20 µL NaOH (0.5 M) at *t* = 100 s of the kinetics experiment, and this data was used as control data. The time axis was normalized according to Equation S1. The time-dependent data were normalized to percent change in fluorescence intensity using Equation S2.

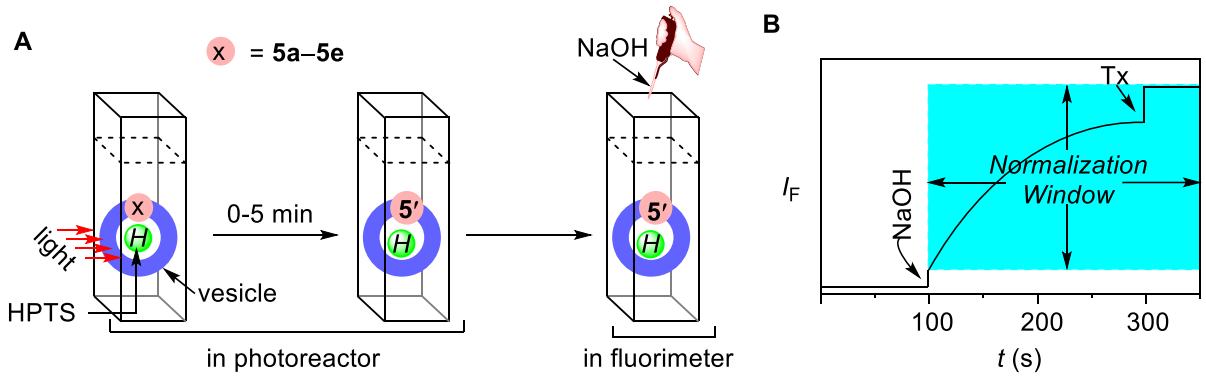

Fig. S33 Description of the phototriggered release of active carrier in the presence of unilamellar vesicles followed by ion transport measurement (**A**). Illustration of ion transport kinetics showing normalization window (**B**).

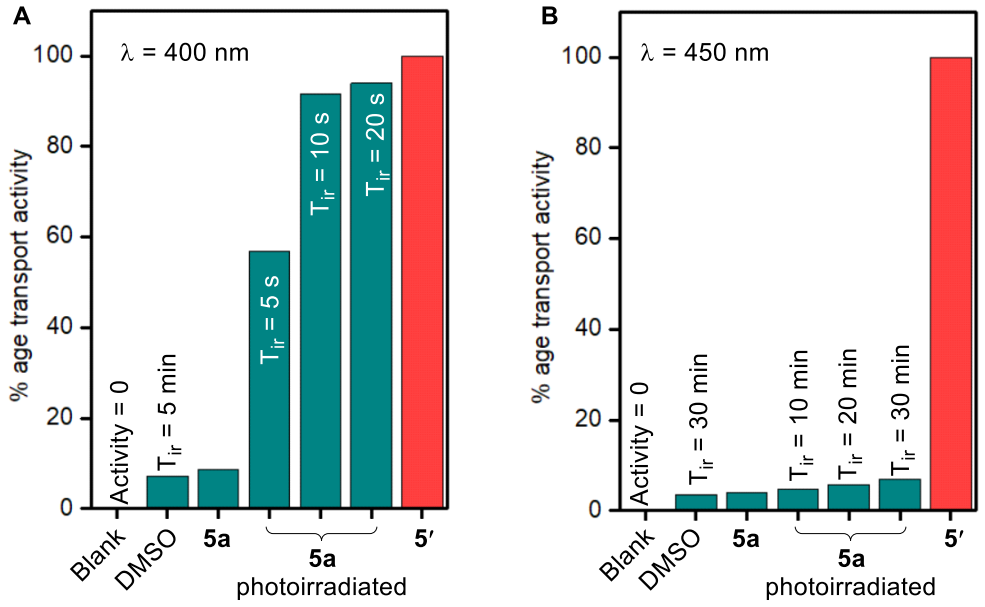

Fig. S34 Normalized ion transport activity data upon photoirradiation of **5a** at 400 nm (**A**) and 450 nm (**B**).

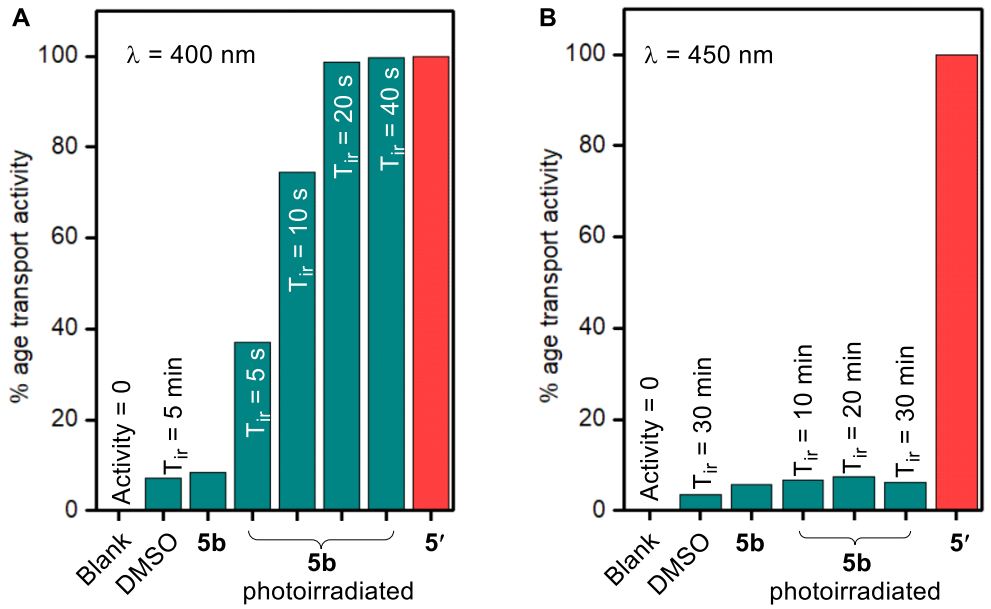

Fig. S35 Normalized ion transport activity data upon photoirradiation of **5b** at 400 nm (**A**) and 450 nm (**B**).

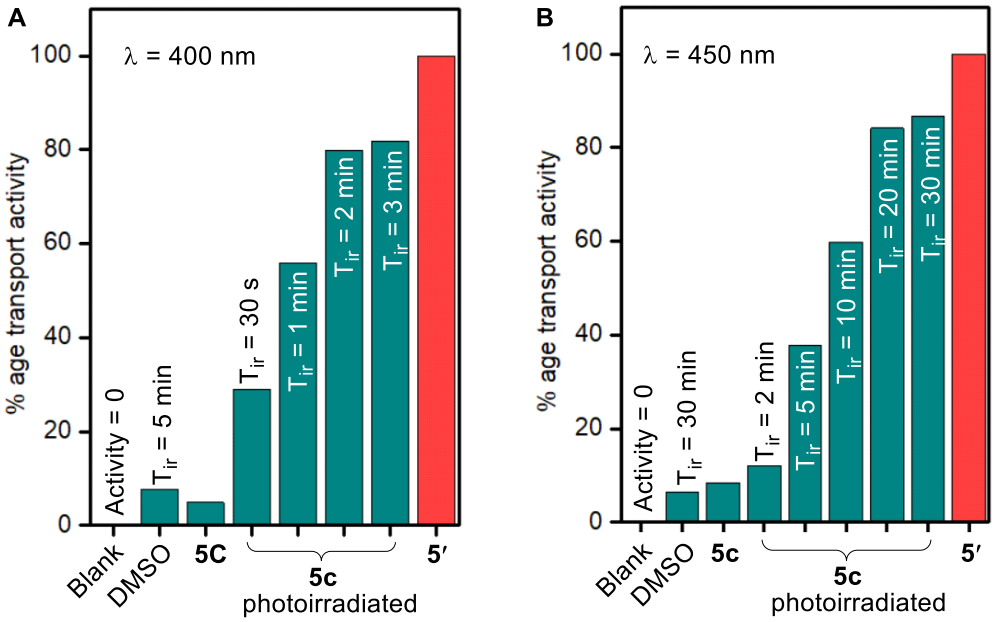

Fig. S36 Normalized ion transport activity data upon photoirradiation of **5c** at 400 nm (**A**) and 450 nm (**B**).

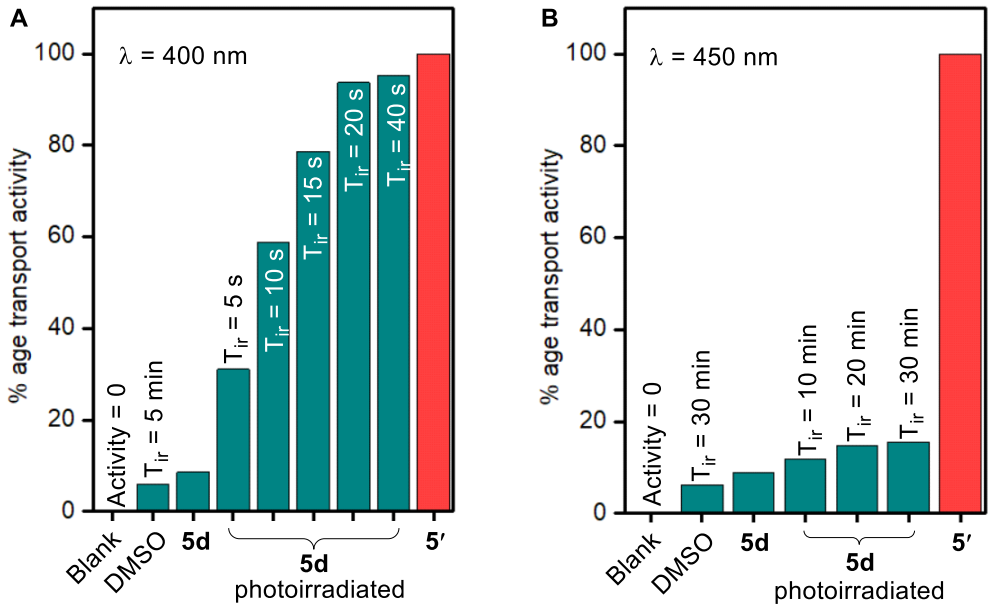

Fig. S37 Normalized ion transport activity data upon photoirradiation of **5d** at 400 nm (**A**) and 450 nm (**B**).

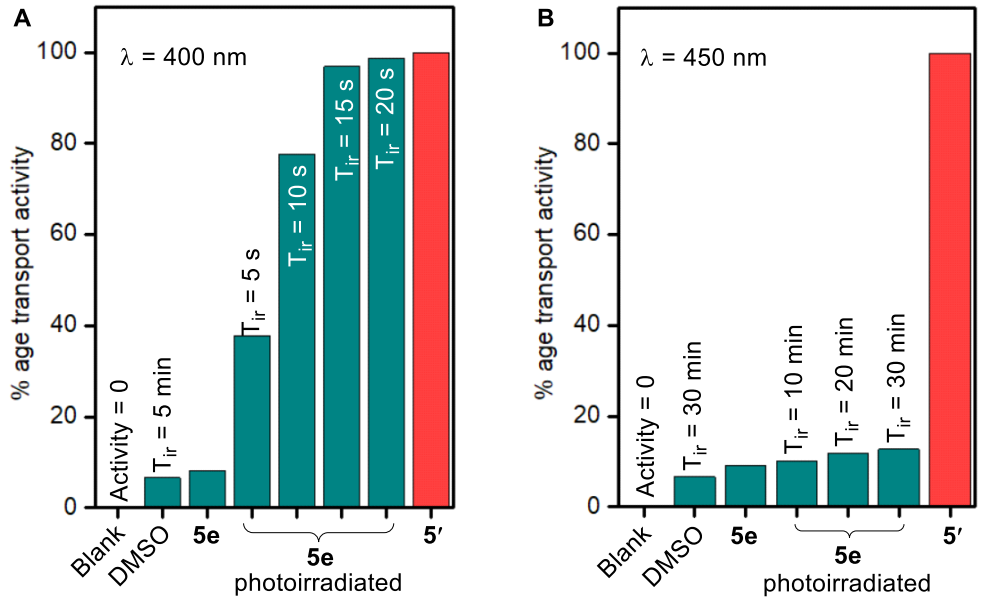

Fig. S38 Normalized ion transport activity data upon photoirradiation of **5e** at 400 nm (**A**) and 450 nm (**B**).

VIII. Biological Studies

Cell culture protocol: The MCF 7 cells were grown in high glucose Dulbecco's Modified Eagle Medium (DMEM; Lonza) containing 2 mM L-glutamine. The media was supplemented with 10% (v/v) heat-inactivated fetal bovine serum (FBS; Invitrogen) and 100 units/mL

penicillin-streptomycin (Invitrogen). Cells were maintained in 100 mm tissue culture-treated dishes (Eppendorf) at 37 °C in a humidified 5% CO_2 incubator (Thermo Scientific).

MTT-based cytotoxicity assay: The cells were dispersed in a 96-well flat bottom tissue culture treated plates (Eppendorf) at a density of 8000 cells/well (per 100 µL) and incubated at 37 ^oC in a humidified 5% CO_2 incubator for 24 h. Compounds were added to each well at the required concentrations, maintaining the maximum amount of DMSO at 1 µL. Following 24 h incubation at 37 ^oC the media was aspirated out and replaced with 110 µL of MTT solution (0.5 mg/mL) in DMEM and incubated for 4 h in identical conditions. Then, the media was removed, and 100 µL of DMSO was added to each well to dissolve the formazan crystals. The absorbance was recorded in a Varioskan Flash (Thermo Scientific) multimode plate reader at 570 nm wavelength. All experiments were performed in triplicate, and the relative cell viability (%) was expressed as a percentage of vehicle (DMSO- 1 µL) treated control.

MCF-7 cells were treated with **5´** in the 0-20 µM concentration range, and the cell viability was assessed through an MTT assay to obtain an IC_{50} of 6.02 µM for the carrier (Fig. S38).

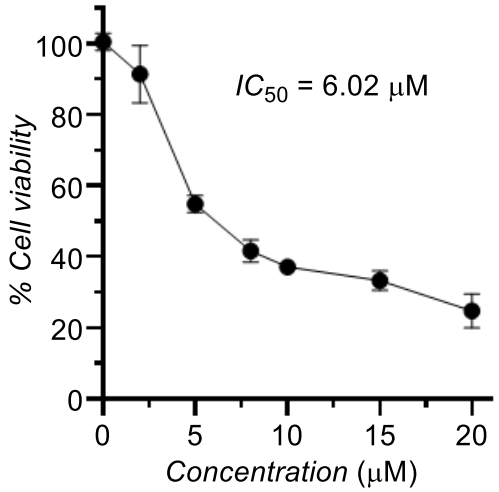

Fig. S39 Dose-dependent toxicity of **5´** towards MCF-7 cells.

MQAE assay: MCF-7 cells were seeded in 96-well black flat bottom tissue culture treated plates (BD Falcon) in complete L-15 media at a density of 10000 cells/well (per 100 µL) and incubated at 37°C in a 5% CO_2 incubator for 18 h. The media was aspirated and replaced with L-15 media containing 5 mM MQAE dye. The plate was then incubated for 4.5 h at 37 °C in 5% CO_2. Post incubation, the media was aspirated, and the cells were washed twice with prewarmed (37 °C) DPBS (100 µL each). Then, L-15 media (100 µL) containing the carrier **5'** (at 5, 10 and 25 µM concentrations) was added. The fluorescence of the dye was then recorded (λ_{ex} = 350 nm, λ_{em} = 460 nm) at different time points (0, 15, 30, 45, 60, 90, 120, and 150 min)

on a PerkinElmer EnSight™ multimode plate reader maintaining plate temperature at 37°C throughout the duration of the measurement (Fig. 5A).

Immunoblot analysis: MCF-7 cells were seeded at a density of 4 x10^5 cells per well in 35 mm tissue culture-treated dishes (ThermoScientific) in a complete DMEM medium and incubated at 37 °C in a humidified 5% CO_2 incubator for 16 h. The cells were then treated with the carrier **5'** at 5 µM concentration. One dish was kept as a control, and the cells were treated with an equal volume of DMSO. Following 16 h of treatment, the medium containing compounds was aspirated out, and the cells were washed with 1 mL 1X Dulbecco's phosphate buffered saline (DPBS; Lonza). Then, 1X sample buffer (containing 60 mM Tris (pH 6.8), 6% glycerol, 2% sodium dodecyl sulfate (SDS), 0.1 M dithiothreitol (DTT) and 0.006% bromophenol blue) was added to each well, cells scraped out using a scraper and transferred to 1.5 mL centrifuge tubes. The cells were lysed by heating the samples at 95 °C for 10 min, and the lysates were stored at –55°C.

The cell lysates were resolved by sodium dodecyl sulphate-polyacrylamide gel electrophoresis (SDS-PAGE). The lysates were run on 13.4 % acrylamide gel in a miniVE vertical electrophoresis system (GE Healthcare) at 130 V. The proteins were transferred to a polyvinylidenedifluoride (PVDF) membrane (Immobilon, Millipore) for 2 h at 4 °C using a TE 22 Mini Tank Transfer Unit (GE Healthcare), with a 245 mA constant current supply. Blocking was performed in 3% BSA prepared in 1X Tris buffered saline containing 0.1% Tween 20 (1X TBS-T) over 16 h at 4 °C. The blots were incubated in the primary antibody solution (1 h at RT for GAPDH and 16 h at 4 °C for PARP1). Following 3 x 10 min washes in 1X TBS-T, the blots were incubated with peroxidase-conjugated secondary antibody solution prepared in 3% BSA in 1X TBS-T for 1 h at RT. The blots were then developed using Amersham ECL Prime Western Blotting Detection Reagent (GE Healthcare) and visualized using ImageQuant LAS400Imaging System (GE Healthcare). The images were processed and quantified using ImageJ software (https://imagej.nih.gov/ij/download.html), and the quantitation is depicted in Fig. 7B.

Phototriggered activation in cells:

MCF 7 were dispersed in a 96-well flat bottom tissue culture treated plates (Eppendorf) in complete DMEM medium at a density of 10000 cells/well (per 100 µL) and incubated at 37ºC in a 5% CO_2 incubator for 24 h. The media was then replaced with 100 µL prewarmed (37ºC)

complete L-15 media, and the cells were treated with the procarriers **5a-5e** (as a solution in DMSO) at 10 µM concentration, maintaining the amount of DMSO at 1 µL per well.

The plates were irradiated for either 20 minutes at 400 nm (using 1 × 12 W LED) or for 2 h at 450 nm (using 3 ×1 W LEDs) in two separate experiments for the two different wavelengths (the plate was positioned at a distance of 8 cm from the LEDs). The plate was then incubated for 24 h at 37°C (5% CO_2). Post incubation, the media was aspirated out and replaced with 110 µL (per well) of MTT solution (0.5 mg/mL) in DMEM. Following incubation at 37°C (5% CO_2) for 4 h, the media was removed, and the formazan crystals formed were dissolved using 100 µl DMSO. The absorbance for each well was measured at 570 nm using a Varioskan Flash (Thermo Scientific) multimode plate reader. All experiments were performed in triplicate, and the relative cell viability (%) was expressed as a percentage of vehicle (DMSO- 1 µL) treated control.

Assessment of cytotoxicity of the *o*-nitrosobenzaldehyde byproducts 1´´, 5b´´-5e´´: To evaluate the cytotoxicity of the *o*-nitrosobenzaldehyde byproducts obtained during the photocleavage of the procarriers **5a-5e** on photoirradiation at 400 nm and by **5c** by photoirradiation at 450 nm, the amine derivatives **6a-6e** were used for cell viability studies in the presence of light (**6a-6e** for 400 nm and **6c** 450 nm). These compounds gave 4-trifluoromethylaniline and *o*-nitrosobenzaldehyde byproducts **1´´** and **5b´´-5e´´**, respectively, for 400 nm activation and **5c´´** for 450 nm activation. 4-Trifluoromethylaniline **6´** did not show significant cellular toxicity. Thus, any excess toxicity observed for the photoirradiated controls would be due to the formation of *o*-nitrosobenzaldehyde byproducts.

Photoactivation studies were performed for the control compounds as described in the protocol above, and the cell viability was assessed through an MTT assay.

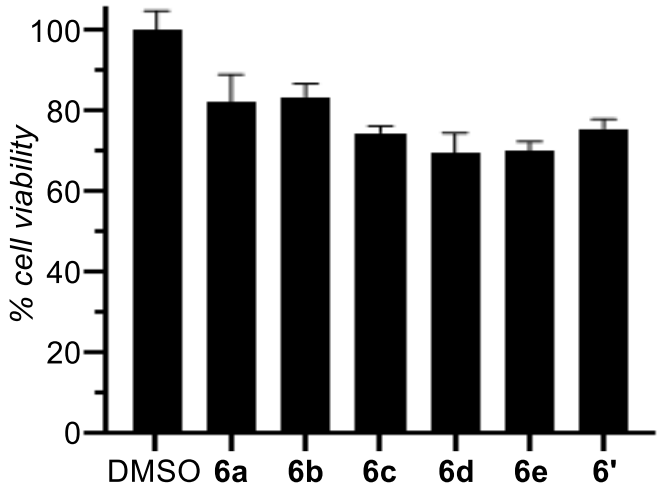

Fig. S40 Cell viability obtained from MTT assay on the treatment of MCF-7 cells with **6a-6e** and **6´** followed by photoirradiation under 400 nm light for 20 min. DMSO was used as a negative control.

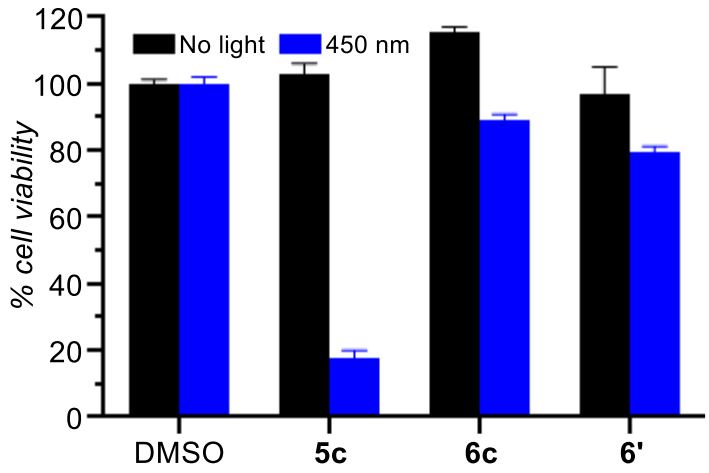

Fig. S41 Comparison of cell viabilities obtained from MTT assay on the treatment of MCF-7 cells with procarrier **5c**, photoactivation byproduct control **6c** and 4-trifluoromethylaniline **6´** in the absence of light (**black**) and upon photoirradiation under 450 nm light for 2 h (**blue**). DMSO was used as a negative control.

IX. Single Crystal X-ray Diffraction Studies

The single-crystal X-ray diffraction (SCXRD) analysis of all the compounds was performed on a Bruker Smart Apex Duo diffractometer using Mo Kα radiation (λ = 0.71073Å). The crystal structures were solved using intrinsic methods and then refined by full-matrix least-squares

against F^2 using all data by using SHELXL-2014/7[S6] built in the Apex-3 package. The crystallographic refinement data for compounds are listed in the tables below. All the non-hydrogen atoms were refined anisotropically if not stated otherwise. Hydrogen atoms were constructed in geometric positions to their parent atoms.[S7] Some of the atom positions (CF_3 group) disordered sites and their occupancies were modeled using the different crystallographic constrain commands. The DIAMOND-3.1 and Mercury software were used to describe the bond length, bond angles, and various structural illustrations of compounds.

Crystallization for 5´

5´ (10 mg) in 2 mL of acetonitrile was shortly heated, and the solution was filtered through a cotton plug to separate any undissolved compound. Suitable crystals for X-ray analysis were obtained by slow evaporation of the solvent.

Table S1. Crystallographic data of **5´** at 100 K.

Crystallographic details	**5´**
Chemical formula	$C_{23}H_{14}F_6N_2O$
Formula weight (g/mol)	448.36
Temperature	100(2)K
Crystal system	Triclinic
Space group	*P-1*
a (Å); α (°)	7.6045(15); 76.190(6)
b (Å); β (°)	9.8170(19); 74.705(6)
c (Å); γ (°)	14.024(3); 74.570(6)
V ($Å^3$); Z	957.3(3); 2
ρ (calc.) g cm^{-3}	1.555
μ(Mo K_α) mm^{-1}	0.137
$2\theta_{max}$ (°)	56.60
R(int)	0.0540
Completeness to θ	99.7
Data / param.	4748/290
GOF	1.054
R1 [F>4σ(F)]	0.0504
wR2 (all data)	0.1404
max. peak/hole (e.$Å^{-3}$)	0.487/-0.547

Table S2. Selected bond lengths [Å] for **5´** at 100 K.

Type of bond	Bond length	Type of bond	Bond length
F3-C12	1.326(2)	**F5-C23**	1.339(2)
F4-C23	1.344(2)	**O1-C16**	1.230(2)
F6-C23	1.344(2)	**F1-C12**	1.340(3)
N1-C6	1.365(2)	**N1-C7**	1.382(2)
N1-H1	0.88	**N2-C16**	1.364(2)
N2-C18	1.417(2)	**N2-H2**	0.88
F2-C12	1.314(3)	**C6-C1**	1.399(3)
C6-C5	1.419(2)	**C16-C7**	1.476(3)
C5-C4	1.411(3)	**C5-C8**	1.428(3)
C7-C8	1.388(2)	**C13-C14**	1.384(3)
C13-C11	1.390(3)	**C13-C12**	1.504(2)
C15-C14	1.397(2)	**C15-C9**	1.397(3)
C15-H15	0.95	**C9-C10**	1.398(3)
C9-C8	1.490(2)	**C18-C17**	1.395(3)
C18-C19	1.398(3)	**C14-H14**	0.95
C17-C22	1.388(3)	**C17-H17**	0.95
C11-C10	1.391(2)	**C11-H11**	0.95
C10-H10	0.95	**C1-C2**	1.374(3)
C1-H1A	0.95	**C4-C3**	1.381(3)
C4-H4	0.95	**C2-C3**	1.413(3)
C2-H2A	0.95	**C22-C21**	1.394(3)
C22-H22	0.95	**C19-C20**	1.398(3)
C19-H19	0.95	**C3-H3**	0.95
C21-C20	1.378(3)	**C21-C23**	1.491(3)
C20-H20	0.95		

Table S3. Selected bond angles [°] for **5´** at 100 K.

Type of bond	Bond angle	Type of bond	Bond angle
C6-N1-C7	109.45(14)	**C6-N1-H1**	125.3
C7-N1-H1	125.3	**C16-N2-C18**	125.25(15)
C16-N2-H2	117.4	**C18-N2-H2**	117.4
N1-C6-C1	130.20(16)	**N1-C6-C5**	107.49(16)
C1-C6-C5	122.31(17)	**O1-C16-N2**	122.23(17)
O1-C16-C7	120.64(16)	**N2-C16-C7**	117.13(15)
C4-C5-C6	118.93(17)	**C4-C5-C8**	133.56(16)
C6-C5-C8	107.51(15)	**N1-C7-C8**	109.34(16)
N1-C7-C16	115.84(15)	**C8-C7-C16**	134.71(17)
C14-C13-C11	120.51(16)	**C14-C13-C12**	120.32(17)
C11-C13-C12	119.17(16)	**C14-C15-C9**	120.41(16)
C14-C15-H15	119.8	**C9-C15-H15**	119.8
C15-C9-C10	118.79(16)	**C15-C9-C8**	121.62(16)
C10-C9-C8	119.51(16)	**C17-C18-C19**	119.91(17)
C17-C18-N2	121.48(17)	**C19-C18-N2**	118.57(16)

C7-C8-C5	106.20(15)	**C7-C8-C9**	130.19(17)
C5-C8-C9	123.61(15)	**C13-C14-C15**	119.86(17)
C13-C14-H14	120.1	**C15-C14-H14**	120.1
C22-C17-C18	119.37(17)	**C22-C17-H17**	120.3
C18-C17-H17	120.3	**C13-C11-C10**	119.52(17)
C13-C11-H11	120.2	**C10-C11-H11**	120.2
C11-C10-C9	120.90(17)	**C11-C10-H10**	119.6
C9-C10-H10	119.6	**C2-C1-C6**	117.30(17)
C2-C1-H1A	121.3	**C6-C1-H1A**	121.3
C3-C4-C5	118.61(17)	**C3-C4-H4**	120.7
C5-C4-H4	120.7	**C1-C2-C3**	121.70(18)
C1-C2-H2A	119.2	**C3-C2-H2A**	119.2
C17-C22-C21	120.34(17)	**C17-C22-H22**	119.8
C21-C22-H22	119.8	**C18-C19-C20**	120.44(17)
C18-C19-H19	119.8	**C20-C19-H19**	119.8
C4-C3-C2	121.16(17)	**C4-C3-H3**	119.4
C2-C3-H3	119.4	**C20-C21-C22**	120.87(18)
C20-C21-C23	120.71(18)	**C22-C21-C23**	118.42(17)
F2-C12-F3	107.72(18)	**F2-C12-F1**	106.73(19)
F3-C12-F1	104.34(16)	**F2-C12-C13**	112.50(16)
F3-C12-C13	113.12(16)	**F1-C12-C13**	111.88(17)
C21-C20-C19	119.06(18)	**C21-C20-H20**	120.5
C19-C20-H20	120.5	**F5-C23-F4**	105.95(17)
F5-C23-F6	106.09(17)	**F4-C23-F6**	105.76(16)
F5-C23-C21	112.85(16)	**F4-C23-C21**	113.76(17)
F6-C23-C21	111.82(18)		

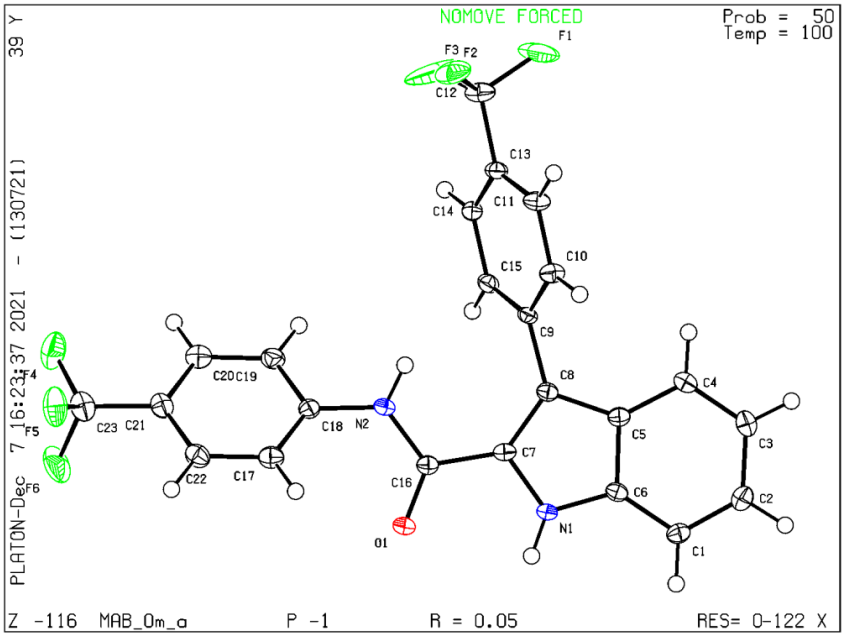

Fig. S42 ORTEP diagram of **5´**. Ellipsoids are drawn at 50% probability. (CCDC: 2127603).

Crystallization for 5´·Cl⁻

5´ (10 mg) in 2 mL of acetonitrile and TBACl, in a ratio of **5´**:TBACl of 1:3 and 1:6 in two different glass vials, were shortly heated, and the solution was filtered through a cotton plug to separate any undissolved compound. Suitable crystals for X-ray analysis were obtained by slow evaporation of the sample containing **5´**:TBACl in a 1:6 ratio.

Table S4. Crystallographic data of **5´·Cl** at 100 K

Crystallographic details	**5´▪Cl**
Chemical formula	$C_{39}H_{50}ClF_6N_3O$
Formula weight (g/mol)	726.27
Temperature	100(2)K
Crystal system	Monoclinic
Space group	*P1 21/c 1*
a (Å); α (°)	24.4975(12); 90
b (Å); β (°)	8.6281(5); 106.476(2)
c (Å); γ (°)	18.2798(9); 90
V (Å^3); Z	3705.1(3); 4
ρ (calc.) g cm^{-3}	1.302
μ(Mo K$_\alpha$) mm^{-1}	0.168
2θ$_{max}$ (°)	50.06
R(int)	0.1637
Completeness to θ	100
Data / param.	6538/456
GOF	1.045
R1 [F>4σ(F)]	0.0575
wR2 (all data)	0.1095
max. peak/hole (e.Å^{-3})	0.259/-0.280

Table S5. Selected bond lengths [Å] for **5´·Cl** at 100 K.

Type of bond	**Bond length**	**Type of bond**	**Bond length**
F5-C22	1.346(3)	**F3-C23**	1.350(3)
F6-C22	1.345(3)	**F4-C22**	1.337(3)
O1-C15	1.226(3)	**F2-C23**	1.333(3)
F1-C23	1.331(3)	**N1-C13**	1.369(3)
N1-C14	1.387(3)	**N1-H1**	0.88
N2-C15	1.367(3)	**N2-C16**	1.407(3)

N2-H2	0.88	**N1A-C5A**	1.517(3)
N1A-C13A	1.521(3)	**N1A-C9A**	1.523(3)
N1A-C1A	1.524(3)	**C21-C20**	1.382(4)
C21-C16	1.390(4)	**C21-H21**	0.95
C20-C19	1.386(4)	**C20-H20**	0.95
C15-C14	1.475(4)	**C14-C7**	1.384(4)
C13A-C14A	1.515(3)	**C13A-H13A**	0.99
C13A-H13B	0.99	**C6-C1**	1.380(4)
C6-C5	1.384(4)	**C6-H6**	0.95
C19-C18	1.382(4)	**C19-C22**	1.489(4)
C8-C13	1.405(4)	**C8-C9**	1.407(4)
C8-C7	1.438(4)	**C5-C4**	1.389(4)
C5-H5	0.95	**C5A-C6A**	1.514(4)
C5A-H5A1	0.99	**C5A-H5A2**	0.99
C9A-C10A	1.516(4)	**C9A-H9A1**	0.99
C9A-H9A2	0.99	**C17-C18**	1.372(4)
C17-C16	1.401(4)	**C17-H17**	0.95
C10A-C11A	1.530(4)	**C10A-H10A**	0.99
C10A-H10B	0.99	**C1A-C2A**	1.520(4)
C1A-H1A1	0.99	**C1A-H1A2**	0.99
C12A-C11A	1.519(4)	**C12A-H12A**	0.98
C12A-H12B	0.98	**C12A-H12C**	0.98
C4-C3	1.389(4)	**C4-C7**	1.477(4)
C14A-C15A	1.523(4)	**C14A-H14A**	0.99
C14A-H14B	0.99	**C1-C2**	1.381(4)
C1-C23	1.491(4)	**C13-C12**	1.396(4)
C18-H18	0.95	**C15A-C16A**	1.518(4)
C15A-H15A	0.99	**C15A-H15B**	0.99
C11A-H11A	0.99	**C11A-H11B**	0.99
C3-C2	1.389(4)	**C3-H3**	0.95
C2A-C3A	1.525(4)	**C2A-H2A1**	0.99
C2A-H2A2	0.99	**C12-C11**	1.372(4)
C12-H12	0.95	**C9-C10**	1.377(4)
C9-H9	0.95	**C2-H2A**	0.95
C11-C10	1.404(4)	**C11-H11**	0.95
C10-H10	0.95	**C3A-C4A**	1.510(4)
C3A-H3A1	0.99	**C3A-H3A2**	0.99
C6A-C7A	1.515(4)	**C6A-H6A1**	0.99
C6A-H6A2	0.99	**C4A-H4A1**	0.98
C4A-H4A2	0.98	**C4A-H4A3**	0.98
C8A-C7A	1.520(4)	**C8A-H8A1**	0.98
C8A-H8A2	0.98	**C8A-H8A3**	0.98
C16A-H16A	0.98	**C16A-H16B**	0.98
C16A-H16C	0.98	**C7A-H7A1**	0.99
C7A-H7A2	0.99		

Table S6. Selected bond angles [°] for **5´·Cl** at 100 K.

Type of bond	Bond angle	Type of bond	Bond angle
C13-N1-C14	109.2(2)	**C13-N1-H1**	125.4
C14-N1-H1	125.4	**C15-N2-C16**	127.4(2)
C15-N2-H2	116.3	**C16-N2-H2**	116.3
C5A-N1A-C13A	111.44(19)	**C5A-N1A-C9A**	105.87(19)
C13A-N1A-C9A	111.3(2)	**C5A-N1A-C1A**	111.5(2)
C13A-N1A-C1A	105.71(19)	**C9A-N1A-C1A**	111.08(19)
C20-C21-C16	120.2(3)	**C20-C21-H21**	119.9
C16-C21-H21	119.9	**C21-C20-C19**	120.4(3)
C21-C20-H20	119.8	**C19-C20-H20**	119.8
O1-C15-N2	122.8(2)	**O1-C15-C14**	121.0(2)
N2-C15-C14	116.1(2)	**C7-C14-N1**	109.1(2)
C7-C14-C15	128.2(2)	**N1-C14-C15**	122.7(2)
C14A-C13A-N1A	116.7(2)	**C14A-C13A-H13A**	108.1
N1A-C13A-H13A	108.1	**C14A-C13A-H13B**	108.1
N1A-C13A-H13B	108.1	**H13A-C13A-H13B**	107.3
C1-C6-C5	119.4(3)	**C1-C6-H6**	120.3
C5-C6-H6	120.3	**C18-C19-C20**	119.4(3)
C18-C19-C22	121.3(3)	**C20-C19-C22**	119.3(3)
C13-C8-C9	118.8(3)	**C13-C8-C7**	107.4(2)
C9-C8-C7	133.8(3)	**C6-C5-C4**	121.3(3)
C6-C5-H5	119.3	**C4-C5-H5**	119.3
C6A-C5A-N1A	116.4(2)	**C6A-C5A-H5A1**	108.2
N1A-C5A-H5A1	108.2	**C6A-C5A-H5A2**	108.2
N1A-C5A-H5A2	108.2	**H5A1-C5A-H5A2**	107.3
C10A-C9A-N1A	115.7(2)	**C10A-C9A-H9A1**	108.4
N1A-C9A-H9A1	108.4	**C10A-C9A-H9A2**	108.4
N1A-C9A-H9A2	108.4	**H9A1-C9A-H9A2**	107.4
C18-C17-C16	120.2(3)	**C18-C17-H17**	119.9
C16-C17-H17	119.9	**C9A-C10A-C11A**	110.4(2)
C9A-C10A-H10A	109.6	**C11A-C10A-H10A**	109.6
C9A-C10A-H10B	109.6	**C11A-C10A-H10B**	109.6
H10A-C10A-H10B	108.1	**C21-C16-C17**	119.0(2)
C21-C16-N2	124.6(2)	**C17-C16-N2**	116.4(2)
C2A-C1A-N1A	116.0(2)	**C2A-C1A-H1A1**	108.3
N1A-C1A-H1A1	108.3	**C2A-C1A-H1A2**	108.3
N1A-C1A-H1A2	108.3	**H1A1-C1A-H1A2**	107.4
C11A-C12A-H12A	109.5	**C11A-C12A-H12B**	109.5
H12A-C12A-H12B	109.5	**C11A-C12A-H12C**	109.5
H12A-C12A-H12C	109.5	**H12B-C12A-H12C**	109.5
C3-C4-C5	118.2(2)	**C3-C4-C7**	120.8(2)
C5-C4-C7	120.8(2)	**C13A-C14A-C15A**	108.8(2)
C13A-C14A-H14A	109.9	**C15A-C14A-H14A**	109.9
C13A-C14A-H14B	109.9	**C15A-C14A-H14B**	109.9
H14A-C14A-H14B	108.3	**C6-C1-C2**	120.6(3)
C6-C1-C23	119.7(3)	**C2-C1-C23**	119.6(3)
N1-C13-C12	129.4(3)	**N1-C13-C8**	107.9(2)

C12-C13-C8	122.7(3)	**C17-C18-C19**	120.8(3)
C17-C18-H18	119.6	**C19-C18-H18**	119.6
C14-C7-C8	106.4(2)	**C14-C7-C4**	129.5(3)
C8-C7-C4	123.9(2)	**C16A-C15A-C14A**	112.6(2)
C16A-C15A-H15A	109.1	**C14A-C15A-H15A**	109.1
C16A-C15A-H15B	109.1	**C14A-C15A-H15B**	109.1
H15A-C15A-H15B	107.8	**C12A-C11A-C10A**	113.4(2)
C12A-C11A-H11A	108.9	**C10A-C11A-H11A**	108.9
C12A-C11A-H11B	108.9	**C10A-C11A-H11B**	108.9
H11A-C11A-H11B	107.7	**C4-C3-C2**	121.1(3)
C4-C3-H3	119.5	**C2-C3-H3**	119.5
C1A-C2A-C3A	109.7(2)	**C1A-C2A-H2A1**	109.7
C3A-C2A-H2A1	109.7	**C1A-C2A-H2A2**	109.7
C3A-C2A-H2A2	109.7	**H2A1-C2A-H2A2**	108.2
C11-C12-C13	117.1(3)	**C11-C12-H12**	121.5
C13-C12-H12	121.5	**C10-C9-C8**	118.6(3)
C10-C9-H9	120.7	**C8-C9-H9**	120.7
C1-C2-C3	119.4(3)	**C1-C2-H2A**	120.3
C3-C2-H2A	120.3	**C12-C11-C10**	121.6(3)
C12-C11-H11	119.2	**C10-C11-H11**	119.2
F4-C22-F6	106.6(2)	**F4-C22-F5**	105.8(2)
F6-C22-F5	105.5(2)	**F4-C22-C19**	113.2(2)
F6-C22-C19	112.5(2)	**F5-C22-C19**	112.6(2)
C9-C10-C11	121.2(3)	**C9-C10-H10**	119.4
C11-C10-H10	119.4	**C4A-C3A-C2A**	113.6(2)
C4A-C3A-H3A1	108.8	**C2A-C3A-H3A1**	108.8
C4A-C3A-H3A2	108.8	**C2A-C3A-H3A2**	108.8
H3A1-C3A-H3A2	107.7	**F1-C23-F2**	107.0(3)
F1-C23-F3	105.4(2)	**F2-C23-F3**	105.1(2)
F1-C23-C1	113.3(2)	**F2-C23-C1**	114.0(3)
F3-C23-C1	111.3(2)	**C5A-C6A-C7A**	109.5(2)
C5A-C6A-H6A1	109.8	**C7A-C6A-H6A1**	109.8
C5A-C6A-H6A2	109.8	**C7A-C6A-H6A2**	109.8
H6A1-C6A-H6A2	108.2	**C3A-C4A-H4A1**	109.5
C3A-C4A-H4A2	109.5	**H4A1-C4A-H4A2**	109.5
C3A-C4A-H4A3	109.5	**H4A1-C4A-H4A3**	109.5
H4A2-C4A-H4A3	109.5	**C7A-C8A-H8A1**	109.5
C7A-C8A-H8A2	109.5	**H8A1-C8A-H8A2**	109.5
C7A-C8A-H8A3	109.5	**H8A1-C8A-H8A3**	109.5
H8A2-C8A-H8A3	109.5	**C15A-C16A-H16A**	109.5
C15A-C16A-H16B	109.5	**H16A-C16A-H16B**	109.5
C15A-C16A-H16C	109.5	**H16A-C16A-H16C**	109.5
H16B-C16A-H16C	109.5	**C6A-C7A-C8A**	112.1(2)
C6A-C7A-H7A1	109.2	**C8A-C7A-H7A1**	109.2
C6A-C7A-H7A2	109.2	**C8A-C7A-H7A2**	109.2
H7A1-C7A-H7A2	107.9		

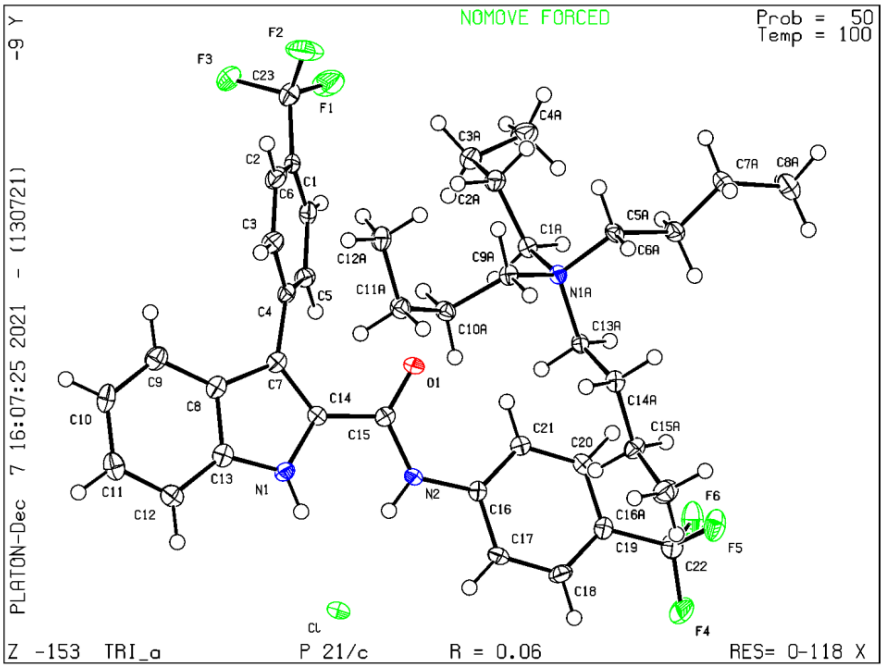

Fig. S43 ORTEP diagram of **5´** co-crystalized TBACl. Ellipsoids are drawn at 50% probability. (CCDC: 2127604).

Crystallization for 5a

5a (10mg) in 2 mL of acetonitrile was shortly heated, and the solution was filtered through a cotton plug to separate any undissolved compound. Suitable crystals for X-ray analysis were obtained by slow evaporation of the solvent.

Table S7. Crystallographic data of **5a** at 100 K.

Crystallographic details	**5a**
Chemical formula	$C_{30}H_{19}F_6N_3O_3$
Formula weight (g/mol)	585.48
Temperature	100(2)K
Crystal system	Monoclinic
Space group	*P 1 21/c 1*
a (Å); α (°)	19.6161(11); 90
b (Å); β (°)	18.8098(10); 94.641(2)
c (Å); γ (°)	8.1114(5); 90
V (Å^3); Z	2983.1(3); 4
ρ (calc.) g cm^{-3}	1.299
μ(Mo Kα) mm^{-1}	0.110

$2\theta_{max}$ (°)	50.04
R(int)	0.0761
Completeness to θ	99.6
Data / param.	5253/343
GOF	2.088
R1 [F>4σ(F)]	0.1755
wR2 (all data)	0.5122
max. peak/hole (e.Å^{-3})	1.717/-0.995

Table S8. Selected bond lengths [Å] for **5a** at 100 K.

Type of bond	Bond length	Type of bond	Bond length
C22-C23	1.39	**C22-C27**	1.39
C22-C28	1.674(12)	**C23-N3**	1.233(16)
C23-C24	1.39	**C24-C25**	1.39
C24-H24	0.95	**C25-C26**	1.39
C25-H25	0.95	**C26-C27**	1.39
C26-H26	0.95	**C27-H27**	0.95
N1-C8	1.351(8)	**N1-C5**	1.420(5)
N1-C28	1.455(9)	**C2-C3**	1.39
C2-C7	1.39	**C2-C1**	1.436(6)
C3-C4	1.39	**C3-H3**	0.95
C4-C5	1.39	**C4-H4**	0.95
C5-C6	1.39	**C6-C7**	1.39
C6-H6	0.95	**C7-H7**	0.95
O1-C8	1.229(7)	**C16-C17**	1.39
C16-C21	1.39	**C16-C30**	1.476(7)
C17-C18	1.39	**C17-H17**	0.95
C18-C19	1.39	**C18-H18**	0.95
C19-C20	1.39	**C19-C29**	1.466(15)
C20-C21	1.39	**C20-H20**	0.95
C21-H21	0.95	**N2-C15**	1.360(7)
N2-C9	1.384(8)	**N2-H2**	0.88
F1-C1	1.310(11)	**C14-C13**	1.384(9)
C14-C15	1.394(9)	**C14-H14**	0.95
F2-C1	1.475(13)	**F3-C1**	1.174(11)
C30-C9	1.355(9)	**C30-C10**	1.437(8)
C8-C9	1.504(9)	**C28-H28A**	0.99
C28-H28B	0.99	**O2-N3**	1.348 (16)
N3-O3	1.414(16)	**C10-C15**	1.399(8)
C10-C11	1.424(9)	**C13-C12**	1.406(9)
C13-H13	0.95	**C12-C11**	1.346(9)
C12-H12	0.95	**C11-H11**	0.95
F4-C29	1.241(18)	**F5-C29**	1.49(4)
F6-C29	1.15(3)		

Table S9. Selected bond angles [°] for **5a** at 100 K.

Type of bond	Bond angle	Type of bond	Bond angle
C23-C22-C27	120.0	**C23-C22-C28**	120.2(6)
C27-C22-C28	119.7(5)	**N3-C23-C24**	119.4(9)
N3-C23-C22	120.6(9)	**C24-C23-C22**	120.0
C25-C24-C23	120.0	**C25-C24-H24**	120.0
C23-C24-H24	120.0	**C24-C25-C26**	120.0
C24-C25-H25	120.0	**C26-C25-H25**	120.0
C25-C26-C27	120.0	**C25-C26-H26**	120.0
C27-C26-H26	120.0	**C26-C27-C22**	120.0
C26-C27-H27	120.0	**C22-C27-H27**	120.0
C8-N1-C5	124.2(5)	**C8-N1-C28**	116.7(5)
C5-N1-C28	118.9(5)	**C3-C2-C7**	120.0
C3-C2-C1	120.3(5)	**C7-C2-C1**	119.7(5)
C4-C3-C2	120.0	**C4-C3-H3**	120.0
C2-C3-H3	120.0	**C3-C4-C5**	120.0
C3-C4-H4	120.0	**C5-C4-H4**	120.0
C6-C5-C4	120.0	**C6-C5-N1**	119.5(3)
C4-C5-N1	120.5(3)	**C5-C6-C7**	120.0
C5-C6-H6	120.0	**C7-C6-H6**	120.0
C6-C7-C2	120.0	**C6-C7-H7**	120.0
C2-C7-H7	120.0	**C17-C16-C21**	120.0
C17-C16-C30	120.0(4)	**C21-C16-C30**	119.8(4)
C16-C17-C18	120.0	**C16-C17-H17**	120.0
C18-C17-H17	120.0	**C19-C18-C17**	120.0
C19-C18-H18	120.0	**C17-C18-H18**	120.0
C18-C19-C20	120.0	**C18-C19-C29**	114.6(14)
C20-C19-C29	125.3(14)	**C19-C20-C21**	120.0
C19-C20-H20	120.0	**C21-C20-H20**	120.0
C20-C21-C16	120.0	**C20-C21-H21**	120.0
C16-C21-H21	120.0	**C15-N2-C9**	108.4(5)
C15-N2-H2	125.8	**C9-N2-H2**	125.8
C13-C14-C15	115.8(6)	**C13-C14-H14**	122.1
C15-C14-H14	122.1	**C9-C30-C10**	105.7(5)
C9-C30-C16	129.1(5)	**C10-C30-C16**	125.1(5)
O1-C8-N1	121.5(6)	**O1-C8-C9**	119.4(5)
N1-C8-C9	119.1(5)	**C30-C9-N2**	110.5(5)
C30-C9-C8	132.3(5)	**N2-C9-C8**	117.2(5)
F3-C1-F1	114.1(9)	**F3-C1-C2**	119.1(9)
F1-C1-C2	116.8(8)	**F3-C1-F2**	100.0(11)
F1-C1-F2	91.6(8)	**C2-C1-F2**	109.6(8)
N1-C28-C22	108.8(7)	**N1-C28-H28A**	109.9
C22-C28-H28A	109.9	**N1-C28-H28B**	109.9
C22-C28-H28B	109.9	**H28A-C28-H28B**	108.3
C23-N3-O2	136.1(12)	**C23-N3-O3**	131.7(13)
O2-N3-O3	91.3(13)	**C15-C10-C11**	118.5(5)
C15-C10-C30	107.5(5)	**C11-C10-C30**	134.0(6)

N2-C15-C14	128.7(6)	**N2-C15-C10**	107.9(5)
C14-C15-C10	123.4(5)	**C14-C13-C12**	121.9(6)
C14-C13-H13	119.0	**C12-C13-H13**	119.0
C11-C12-C13	121.8(6)	**C11-C12-H12**	119.1
C13-C12-H12	119.1	**C12-C11-C10**	118.5(6)
C12-C11-H11	120.7	**C10-C11-H11**	120.7
F6-C29-F4	110.(2)	**F6-C29-C19**	122.(2)
F4-C29-C19	117.8(12)	**F6-C29-F5**	98.9(17)
F4-C29-F5	97.(2)	**C19-C29-F5**	106.(2)

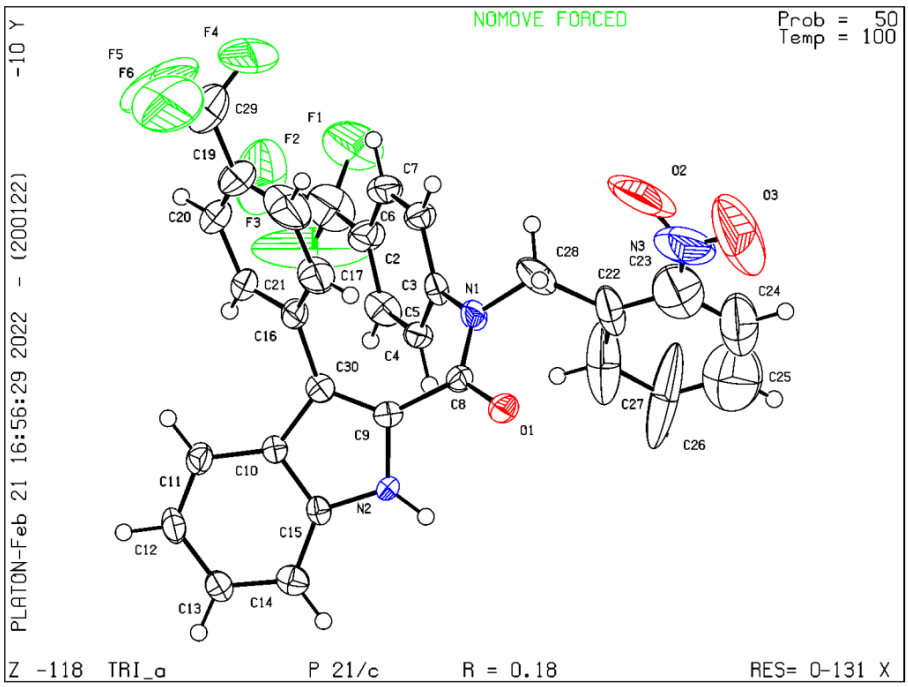

Fig. S44 ORTEP diagram of **5a.** Ellipsoids are drawn at 50% probability. (CCDC: 2155430).

Crystallization for 5c

5c (10 mg) in 2 mL of acetonitrile was shortly heated, and the solution was filtered through a cotton plug to separate any undissolved compound. Suitable crystals for X-ray analysis were obtained by slow evaporation of the solvent.

Table S10. Crystallographic data of **5c** at 100 K.

Crystallographic details	**5c**
Chemical formula	$C_{32}H_{24}F_6N_4O_3$
Formula weight (g/mol)	626.55
Temperature	100(2)K
Crystal system	Triclinic

Space group	*P-1*
a (Å); α (°)	10.851(2); 81.019(8)
b (Å); β (°)	11.560(2); 72.671(9)
c (Å); γ (°)	11.920(2); 78.352(9)
V (Å^3); Z	1390.6(5); 2
ρ (calc.) g cm^{-3}	1.496
μ(Mo K$_\alpha$) mm^{-1}	1.076
2θ$_{max}$ (°)	131.54
R(int)	0.0455
Completeness to θ	97.1
Data / param.	4677/409
GOF	1.073
R1 [F>4σ(F)]	0.0604
wR2 (all data)	0.1506
max. peak/hole (e.Å^{-3})	1.121/-0.961

Table S11. Selected bond lengths [Å] for **5c** at 100 K.

Type of bond	Bond length	Type of bond	Bond length
F6-C23	1.348(3)	**F4-C23**	1.343(3)
F5-C23	1.342(3)	**O1-C16**	1.233(3)
F1-C15	1.284(4)	**F2-C15**	1.312(4)
N1-C8	1.365(3)	**N1-C5**	1.375(3)
N1-H1	0.88	**N2-C16**	1.360(4)
N2-C17	1.437(4)	**N2-C24**	1.475(3)
O2-N4	1.212(3)	**N4-O3**	1.218(3)
N4-C30	1.468(4)	**N3-C28**	1.376(4)
N3-C31	1.447(4)	**N3-C32**	1.453(4)
F3-C15	1.344(4)	**C7-C8**	1.377(4)
C7-C6	1.448(4)	**C7-C9**	1.472(4)
C25-C26	1.393(4)	**C25-C30**	1.407(4)
C25-C24	1.518(4)	**C16-C8**	1.490(4)
C17-C18	1.384(4)	**C17-C22**	1.397(4)
C6-C1	1.404(4)	**C6-C5**	1.408(4)
C9-C10	1.392(4)	**C9-C14**	1.403(4)
C20-C21	1.389(4)	**C20-C19**	1.389(4)
C20-C23	1.495(4)	**C26-C27**	1.374(4)
C26-H26	0.95	**C10-C11**	1.376(4)
C10-H10	0.95	**C30-C29**	1.385(4)
C18-C19	1.383(4)	**C18-H18**	0.95
C27-C28	1.403(4)	**C27-H27**	0.95
C5-C4	1.396(4)	**C19-H19**	0.95
C11-C12	1.387(4)	**C11-H11**	0.95
C28-C29	1.398(4)	**C29-H29**	0.95

C4-C3	1.377(4)	**C4-H4**	0.95
C22-C21	1.383(4)	**C22-H22**	0.95
C21-H21	0.95	**C13-C14**	1.381(4)
C13-C12	1.392(4)	**C13-H13**	0.95
C14-H14	0.95	**C1-C2**	1.372(4)
C1-H1A	0.95	**C12-C15**	1.484(4)
C3-C2	1.400(4)	**C3-H3**	0.95
C24-H24A	0.99	**C24-H24B**	0.99
C2-H2	0.95	**C32-H32A**	0.98
C32-H32B	0.98	**C32-H32C**	0.98
C31-H31A	0.98	**C31-H31B**	0.98
C31-H31C	0.98		

Table S12. Selected bond angles [°] for **5c** at 100 K.

Type of bond	Bond angle	Type of bond	Bond angle
C8-N1-C5	108.9(2)	**C8-N1-H1**	125.5
C5-N1-H1	125.5	**C16-N2-C17**	124.3(2)
C16-N2-C24	117.6(2)	**C17-N2-C24**	117.8(2)
O2-N4-O3	121.4(2)	**O2-N4-C30**	119.3(2)
O3-N4-C30	119.3(2)	**C28-N3-C31**	119.4(2)
C28-N3-C32	119.1(2)	**C31-N3-C32**	118.1(2)
C8-C7-C6	105.8(2)	**C8-C7-C9**	126.0(2)
C6-C7-C9	128.1(2)	**C26-C25-C30**	114.3(2)
C26-C25-C24	120.8(2)	**C30-C25-C24**	124.8(2)
O1-C16-N2	122.0(2)	**O1-C16-C8**	120.2(2)
N2-C16-C8	117.8(2)	**C18-C17-C22**	119.5(3)
C18-C17-N2	119.3(2)	**C22-C17-N2**	121.1(2)
C1-C6-C5	118.1(2)	**C1-C6-C7**	135.1(3)
C5-C6-C7	106.7(2)	**C10-C9-C14**	118.2(3)
C10-C9-C7	119.6(2)	**C14-C9-C7**	122.2(2)
N1-C8-C7	110.4(2)	**N1-C8-C16**	118.0(2)
C7-C8-C16	131.5(2)	**C21-C20-C19**	120.0(3)
C21-C20-C23	119.0(3)	**C19-C20-C23**	120.9(3)
C27-C26-C25	123.4(3)	**C27-C26-H26**	118.3
C25-C26-H26	118.3	**C11-C10-C9**	121.3(3)
C11-C10-H10	119.3	**C9-C10-H10**	119.3
C29-C30-C25	123.7(3)	**C29-C30-N4**	115.3(2)
C25-C30-N4	121.0(2)	**C19-C18-C17**	120.4(3)
C19-C18-H18	119.8	**C17-C18-H18**	119.8
C26-C27-C28	121.5(3)	**C26-C27-H27**	119.3
C28-C27-H27	119.3	**N1-C5-C4**	129.4(3)
N1-C5-C6	108.1(2)	**C4-C5-C6**	122.5(2)
C18-C19-C20	120.0(3)	**C18-C19-H19**	120.0
C20-C19-H19	120.0	**C10-C11-C12**	120.0(3)
C10-C11-H11	120.0	**C12-C11-H11**	120.0
N3-C28-C29	121.5(2)	**N3-C28-C27**	121.8(3)
C29-C28-C27	116.7(2)	**C30-C29-C28**	120.5(2)

C30-C29-H29	119.8	**C28-C29-H29**	119.8
C3-C4-C5	117.7(3)	**C3-C4-H4**	121.1
C5-C4-H4	121.1	**C21-C22-C17**	120.2(3)
C21-C22-H22	119.9	**C17-C22-H22**	119.9
C22-C21-C20	119.8(3)	**C22-C21-H21**	120.1
C20-C21-H21	120.1	**C14-C13-C12**	120.0(3)
C14-C13-H13	120.0	**C12-C13-H13**	120.0
C13-C14-C9	120.7(3)	**C13-C14-H14**	119.6
C9-C14-H14	119.6	**C2-C1-C6**	119.2(3)
C2-C1-H1A	120.4	**C6-C1-H1A**	120.4
C11-C12-C13	119.7(3)	**C11-C12-C15**	120.4(3)
C13-C12-C15	119.8(3)	**C4-C3-C2**	120.6(3)
C4-C3-H3	119.7	**C2-C3-H3**	119.7
N2-C24-C25	112.7(2)	**N2-C24-H24A**	109.1
C25-C24-H24A	109.1	**N2-C24-H24B**	109.1
C25-C24-H24B	109.1	**H24A-C24-H24B**	107.8
F5-C23-F4	107.0(2)	**F5-C23-F6**	105.6(2)
F4-C23-F6	105.4(2)	**F5-C23-C20**	113.2(2)
F4-C23-C20	113.2(2)	**F6-C23-C20**	111.8(2)
C1-C2-C3	121.7(3)	**C1-C2-H2**	119.1
C3-C2-H2	119.1	**N3-C32-H32A**	109.5
N3-C32-H32B	109.5	**H32A-C32-H32B**	109.5
N3-C32-H32C	109.5	**H32A-C32-H32C**	109.5
H32B-C32-H32C	109.5	**F1-C15-F2**	108.5(3)
F1-C15-F3	104.6(4)	**F2-C15-F3**	102.8(3)
F1-C15-C12	113.0(3)	**F2-C15-C12**	114.4(3)
F3-C15-C12	112.6(3)	**N3-C31-H31A**	109.5
N3-C31-H31B	109.5	**H31A-C31-H31B**	109.5
N3-C31-H31C	109.5	**H31A-C31-H31C**	109.5
H31B-C31-H31C	109.5		

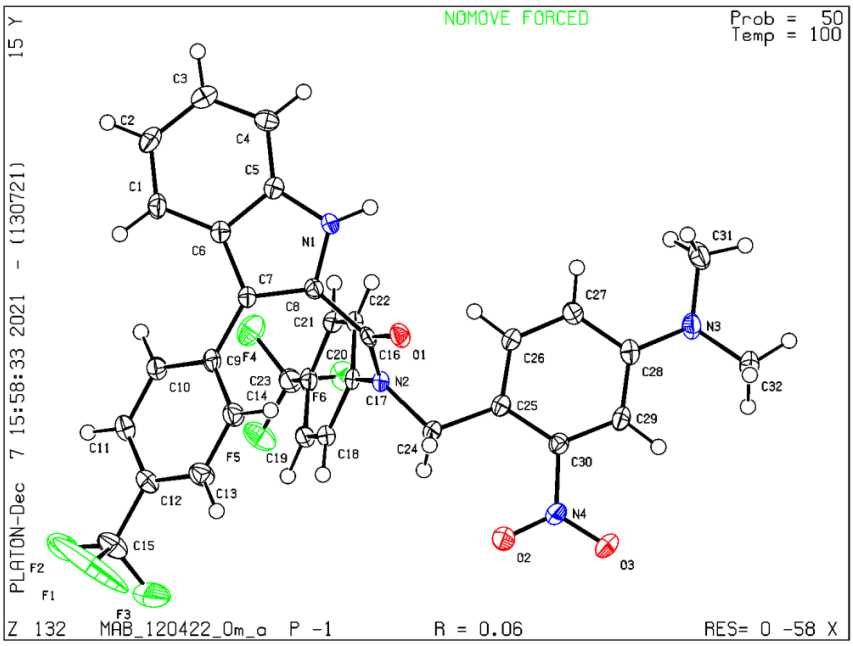

Fig. S45 ORTEP diagram of **5c** co-crystalized TBACl. Ellipsoids are drawn at 50% probability. (CCDC: 2127605).

Crystallization for 5d

5d (10 mg) in 2 mL of acetonitrile was shortly heated, and the solution was filtered through a cotton plug to separate any undissolved compound. Suitable crystals for X-ray analysis were obtained by slow evaporation of the solvent.

Table S13. Crystallographic data of **5d** at 100 K.

Crystallographic details	**5d**
Chemical formula	$C_{37}H_{25}F_6N_3O_4$
Formula weight (g/mol)	689.60
Temperature	100(2)K
Crystal system	Monoclinic
Space group	*P 1 21 1*
a (Å); α (°)	11.639(5); 90
b (Å); β (°)	14.954(7); 98.594(11)
c (Å); γ (°)	18.483(8); 90
V (Å^3); Z	3181.(2); 4
ρ (calc.) g cm^{-3}	1.440
μ(Mo Kα) mm^{-1}	0.118
$2\theta_{max}$ (°)	49.54

R(int)	0.1464
Completeness to θ	99.8
Data / param.	10653/903
GOF	0.954
R1 [F>4σ(F)]	0.0657
wR2 (all data)	0.1689
max. peak/hole (e.Å^{-3})	0.321/-0.336

Table S14. Selected bond lengths [Å] for **5d** at 100 K.

Type of bond	Bond length	Type of bond	Bond length
F1-C22	1.343(12)	**F2-C22**	1.343(11)
F3-C22	1.355(11)	**F4-C38**	1.355(11)
F5-C38	1.334(11)	**F6-C38**	1.325(12)
F7-C60	1.343(14)	**F8-C60**	1.337(12)
F9-C60	1.334(13)	**F10-C75**	1.343(14)
F11-C75	1.342(12)	**F12-C75**	1.355(12)
O5-C40	1.382(11)	**O5-C39**	1.448(10)
O4-C23	1.245(10)	**O7-N4**	1.234(9)
O8-C01O	1.243(10)	**O6-N4**	1.242(9)
O3-N1	1.231(9)	**O1-C2**	1.362(10)
O1-C1	1.437(11)	**O2-N1**	1.224(10)
N4-C51	1.463(11)	**N1-C10**	1.476(12)
N6-C61	1.373(12)	**N6-C64**	1.398(11)
N6-H6	0.88	**N2-C23**	1.377(11)
N2-C16	1.426(11)	**N2-C14**	1.487(11)
N5-C01O	1.372(12)	**N5-C54**	1.434(11)
N5-C52	1.471(11)	**N3-C27**	1.359(11)
N3-C24	1.384(11)	**N3-H3**	0.88
C34-C37	1.380(12)	**C34-C33**	1.387(12)
C34-H34	0.95	**C61-C62**	1.377(12)
C61-C01O	1.477(13)	**C10-C13**	1.392(12)
C10-C9	1.406(11)	**C33-C32**	1.397(13)
C33-H33	0.95	**C37-C36**	1.388(14)
C37-C38	1.476(13)	**C32-C35**	1.399(13)
C32-C25	1.479(13)	**C51-C47**	1.388(11)
C51-C100	1.408(12)	**C54-C55**	1.389(13)
C54-C57	1.393(13)	**C17-C16**	1.390(14)
C17-C19	1.394(13)	**C17-H17**	0.95
C45-C43	1.391(12)	**C45-C44**	1.404(13)
C45-C46	1.481(12)	**C69-C70**	1.390(12)
C69-C72	1.405(11)	**C69-C62**	1.480(13)
C62-C63	1.440(13)	**C19-C21**	1.393(12)
C19-H19	0.95	**C22-C21**	1.489(13)
C23-C24	1.474(13)	**C21-C20**	1.372(14)

C59-C56	1.361(13)	**C59-C58**	1.410(13)
C59-C60	1.477(13)	**C14-C13**	1.531(12)
C14-H14A	0.99	**C14-H14B**	0.99
C44-C42	1.377(12)	**C44-H44**	0.95
C70-C71	1.396(12)	**C70-H70**	0.95
C18-C20	1.392(13)	**C18-C16**	1.394(12)
C18-H18	0.95	**C46-C48**	1.386(12)
C46-C47	1.389(12)	**C27-C28**	1.410(13)
C27-C26	1.417(12)	**C74-C73**	1.385(13)
C74-C71	1.391(12)	**C74-C75**	1.476(14)
C13-C12	1.377(13)	**C6-C7**	1.392(13)
C6-C5	1.392(11)	**C6-H6A**	0.95
C26-C31	1.410(12)	**C26-C25**	1.427(12)
C12-C11	1.390(12)	**C12-H12**	0.95
C8-C9	1.375(13)	**C8-C11**	1.400(13)
C8-C7	1.490(12)	**C24-C25**	1.391(12)
C55-C56	1.394(12)	**C55-H55**	0.95
C11-H11	0.95	**C5-C2**	1.390(13)
C5-H5	0.95	**C66-C65**	1.383(13)
C66-C67	1.411(13)	**C66-H66**	0.95
C40-C41	1.370(13)	**C40-C42**	1.400(12)
C42-H42	0.95	**C36-C35**	1.396(13)
C36-H36	0.95	**C9-H9**	0.95
C64-C65	1.383(14)	**C64-C63**	1.415(12)
C7-C4	1.389(14)	**C52-C100**	1.508(12)
C52-H52A	0.99	**C52-H52B**	0.99
C65-H65	0.95	**C2-C3**	1.373(13)
C43-C41	1.402(12)	**C43-H43**	0.95
C100-C49	1.391(13)	**C28-C29**	1.389(13)
C28-H28	0.95	**C71-H71**	0.95
C30-C31	1.366(13)	**C30-C29**	1.411(13)
C30-H30	0.95	**C4-C3**	1.395(12)
C4-H4	0.95	**C58-C57**	1.388(12)
C58-H58	0.95	**C63-C68**	1.403(12)
C72-C73	1.363(12)	**C72-H72**	0.95
C56-H56	0.95	**C47-H47**	0.95
C68-C67	1.372(14)	**C68-H68**	0.95
C41-H41	0.95	**C48-C49**	1.388(12)
C48-H48	0.95	**C31-H31**	0.95
C57-H57	0.95	**C67-H67**	0.95
C73-H73	0.95	**C49-H49**	0.95
C35-H35	0.95	**C20-H20**	0.95
C3-H3A	0.95	**C29-H29**	0.95
C1-H1A	0.98	**C1-H1B**	0.98
C1-H1C	0.98	**C39-H39A**	0.98
C39-H39B	0.98	**C39-H39C**	0.98

Table S15. Selected bond angles [°] for **5d** at 100 K,

Type of bond	Bond angle	Type of bond	Bond angle
C40-O5-C39	115.6(8)	**C2-O1-C1**	117.8(8)
O7-N4-O6	122.6(8)	**O7-N4-C51**	118.7(7)
O6-N4-C51	118.7(8)	**O2-N1-O3**	125.4(9)
O2-N1-C10	117.7(8)	**O3-N1-C10**	116.9(8)
C61-N6-C64	109.0(7)	**C61-N6-H6**	125.5
C64-N6-H6	125.5	**C23-N2-C16**	124.1(8)
C23-N2-C14	115.8(7)	**C16-N2-C14**	120.0(7)
C01O-N5-C54	124.0(8)	**C01O-N5-C52**	115.8(8)
C54-N5-C52	120.1(8)	**C27-N3-C24**	109.2(7)
C27-N3-H3	125.4	**C24-N3-H3**	125.4
C37-C34-C33	119.8(9)	**C37-C34-H34**	120.1
C33-C34-H34	120.1	**N6-C61-C62**	110.0(9)
N6-C61-C01O	117.1(8)	**C62-C61-C01O**	132.7(9)
C13-C10-C9	121.8(9)	**C13-C10-N1**	121.8(8)
C9-C10-N1	116.3(8)	**C34-C33-C32**	121.1(9)
C34-C33-H33	119.5	**C32-C33-H33**	119.5
C34-C37-C36	120.7(9)	**C34-C37-C38**	119.1(9)
C36-C37-C38	120.2(9)	**C33-C32-C35**	118.2(9)
C33-C32-C25	122.2(9)	**C35-C32-C25**	119.4(9)
C47-C51-C100	123.2(9)	**C47-C51-N4**	117.1(8)
C100-C51-N4	119.5(8)	**C55-C54-C57**	119.8(9)
C55-C54-N5	120.4(9)	**C57-C54-N5**	119.9(9)
F6-C38-F5	107.0(8)	**F6-C38-F4**	105.6(9)
F5-C38-F4	104.6(8)	**F6-C38-C37**	113.0(9)
F5-C38-C37	114.1(9)	**F4-C38-C37**	111.9(8)
C16-C17-C19	120.6(9)	**C16-C17-H17**	119.7
C19-C17-H17	119.7	**C43-C45-C44**	118.1(9)
C43-C45-C46	121.6(9)	**C44-C45-C46**	120.3(8)
C70-C69-C72	117.8(9)	**C70-C69-C62**	122.1(8)
C72-C69-C62	120.1(8)	**C61-C62-C63**	106.6(8)
C61-C62-C69	129.2(9)	**C63-C62-C69**	124.1(8)
C21-C19-C17	119.3(9)	**C21-C19-H19**	120.4
C17-C19-H19	120.4	**F1-C22-F2**	106.3(9)
F1-C22-F3	106.0(8)	**F2-C22-F3**	107.1(8)
F1-C22-C21	112.4(8)	**F2-C22-C21**	112.7(9)
F3-C22-C21	111.9(9)	**O4-C23-N2**	119.6(8)
O4-C23-C24	119.3(9)	**N2-C23-C24**	121.0(8)
C20-C21-C19	120.1(9)	**C20-C21-C22**	120.5(9)
C19-C21-C22	119.3(9)	**C56-C59-C58**	120.5(9)
C56-C59-C60	121.5(10)	**C58-C59-C60**	117.9(9)
N2-C14-C13	111.9(8)	**N2-C14-H14A**	109.2
C13-C14-H14A	109.2	**N2-C14-H14B**	109.2
C13-C14-H14B	109.2	**H14A-C14-H14B**	107.9
C42-C44-C45	121.3(9)	**C42-C44-H44**	119.3
C45-C44-H44	119.3	**C69-C70-C71**	121.3(8)
C69-C70-H70	119.3	**C71-C70-H70**	119.3

C20-C18-C16	119.4(10)	**C20-C18-H18**	120.3
C16-C18-H18	120.3	**C48-C46-C47**	117.7(8)
C48-C46-C45	121.0(8)	**C47-C46-C45**	121.2(8)
C17-C16-C18	119.5(9)	**C17-C16-N2**	119.9(8)
C18-C16-N2	120.6(9)	**N3-C27-C28**	129.9(9)
N3-C27-C26	108.0(8)	**C28-C27-C26**	122.0(9)
C73-C74-C71	120.0(9)	**C73-C74-C75**	120.6(9)
C71-C74-C75	119.3(9)	**C12-C13-C10**	117.0(8)
C12-C13-C14	120.9(8)	**C10-C13-C14**	122.0(9)
C7-C6-C5	121.1(9)	**C7-C6-H6A**	119.4
C5-C6-H6A	119.4	**C31-C26-C27**	118.8(9)
C31-C26-C25	133.9(9)	**C27-C26-C25**	107.3(8)
C13-C12-C11	121.7(9)	**C13-C12-H12**	119.2
C11-C12-H12	119.2	**C9-C8-C11**	117.8(8)
C9-C8-C7	121.4(9)	**C11-C8-C7**	120.7(9)
N3-C24-C25	109.2(8)	**N3-C24-C23**	115.1(8)
C25-C24-C23	135.1(9)	**C54-C55-C56**	119.6(9)
C54-C55-H55	120.2	**C56-C55-H55**	120.2
O8-C01O-N5	119.4(9)	**O8-C01O-C61**	119.8(9)
N5-C01O-C61	120.6(8)	**C12-C11-C8**	121.0(10)
C12-C11-H11	119.5	**C8-C11-H11**	119.5
C2-C5-C6	119.2(9)	**C2-C5-H5**	120.4
C6-C5-H5	120.4	**C24-C25-C26**	106.2(8)
C24-C25-C32	130.4(8)	**C26-C25-C32**	123.3(8)
C65-C66-C67	120.2(10)	**C65-C66-H66**	119.9
C67-C66-H66	119.9	**C41-C40-O5**	126.1(9)
C41-C40-C42	121.0(9)	**O5-C40-C42**	112.9(9)
C44-C42-C40	119.2(10)	**C44-C42-H42**	120.4
C40-C42-H42	120.4	**C37-C36-C35**	119.3(9)
C37-C36-H36	120.4	**C35-C36-H36**	120.4
C8-C9-C10	120.4(9)	**C8-C9-H9**	119.8
C10-C9-H9	119.8	**C65-C64-N6**	129.9(9)
C65-C64-C63	123.2(9)	**N6-C64-C63**	107.0(9)
C4-C7-C6	119.1(9)	**C4-C7-C8**	118.7(9)
C6-C7-C8	122.2(9)	**N5-C52-C100**	111.9(7)
N5-C52-H52A	109.2	**C100-C52-H52A**	109.2
N5-C52-H52B	109.2	**C100-C52-H52B**	109.2
H52A-C52-H52B	107.9	**C66-C65-C64**	117.3(9)
C66-C65-H65	121.4	**C64-C65-H65**	121.4
O1-C2-C3	115.9(9)	**O1-C2-C5**	124.3(9)
C3-C2-C5	119.9(9)	**C45-C43-C41**	121.1(10)
C45-C43-H43	119.5	**C41-C43-H43**	119.5
C49-C100-C51	115.1(9)	**C49-C100-C52**	121.6(8)
C51-C100-C52	123.2(9)	**C29-C28-C27**	116.9(10)
C29-C28-H28	121.6	**C27-C28-H28**	121.6
C74-C71-C70	119.1(9)	**C74-C71-H71**	120.5
C70-C71-H71	120.5	**C31-C30-C29**	121.0(9)
C31-C30-H30	119.5	**C29-C30-H30**	119.5

C7-C4-C3	119.4(10)	**C7-C4-H4**	120.3
C3-C4-H4	120.3	**C57-C58-C59**	118.8(9)
C57-C58-H58	120.6	**C59-C58-H58**	120.6
C68-C63-C64	118.6(9)	**C68-C63-C62**	133.9(9)
C64-C63-C62	107.4(8)	**C73-C72-C69**	121.3(9)
C73-C72-H72	119.4	**C69-C72-H72**	119.4
C59-C56-C55	120.7(9)	**C59-C56-H56**	119.7
C55-C56-H56	119.7	**C51-C47-C46**	120.0(8)
C51-C47-H47	120.0	**C46-C47-H47**	120.0
C67-C68-C63	118.1(9)	**C67-C68-H68**	120.9
C63-C68-H68	120.9	**C40-C41-C43**	119.2(9)
C40-C41-H41	120.4	**C43-C41-H41**	120.4
C46-C48-C49	121.8(9)	**C46-C48-H48**	119.1
C49-C48-H48	119.1	**C30-C31-C26**	119.6(9)
C30-C31-H31	120.2	**C26-C31-H31**	120.2
C58-C57-C54	120.6(9)	**C58-C57-H57**	119.7
C54-C57-H57	119.7	**C68-C67-C66**	122.5(9)
C68-C67-H67	118.7	**C66-C67-H67**	118.7
C72-C73-C74	120.5(9)	**C72-C73-H73**	119.8
C74-C73-H73	119.8	**C48-C49-C100**	122.1(9)
C48-C49-H49	119.0	**C100-C49-H49**	119.0
C36-C35-C32	120.9(10)	**C36-C35-H35**	119.5
C32-C35-H35	119.5	**C21-C20-C18**	121.0(9)
C21-C20-H20	119.5	**C18-C20-H20**	119.5
C2-C3-C4	121.2(10)	**C2-C3-H3A**	119.4
C4-C3-H3A	119.4	**F9-C60-F8**	105.8(10)
F9-C60-F7	104.5(9)	**F8-C60-F7**	105.6(9)
F9-C60-C59	113.4(10)	**F8-C60-C59**	112.9(9)
F7-C60-C59	113.8(10)	**C28-C29-C30**	121.7(10)
C28-C29-H29	119.2	**C30-C29-H29**	119.2
F11-C75-F10	105.4(10)	**F11-C75-F12**	106.2(9)
F10-C75-F12	105.7(10)	**F11-C75-C74**	113.1(10)
F10-C75-C74	113.5(10)	**F12-C75-C74**	112.4(10)
O1-C1-H1A	109.5	**O1-C1-H1B**	109.5
H1A-C1-H1B	109.5	**O1-C1-H1C**	109.5
H1A-C1-H1C	109.5	**H1B-C1-H1C**	109.5
O5-C39-H39A	109.5	**O5-C39-H39B**	109.5
H39A-C39-H39B	109.5	**O5-C39-H39C**	109.5
H39A-C39-H39C	109.5	**H39B-C39-H39C**	109.5

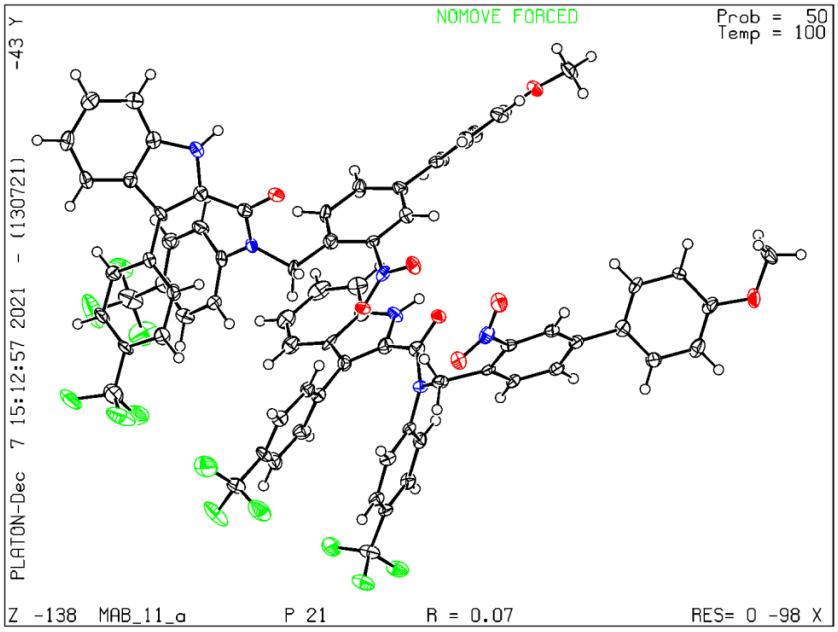

Fig. S46 ORTEP diagram of **5d** co-crystalized TBACl. Ellipsoids are drawn at 50% probability. (CCDC: 2127606).

Crystallization for 6e

6e (10 mg) in 2 mL of acetonitrile was shortly heated, and the solution was filtered through a cotton plug to separate any undissolved compound. Suitable crystals for X-ray analysis were obtained by slow evaporation of the solvent.

Table S16. Crystallographic data of **6e** at 100 K.

Crystallographic details	**6e**
Chemical formula	$C_{15}H_{11}F_3N_2O_4$
Formula weight (g/mol)	340.26
Temperature	100(2)K
Crystal system	Monoclinic
Space group	*P 1 21/n 1*
a (Å); α (°)	8.3389(15); 90
b (Å); β (°)	5.3319(10); 92.827(6)
c (Å); γ (°)	30.853(5); 90
V ($Å^3$); Z	1370.1(4); 4
ρ (calc.) g cm^{-3}	1.650
μ(Mo Kα) mm^{-1}	0.147

$2\theta_{max}$ (°)	49.64
R(int)	0.0690
Completeness to θ	99.3
Data / param.	2344/217
GOF	1.060
R1 [F>4σ(F)]	0.0423
wR2 (all data)	0.1159
max. peak/hole (e.Å^{-3})	0.429/-0.449

Table S17. Selected bond lengths [Å] for **6e** at 100 K,

Type of bond	Bond length	Type of bond	Bond length
F1-C1	1.344(3)	**F2-C1**	1.352(3)
F3-C1	1.332(3)	**O4-C13**	1.376(3)
O4-C15	1.432(3)	**O3-C14**	1.361(3)
O3-C15	1.441(3)	**O2-N2**	1.236(3)
O1-N2	1.231(3)	**N2-C10**	1.456(3)
N1-C7	1.379(3)	**N1-C8**	1.452(3)
N1-H1	0.88	**C3-C6**	1.380(3)
C3-C2	1.390(3)	**C3-H3**	0.95
C4-C5	1.381(3)	**C4-C2**	1.392(3)
C4-H4	0.95	**C5-C7**	1.399(3)
C5-H5	0.95	**C7-C6**	1.401(3)
C2-C1	1.486(4)	**C6-H6**	0.95
C10-C9	1.406(3)	**C10-C11**	1.407(3)
C13-C11	1.357(4)	**C13-C14**	1.380(4)
C9-C12	1.405(3)	**C9-C8**	1.529(3)
C14-C12	1.369(4)	**C11-H11**	0.95
C12-H12	0.95	**C8-H8A**	0.99
C8-H8B	0.99	**C15-H15A**	0.99
C15-H15B	0.99		

Table S18. Selected bond angles [°] for **6e** at 100 K.

Type of bond	Bond angle	Type of bond	Bond angle
C13-O4-C15	105.71(19)	**C14-O3-C15**	105.8(2)
O1-N2-O2	121.9(2)	**O1-N2-C10**	119.6(2)
O2-N2-C10	118.5(2)	**C7-N1-C8**	121.9(2)
C7-N1-H1	119.1	**C8-N1-H1**	119.1
C6-C3-C2	120.8(2)	**C6-C3-H3**	119.6
C2-C3-H3	119.6	**C5-C4-C2**	119.9(2)
C5-C4-H4	120.0	**C2-C4-H4**	120.0
C4-C5-C7	121.1(2)	**C4-C5-H5**	119.5
C7-C5-H5	119.5	**N1-C7-C5**	120.0(2)
N1-C7-C6	121.5(2)	**C5-C7-C6**	118.6(2)

C3-C2-C4	119.4(2)	**C3-C2-C1**	119.4(2)
C4-C2-C1	121.0(2)	**C3-C6-C7**	120.2(2)
C3-C6-H6	119.9	**C7-C6-H6**	119.9
C9-C10-C11	123.4(2)	**C9-C10-N2**	121.5(2)
C11-C10-N2	115.2(2)	**C11-C13-O4**	128.3(2)
C11-C13-C14	121.7(2)	**O4-C13-C14**	110.0(2)
C12-C9-C10	117.6(2)	**C12-C9-C8**	117.7(2)
C10-C9-C8	124.7(2)	**O3-C14-C12**	127.0(2)
O3-C14-C13	110.4(2)	**C12-C14-C13**	122.6(2)
C13-C11-C10	116.3(2)	**C13-C11-H11**	121.8
C10-C11-H11	121.8	**C14-C12-C9**	118.4(2)
C14-C12-H12	120.8	**C9-C12-H12**	120.8
N1-C8-C9	114.6(2)	**N1-C8-H8A**	108.6
C9-C8-H8A	108.6	**N1-C8-H8B**	108.6
C9-C8-H8B	108.6	**H8A-C8-H8B**	107.6
F3-C1-F1	106.8(2)	**F3-C1-F2**	106.0(2)
F1-C1-F2	104.9(2)	**F3-C1-C2**	113.5(2)
F1-C1-C2	113.0(2)	**F2-C1-C2**	111.9(2)
O4-C15-O3	108.0(2)	**O4-C15-H15A**	110.1
O3-C15-H15A	110.1	**O4-C15-H15B**	110.1
O3-C15-H15B	110.1	**H15A-C15-H15B**	108.4

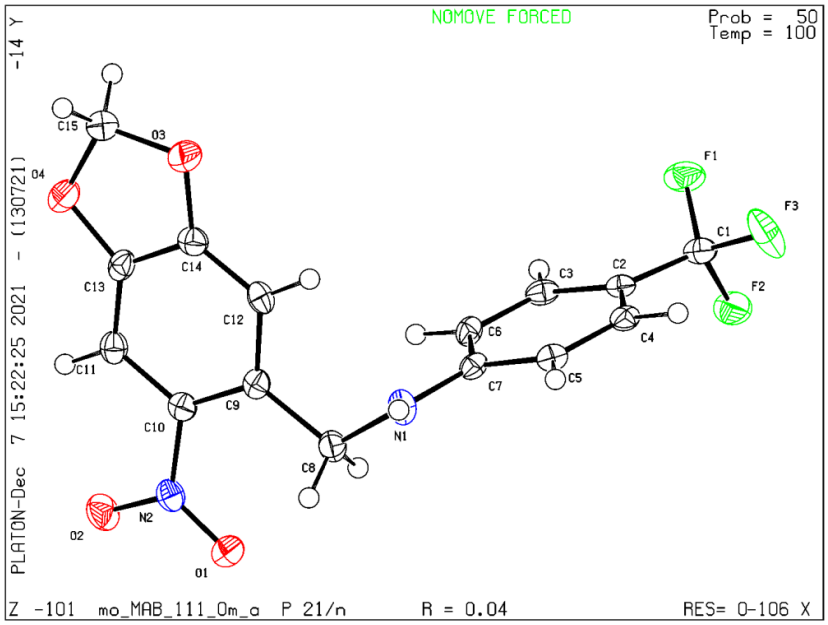

Fig. S47 ORTEP diagram of **6e** co-crystalized TBACl. Ellipsoids are drawn at 50% probability. (CCDC: 2127607).

X. Geometry optimization and binding energy calculations

To get an idea about the conformation of [(**5'**)$_2$+Cl$^-$], several initial geometries of the complex were generated using the CONFLEX 8 software package[S8] using MMFF94s force field. The

calculation provided 10319 conformers, some of which had high Boltzmann populations, as shown in Fig. S48. Among the several conformations, the highest Boltzmann populated structure was used for geometry optimization. The geometry optimization was carried out by the Gaussian 09 program[S9] package using B3LYP functional and 6-311++G(d,p) basis set. The geometry optimized structure is given in the manuscript. For all structures (i.e., free receptors and anionic complexes), the vibrational frequency calculation during the geometry optimization shows no imaginary frequencies, which indicates that all optimized structures are ground state minima.

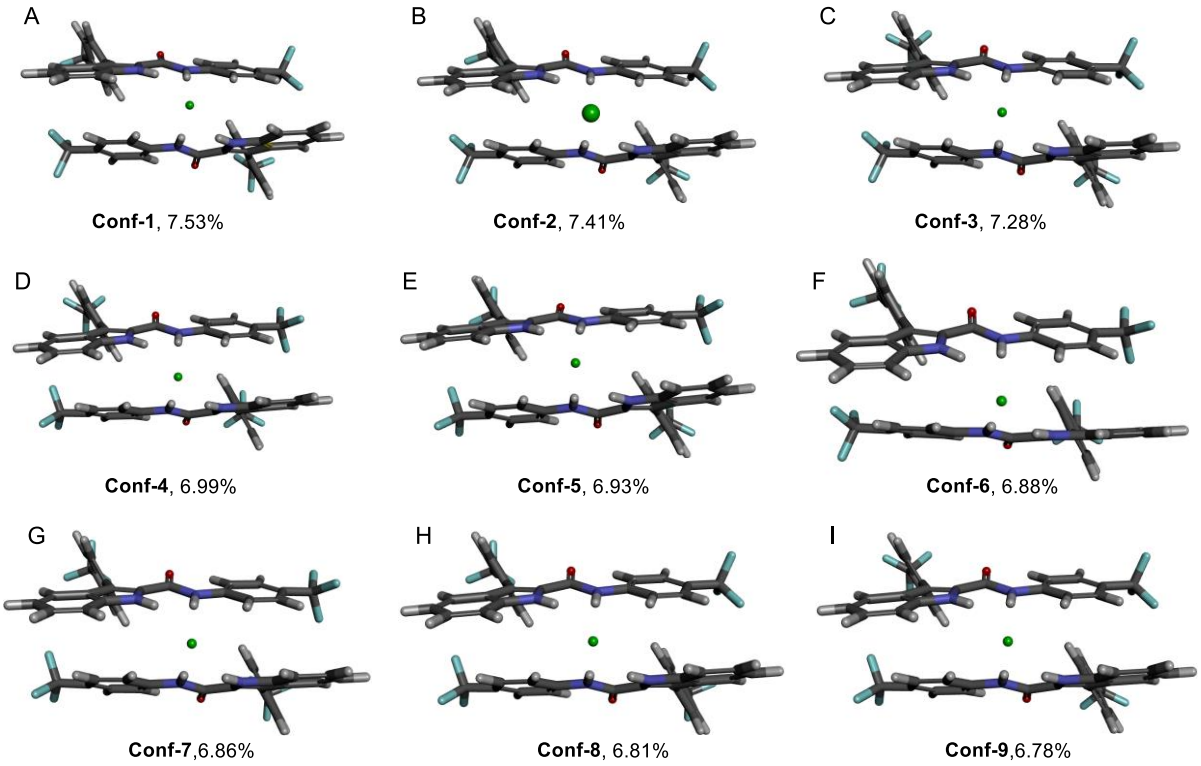

Fig. S48 Initial geometries **Conf-1**–**Conf-9** (**A–I**) for [(**5'**)$_2$+Cl$^-$], optimized by CONFLEX 8 software using MMFF94s force field.

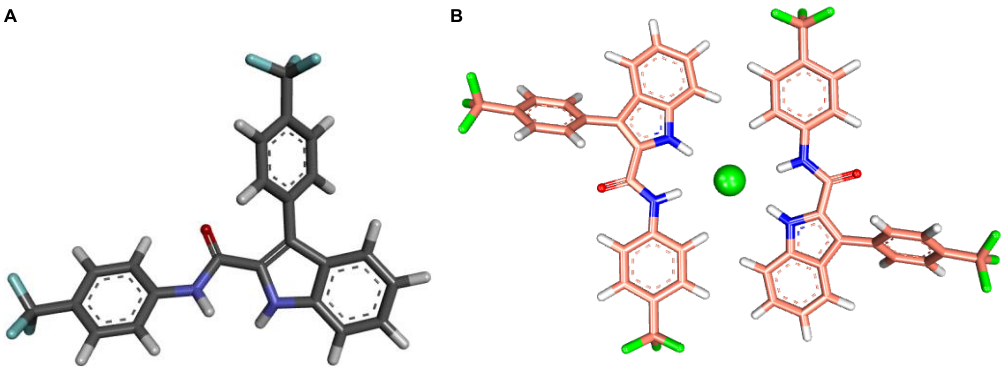

Fig. S49 The geometry optimized structures of **5'** (A) and [(**5'**)$_2$ + Cl$^-$] (B).

The Gaussian 09 program was used to calculate the zero point energy (ZPE) and basis set superposition error (BSSE)[S3, S4] corrected bonding energy of [(**5'**)$_2$ + Cl^-] complex, which was used for the calculation of binding energy (*BE*) using the following equation.

$$BE = [HF_{[M+X^-]} + ZPE_{[M+X^-]} + BSSE_{[M+X^-]}] - 2\times[HF_{\mathbf{M}} + ZPE_{\mathbf{M}}] - [HF_{Cl^-}] \qquad \text{Equation S5}$$

where, $HF_{[M+X^-]}$ = electronic energy of [(**5'**)$_2$ + Cl^-] complex, $ZPE_{[M+X^-]}$ = zero point energy of [(**5'**)$_2$ + Cl^-] complex, $BSSE_{[M+X^-]}$ = BSSE of [(**5'**)$_2$ + Cl^-] complex, $HF_{\mathbf{M}}$ = electronic energy of the receptor **5'**, $ZPE_{\mathbf{M}}$ = zero point energy of the receptor **5'**, and HF_{Cl^-} = electronic energy of Cl^-.

Table S19. The electronic energy (HF), zero point energy (ZPE), basis set superposition error (BSSE) corrected energy (in Hartree unit) for all structures and complexes are calculated at the DFT B3LYP/6-31G(d,p) level of theory.

Structures	Energy
$HF_{[M+X^-]}$ (in Hartree)	–3797.8350322
$ZPE_{[M+X^-]}$ (in Hartree)	0.6579637
$BSSE_{[M+X^-]}$ (in Hartree)	0.014174845
$HF_{\mathbf{M}}$ (in Hartree)	–1668.7285333
$ZPE_{\mathbf{M}}$ (in Hartree)	0.3285074
HF_{Cl^-} (in Hartree)	–460.2522333
BE (in Hartree)	–0.11060852
BE (in kcal/mol)	–69.40784487

Table S20. Atomic coordinates of the optimized structure of lowest energy conformation obtained for **5'** from DFT B3LYP/6-31G(d,p) geometry optimization.

Charge = 0, Multiplicity = 1

Atom #	Atom Type	x	y	Z
1	C	4.178121	4.473606	-0.249254
2	C	3.146254	5.430315	-0.145169
3	C	1.819768	5.046721	0.001966
4	C	1.550875	3.675053	0.055182
5	C	2.574744	2.696019	-0.009324
6	C	3.906257	3.114773	-0.189143
7	N	0.341757	3.010861	0.149915
8	C	0.585015	1.636102	0.226686
9	C	1.943799	1.399818	0.109887
10	C	2.644560	0.102496	0.058379
11	C	3.800439	-0.100206	0.831266
12	C	4.492097	-1.307094	0.781353
13	C	4.039258	-2.335915	-0.046733
14	C	2.890785	-2.150207	-0.820806
15	C	2.203801	-0.942702	-0.768911
16	C	-0.530638	0.676347	0.409820
17	O	-0.393944	-0.403206	0.967843
18	N	-1.738178	1.140519	-0.100342
19	C	-2.999711	0.518699	-0.064576
20	C	-4.036966	1.125388	-0.793500
21	C	-5.313806	0.580884	-0.793552
22	C	-5.578198	-0.581331	-0.063970
23	C	-4.548742	-1.185961	0.660007

24	C	-3.263705	-0.650969	0.666662
25	C	-6.971898	-1.138706	-0.016525
26	F	-6.975460	-2.473297	0.195484
27	F	-7.644612	-0.907077	-1.167753
28	F	-7.705305	-0.583425	0.978948
29	F	4.033736	-4.664276	-0.478805
30	C	4.820713	-3.616022	-0.149653
31	F	5.442285	-3.922255	1.011624
32	F	5.785927	-3.539357	-1.098261
33	H	5.201539	4.810805	-0.380830
34	H	3.392857	6.486596	-0.191575
35	H	1.023400	5.782351	0.064268
36	H	4.704308	2.385142	-0.277920
37	H	-0.484349	3.434199	0.547824
38	H	4.142844	0.686312	1.495750
39	H	5.374111	-1.456051	1.394694
40	H	2.535809	-2.951550	-1.459361
41	H	1.317604	-0.805556	-1.378470
42	H	-1.673116	1.941617	-0.713737
43	H	-3.837943	2.027201	-1.367583
44	H	-6.103740	1.052711	-1.367466
45	H	-4.747906	-2.093515	1.219340
46	H	-2.465002	-1.129753	1.213632

Table S21. Atomic coordinates of the optimized structure of lowest energy conformation obtained for [(**5'**)$_2$ + Cl^-] complex from DFT B3LYP/6-31G(d,p) geometry optimization.

Charge = -1, Multiplicity = 1

Atom #	Atom Type	x	y	Z
1	C	4.560768	-4.869606	1.561212
2	C	4.489207	-3.486969	1.849233
3	C	3.306080	-2.780033	1.696036
4	C	2.182860	-3.493130	1.249238
5	C	2.224340	-4.886351	0.974099
6	C	3.447759	-5.571062	1.125402
7	N	0.915292	-3.050383	0.988834
8	C	0.133223	-4.105706	0.551382
9	C	0.907888	-5.269602	0.532036
10	C	0.545879	-6.645836	0.139849
11	C	0.908284	-7.721591	0.969371
12	C	0.639888	-9.038779	0.604974
13	C	0.000000	-9.309045	-0.605498
14	C	-0.370114	-8.250829	-1.442943
15	C	-0.099925	-6.939148	-1.073941
16	C	-1.313614	-3.978048	0.234757
17	O	-1.994386	-4.975982	-0.000837
18	N	-1.826829	-2.696070	0.218050
19	C	-3.153032	-2.311938	-0.040019
20	C	-3.419974	-0.928218	-0.053308
21	C	-4.702338	-0.456768	-0.293137
22	C	-5.749910	-1.354058	-0.529705
23	C	-5.488129	-2.725431	-0.520266

24	C	-4.206129	-3.213118	-0.280720
25	C	-7.143960	-0.845548	-0.726921
26	F	-7.909615	-1.706297	-1.441846
27	F	-7.167829	0.344148	-1.375185
28	F	-7.794044	-0.647302	0.450794
29	F	-1.354863	-10.853657	-1.787238
30	C	-0.234847	-10.725308	-1.036729
31	F	-0.359556	-11.568617	0.016540
32	F	0.786894	-11.207086	-1.792583
33	H	5.508317	-5.387105	1.680689
34	H	5.379259	-2.967790	2.192927
35	H	3.244523	-1.717833	1.910147
36	H	3.517048	-6.629838	0.896253
37	H	0.625106	-2.076034	1.117645
38	H	1.387249	-7.517473	1.921328
39	H	0.915096	-9.854167	1.265480
40	H	-0.875255	-8.457195	-2.380671
41	H	-0.400614	-6.126393	-1.723099
42	H	-1.205917	-1.908379	0.404280
43	H	-2.606144	-0.232124	0.124820
44	H	-4.886439	0.612628	-0.301161
45	H	-6.294223	-3.426457	-0.709820
46	H	-4.007224	-4.273855	-0.281044
47	C	-4.560768	4.869606	1.561212
48	C	-4.489207	3.486969	1.849233
49	C	-3.306080	2.780033	1.696036

50	C	-2.182860	3.493130	1.249238
51	C	-2.224340	4.886351	0.974099
52	C	-3.447759	5.571062	1.125402
53	N	-0.915292	3.050383	0.988834
54	C	-0.133223	4.105706	0.551382
55	C	-0.907888	5.269602	0.532036
56	C	-0.545879	6.645836	0.139849
57	C	-0.908284	7.721591	0.969371
58	C	-0.639888	9.038779	0.604974
59	C	0.000000	9.309045	-0.605498
60	C	0.370114	8.250829	-1.442943
61	C	0.099925	6.939148	-1.073941
62	C	1.313614	3.978048	0.234757
63	O	1.994386	4.975982	-0.000837
64	N	1.826829	2.696070	0.218050
65	C	3.153032	2.311938	-0.040019
66	C	3.419974	0.928218	-0.053308
67	C	4.702338	0.456768	-0.293137
68	C	5.749910	1.354058	-0.529705
69	C	5.488129	2.725431	-0.520266
70	C	4.206129	3.213118	-0.280720
71	C	7.143960	0.845548	-0.726921
72	F	7.167829	-0.344148	-1.375185
73	F	7.794044	0.647302	0.450794
74	F	7.909615	1.706297	-1.441846
75	F	1.354863	10.853657	-1.787238

76	C	0.234847	10.725308	-1.036729
77	F	0.359556	11.568617	0.016540
78	F	-0.786894	11.207086	-1.792583
79	H	-5.508317	5.387105	1.680689
80	H	-5.379259	2.967790	2.192927
81	H	-3.244523	1.717833	1.910147
82	H	-3.517048	6.629838	0.896253
83	H	-0.625106	2.076034	1.117645
84	H	-1.387249	7.517473	1.921328
85	H	-0.915096	9.854167	1.265480
86	H	0.875255	8.457195	-2.380671
87	H	0.400614	6.126393	-1.723099
88	H	1.205917	1.908379	0.404280
89	H	2.606144	0.232124	0.124820
90	H	4.886439	-0.612628	-0.301161
91	H	6.294223	3.426457	-0.709820
92	H	4.007224	4.273855	-0.281044
93	Cl	0.000000	0.000000	1.117645

XI. NMR Spectra

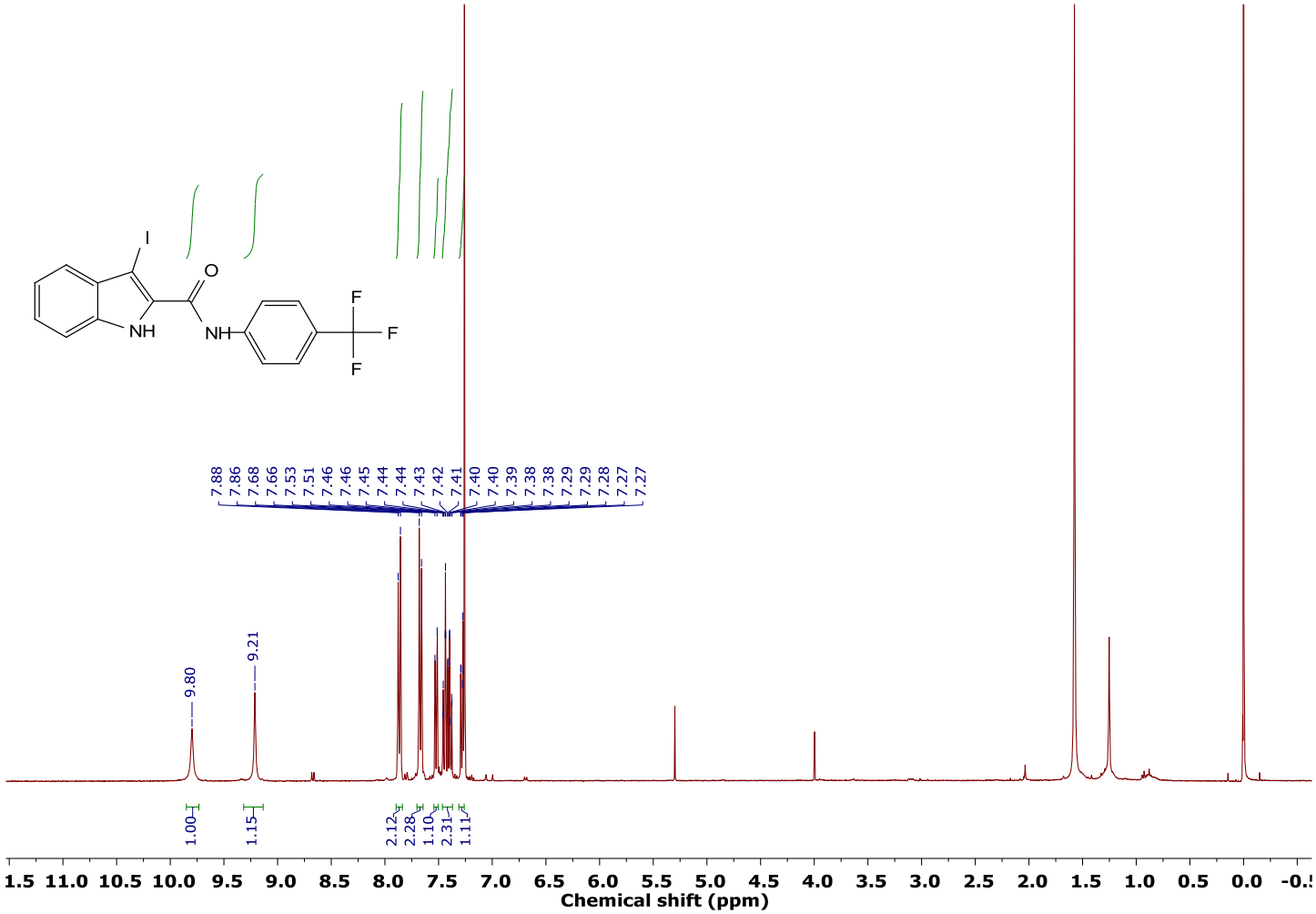

Fig. S50 ^{1}H NMR spectrum (400 MHz) of **9** in $CDCl_3$ at room temperature.

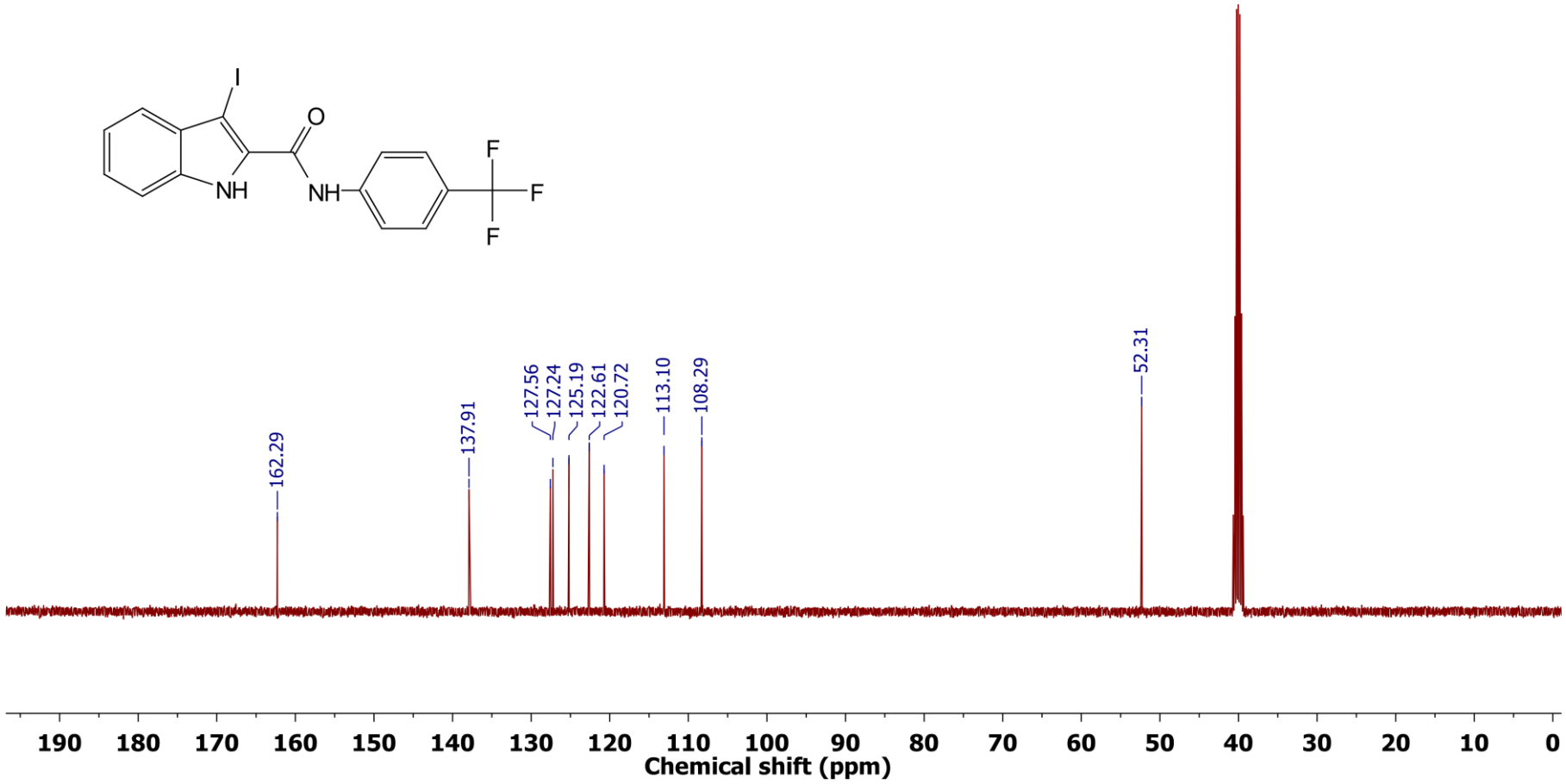

Fig. S51 ^{13}C NMR spectrum (400 MHz) of **9** in $CDCl_3$ at room temperature.

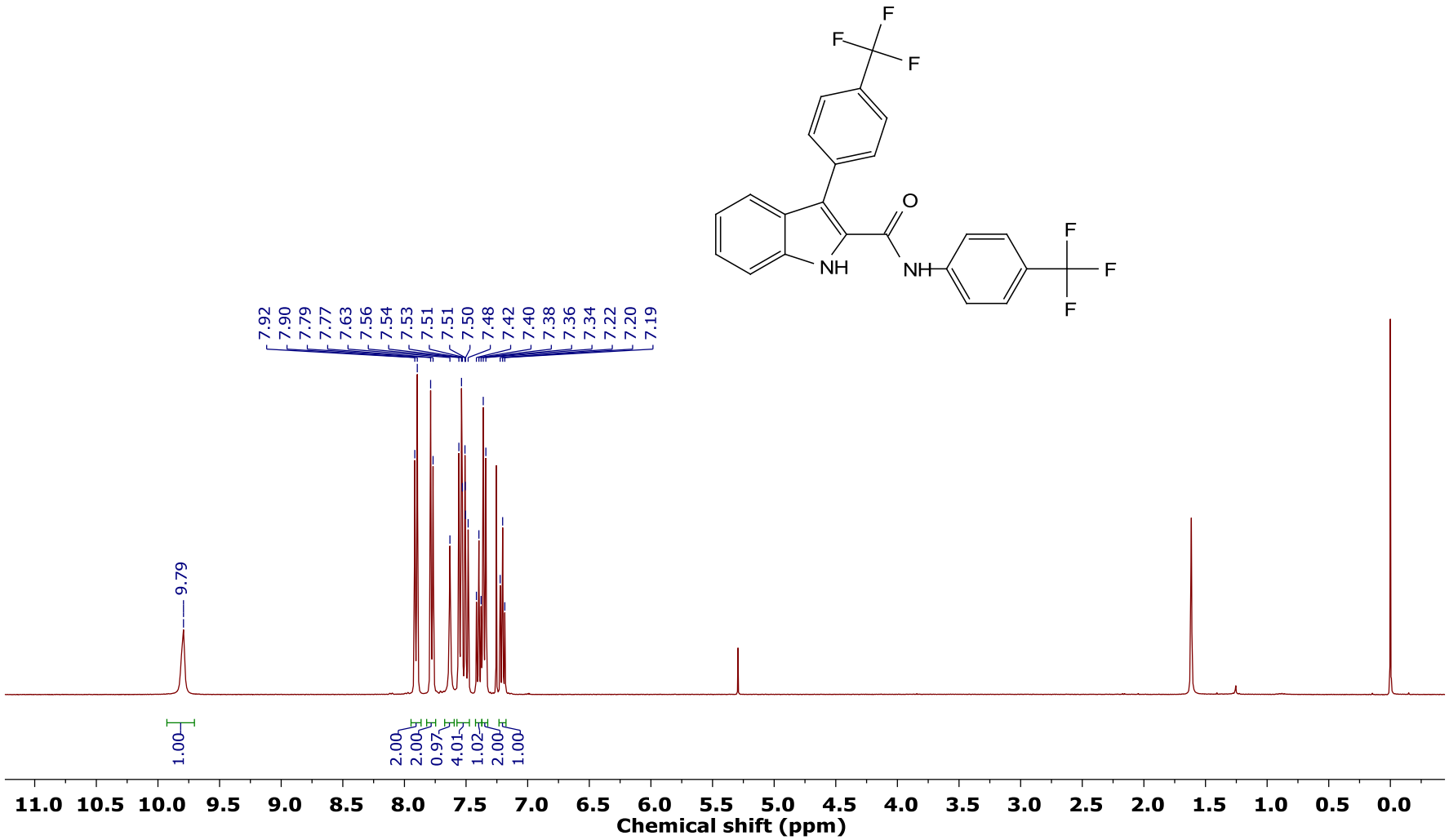

Fig. S52 ^{1}H NMR spectrum (400 MHz) of **5´** in $CDCl_3$ at room temperature.

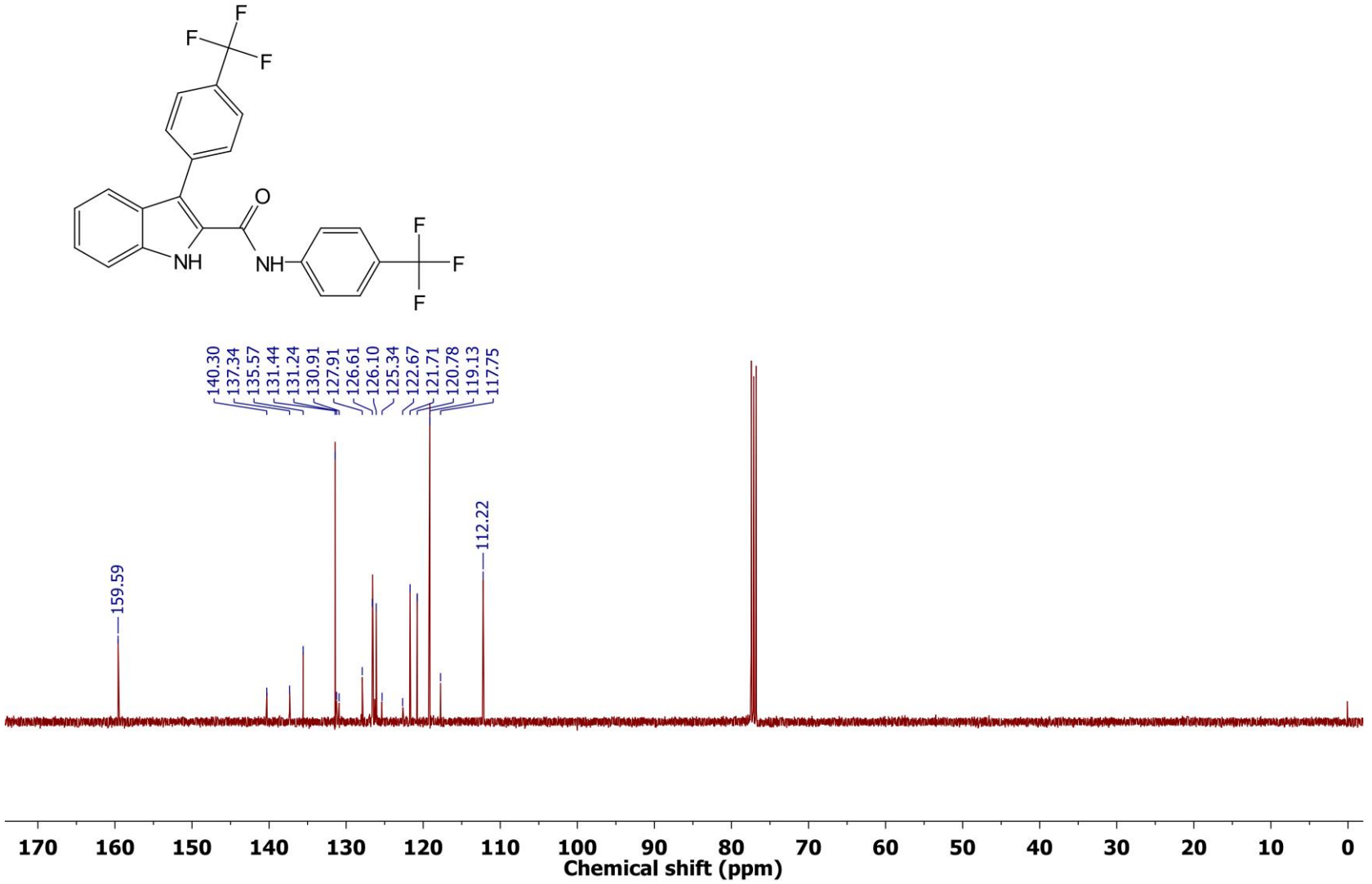

Fig. S53 ^{13}C NMR spectrum (101 MHz) of **5´** in $CDCl_3$ at room temperature.

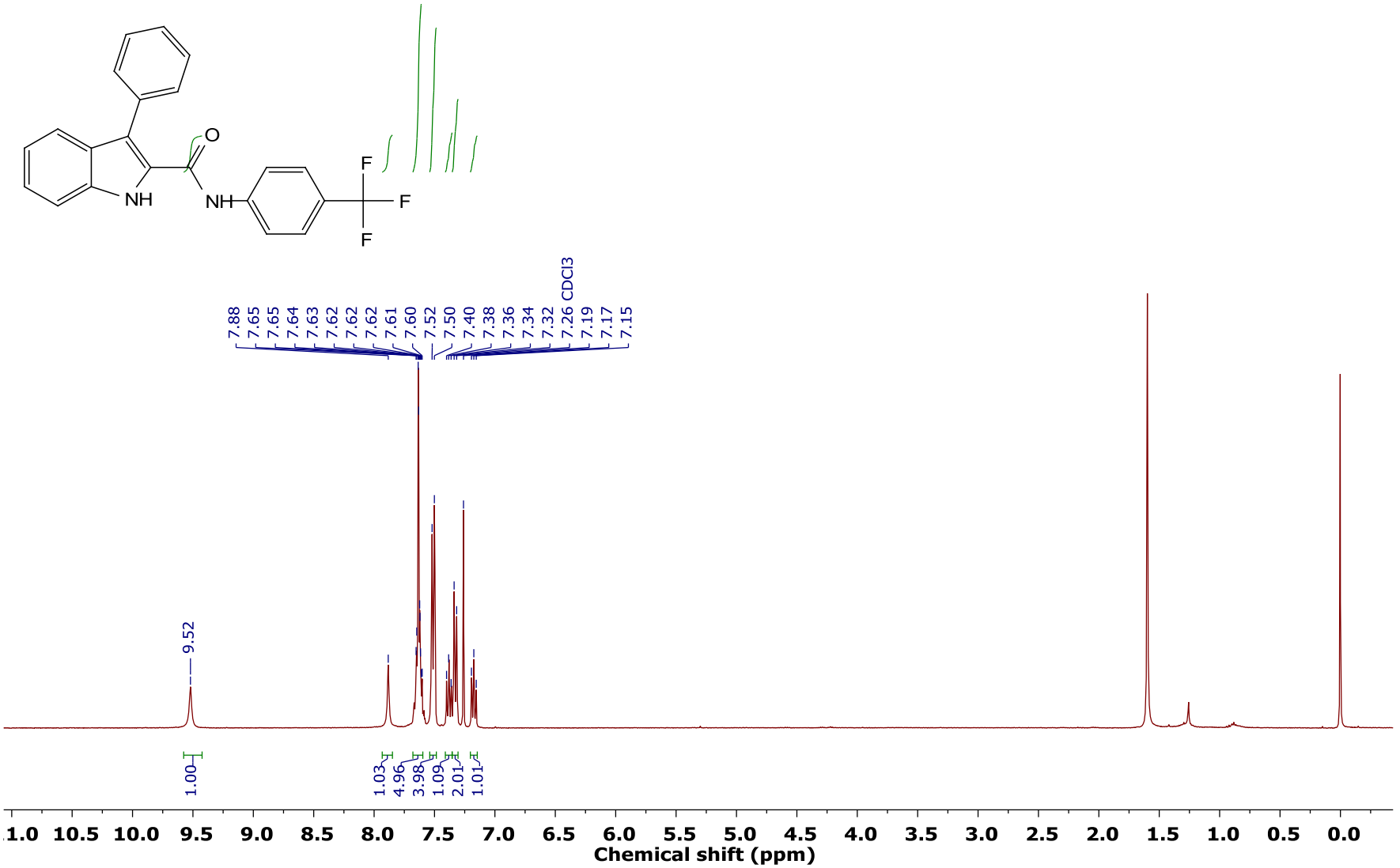

Fig. S54 ^{1}H NMR spectrum (400 MHz) of **2´** in $CDCl_3$ at room temperature.

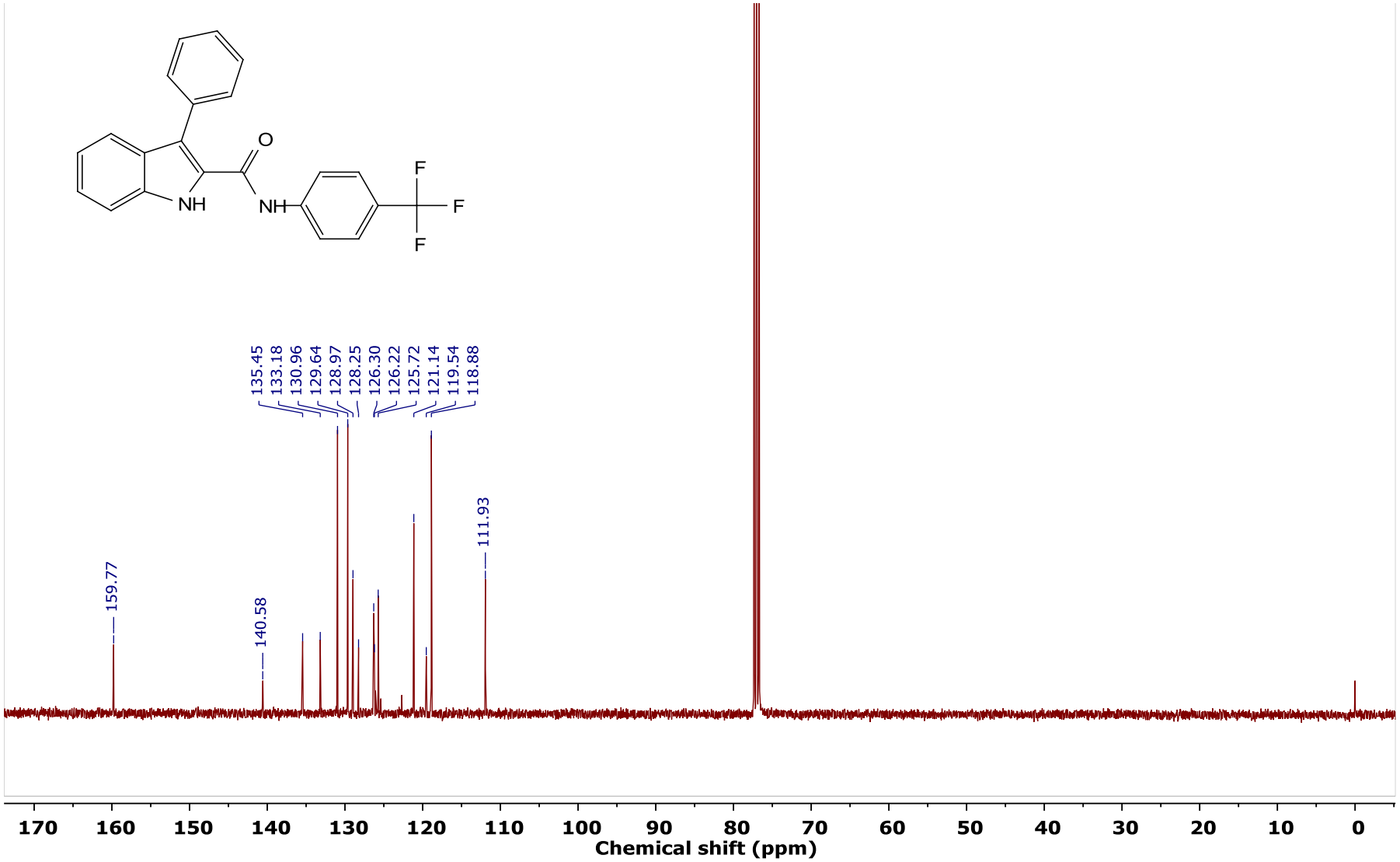

Fig. S55 ^{13}C NMR spectrum (101 MHz) of **2´** in $CDCl_3$ at room temperature.

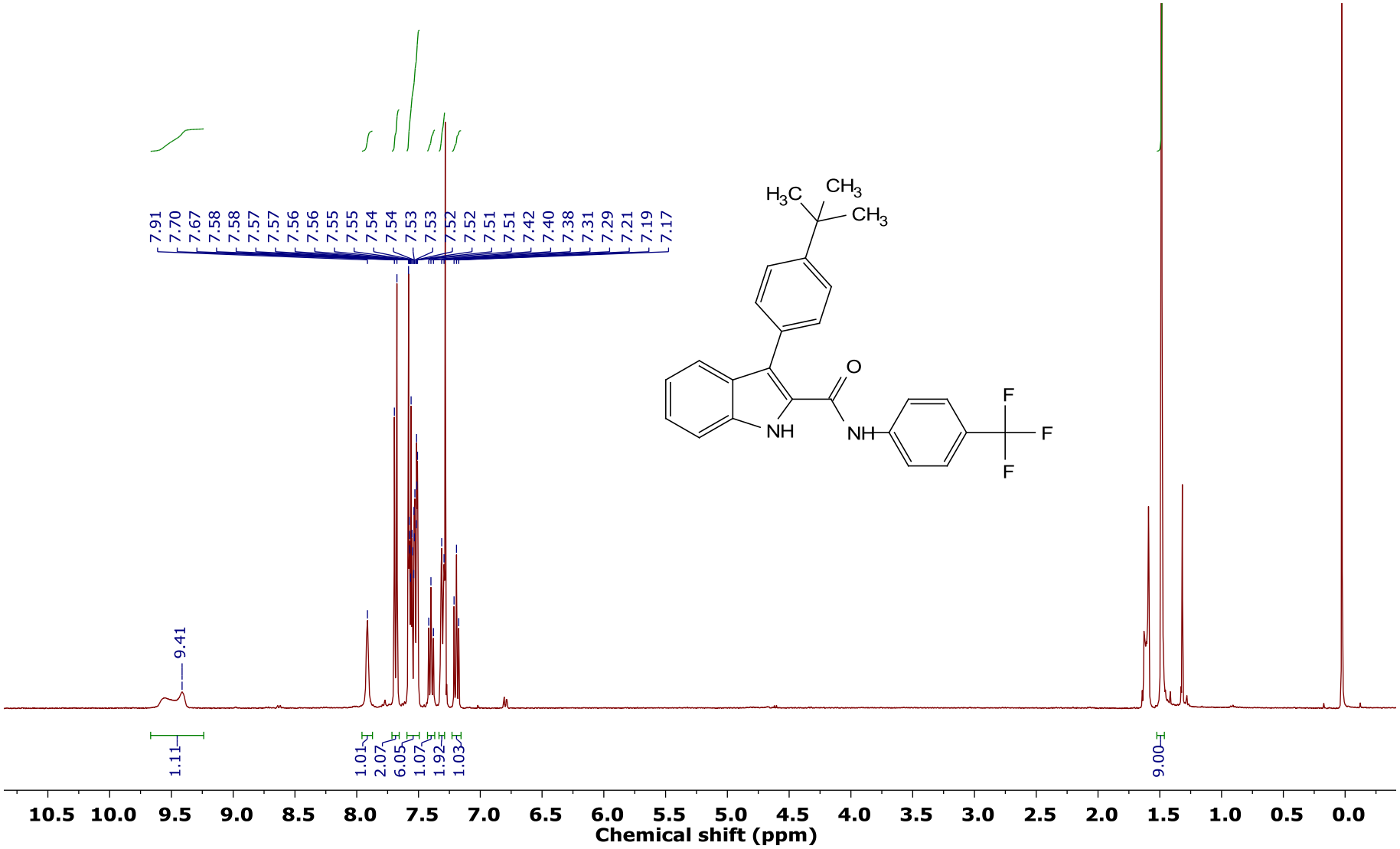

Fig. S56 ^{1}H NMR spectrum (400 MHz) of **4´** in $CDCl_3$ at room temperature.

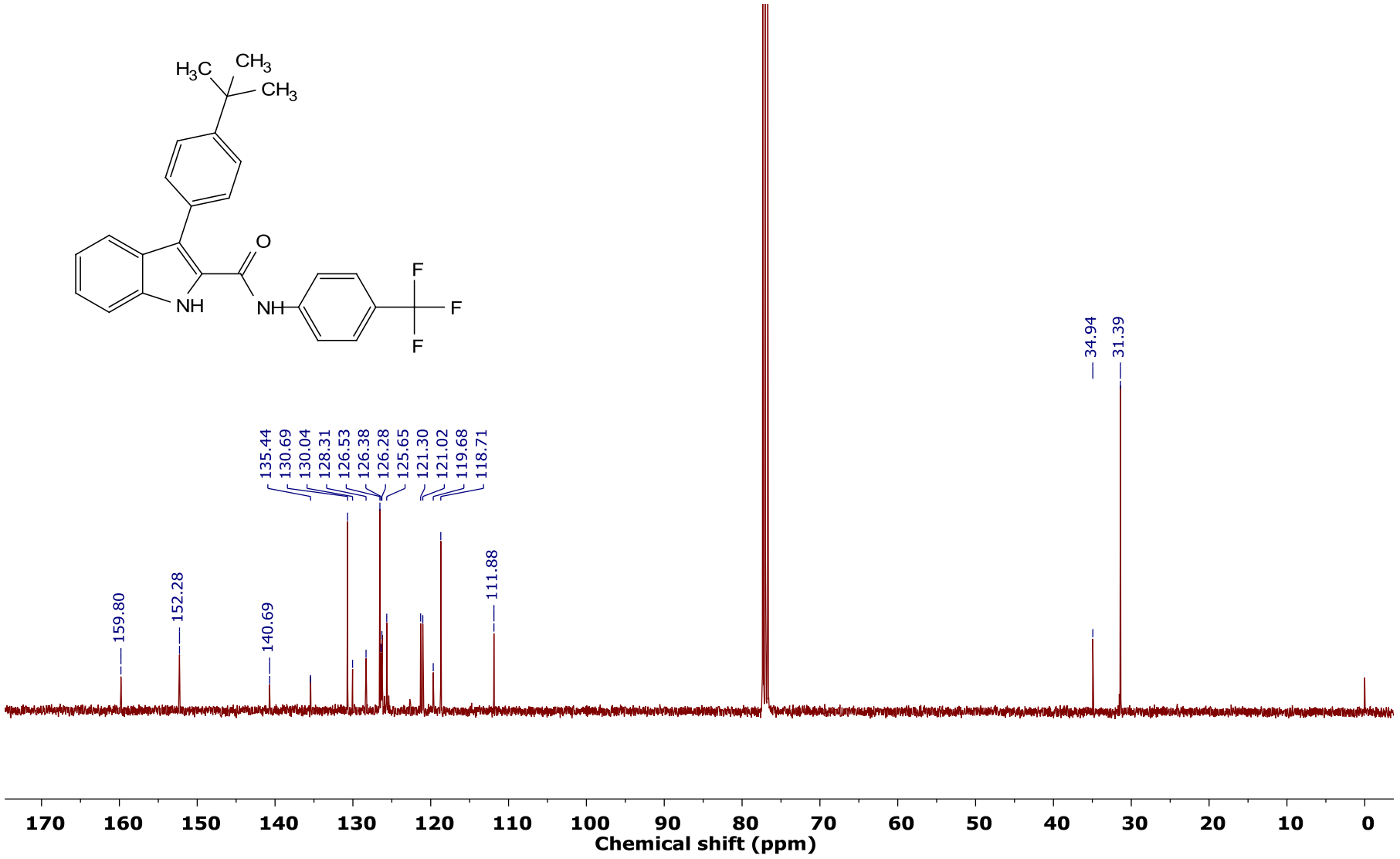

Fig. S57 ^{13}C NMR spectrum (101 MHz) of **4´** in $CDCl_3$ at room temperature.

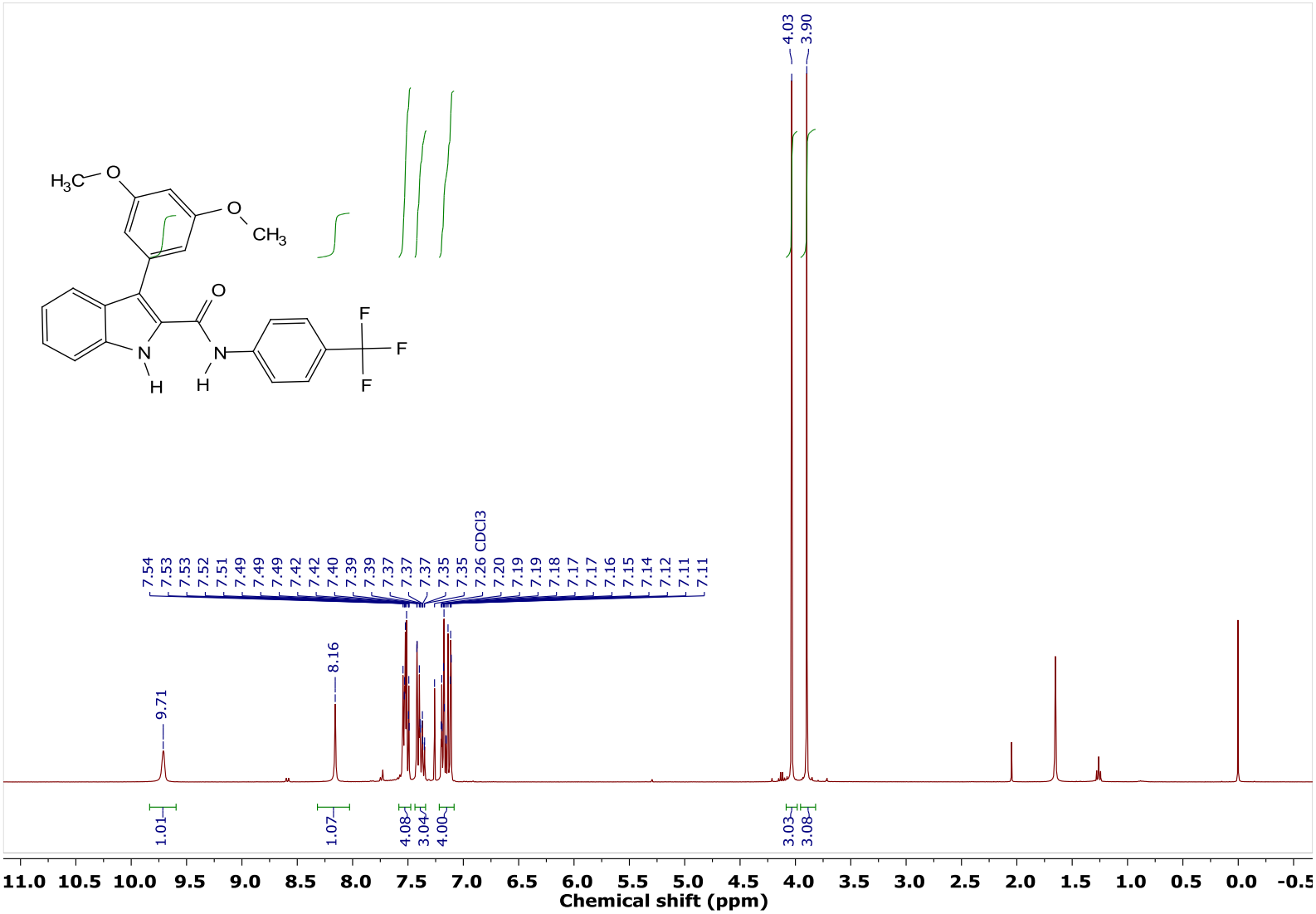

Fig. S58 ^{1}H NMR spectrum (400 MHz) of **3´** in $CDCl_3$ at room temperature.

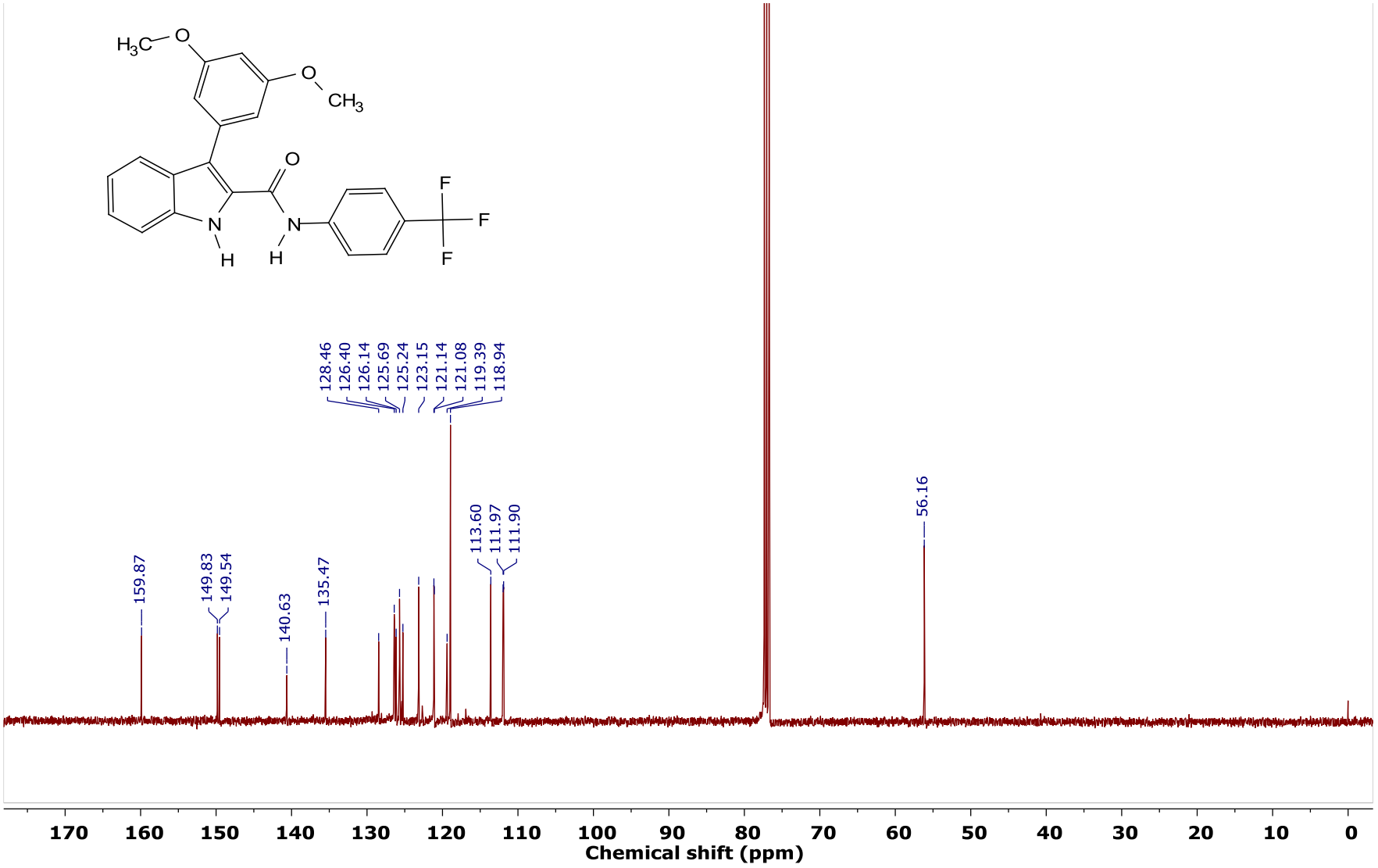

Fig. S59 ^{13}C NMR spectrum (101 MHz) of **3´** in $CDCl_3$ at room temperature.

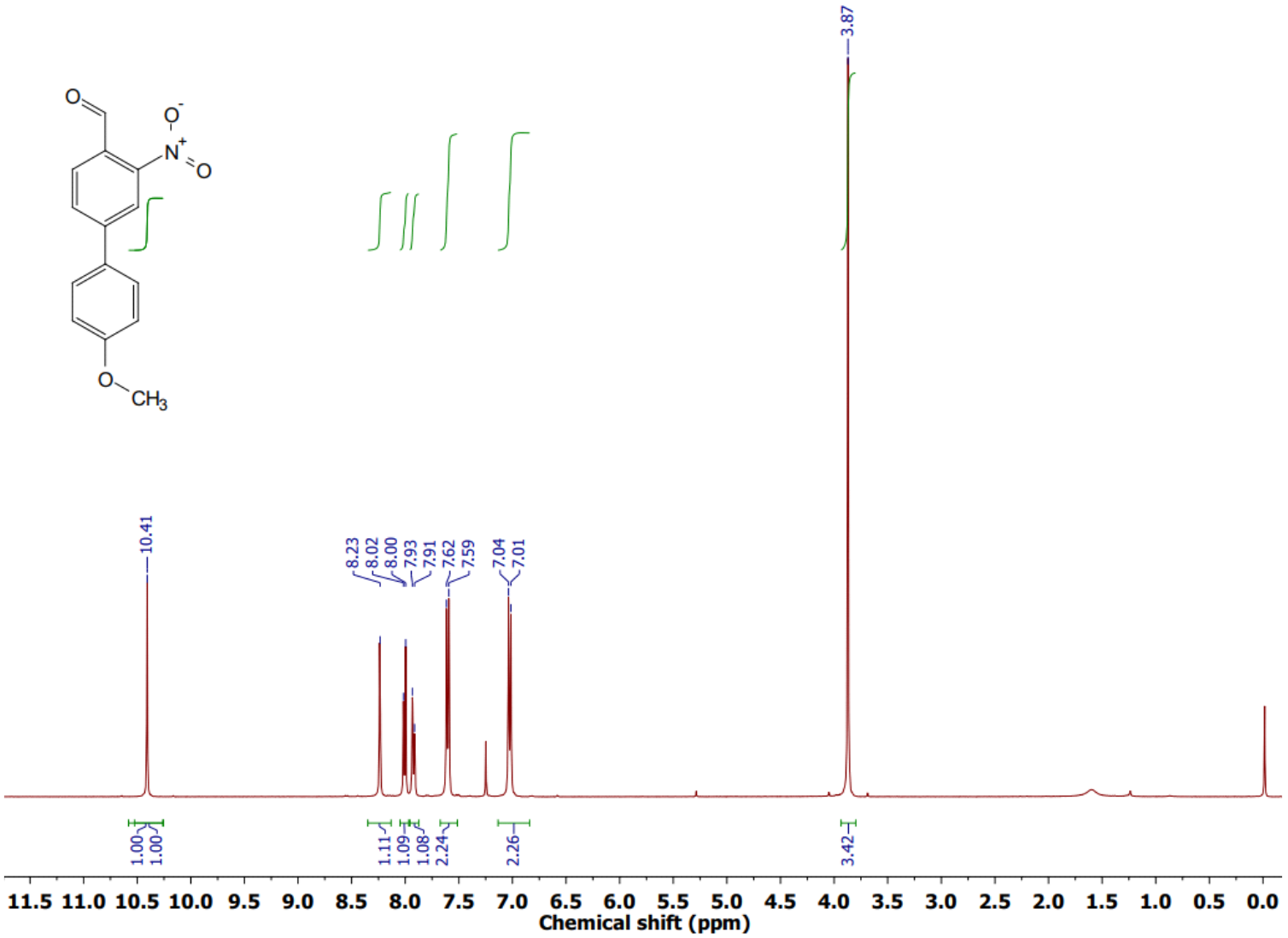

Fig. S60 ^{1}H NMR spectrum (400 MHz) of **10d** in $CDCl_3$ at room temperature.

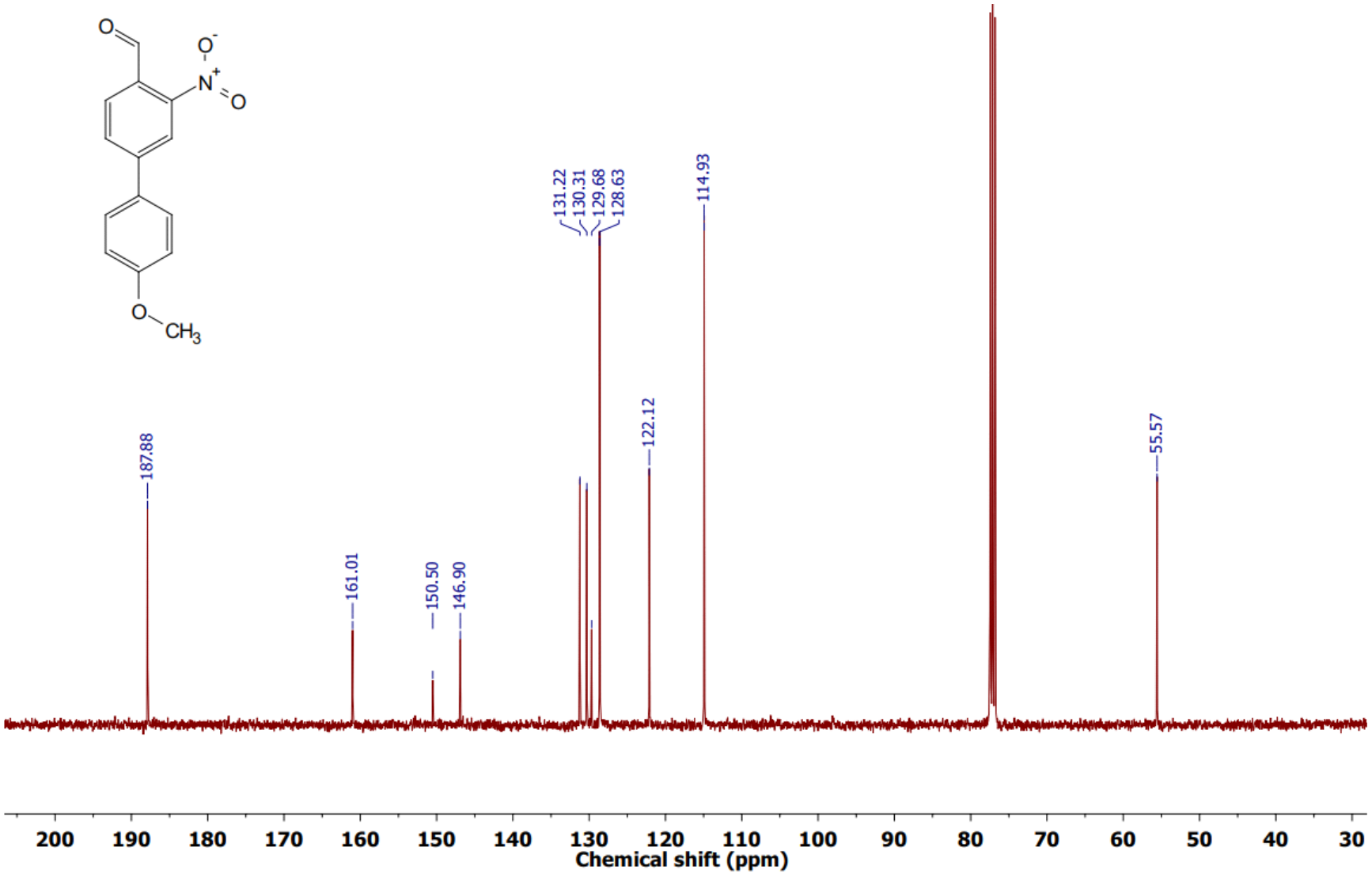

Fig. S61 ^{13}C NMR spectrum (101 MHz) of **10d** in $CDCl_3$ at room temperature.

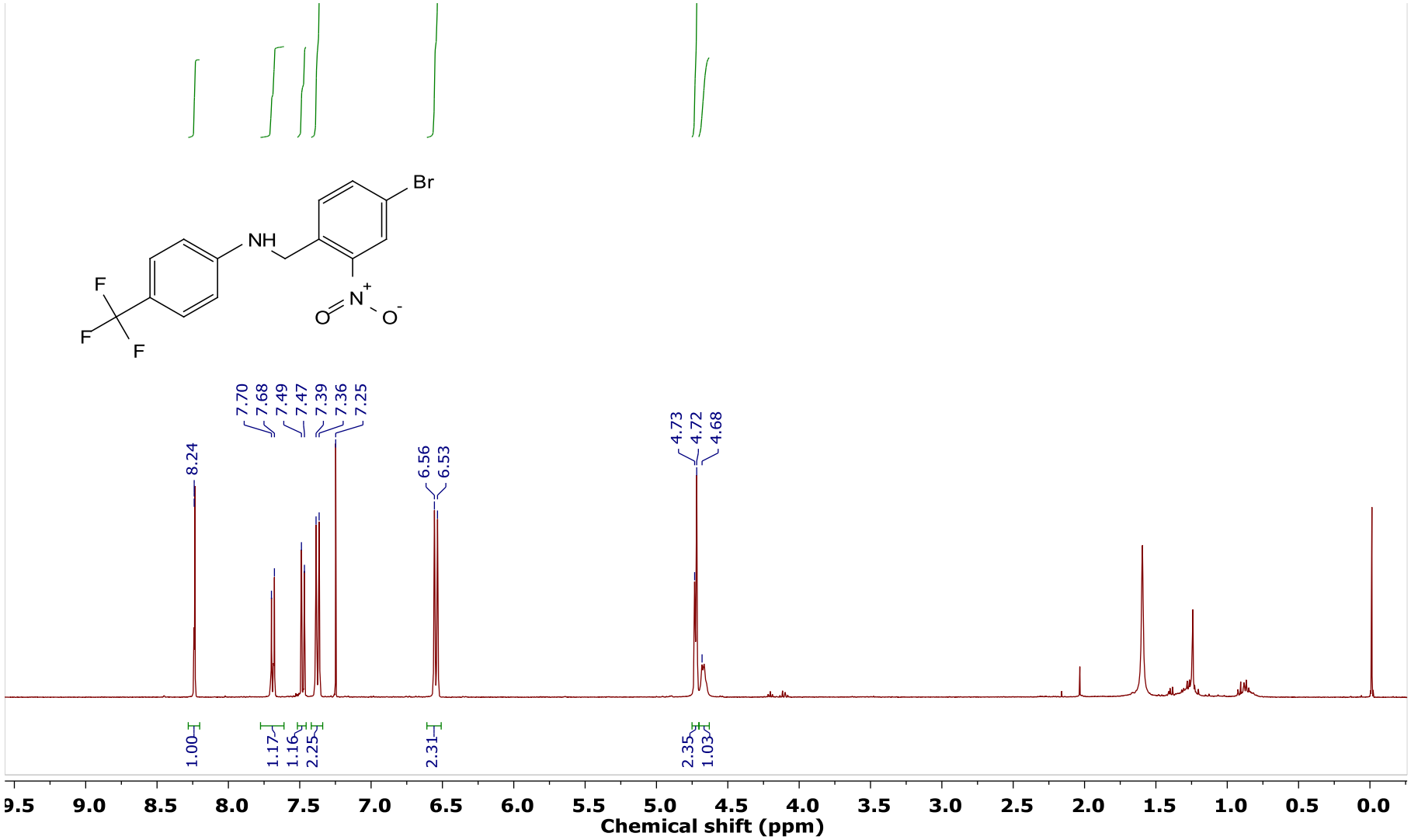

Fig. S62 ^{1}H NMR spectrum (400 MHz) of **6b** in $CDCl_3$ at room temperature.

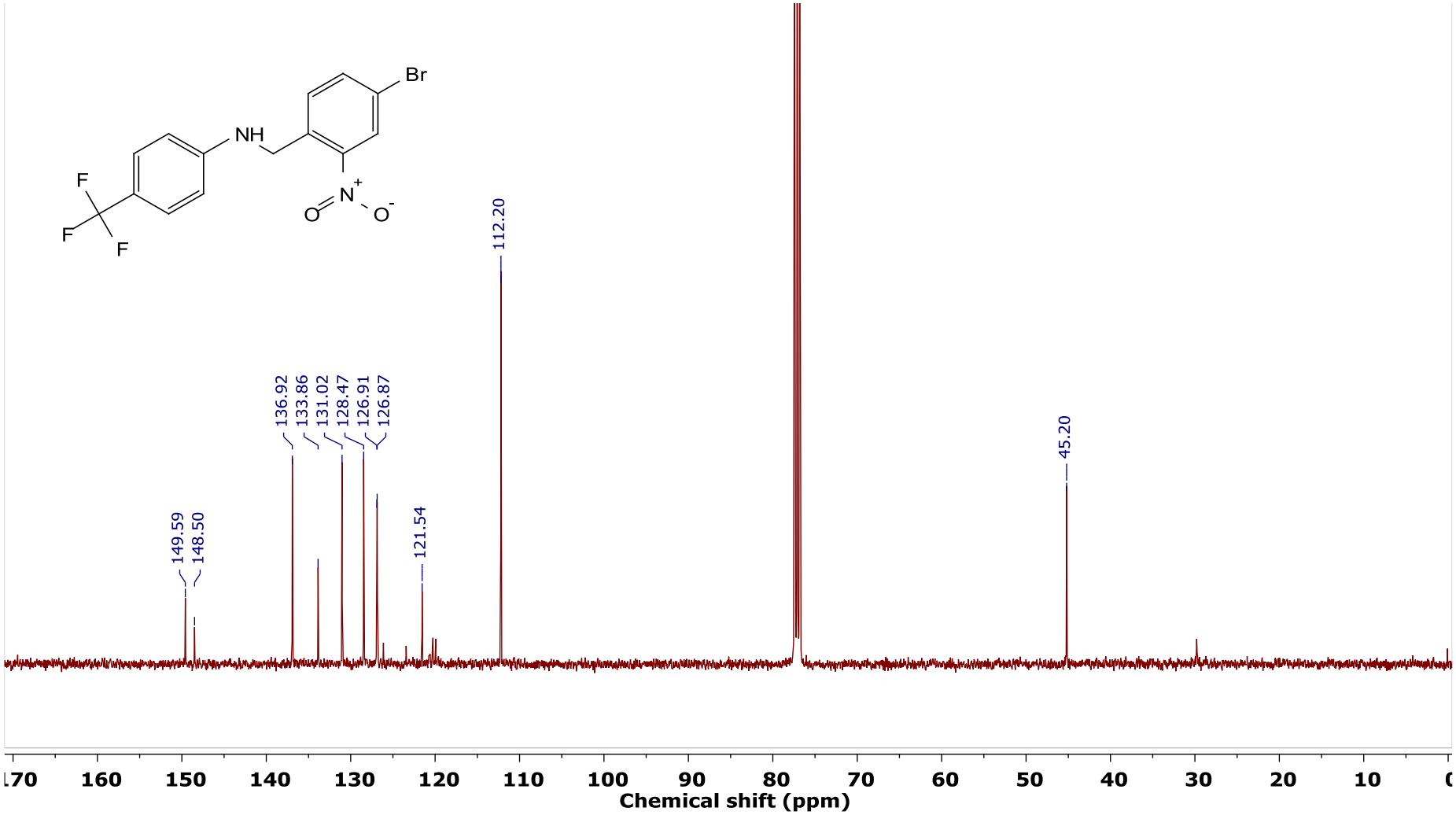

Fig. S63 ^{13}C NMR spectrum (101 MHz) of **6b** in $CDCl_3$ at room temperature.

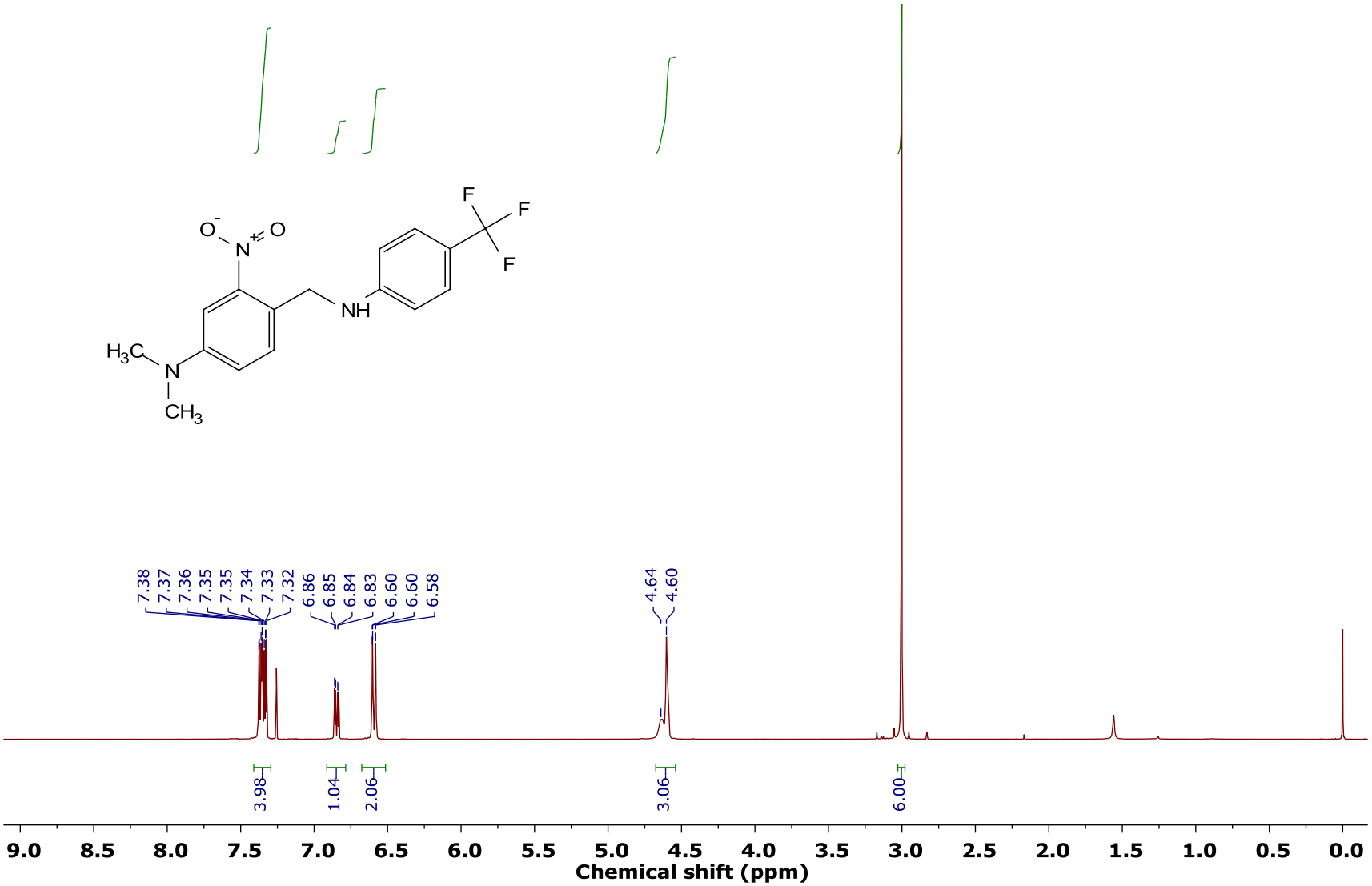

Fig. S64 ^{1}H NMR spectrum (400 MHz) of **6c** in $CDCl_3$ at room temperature.

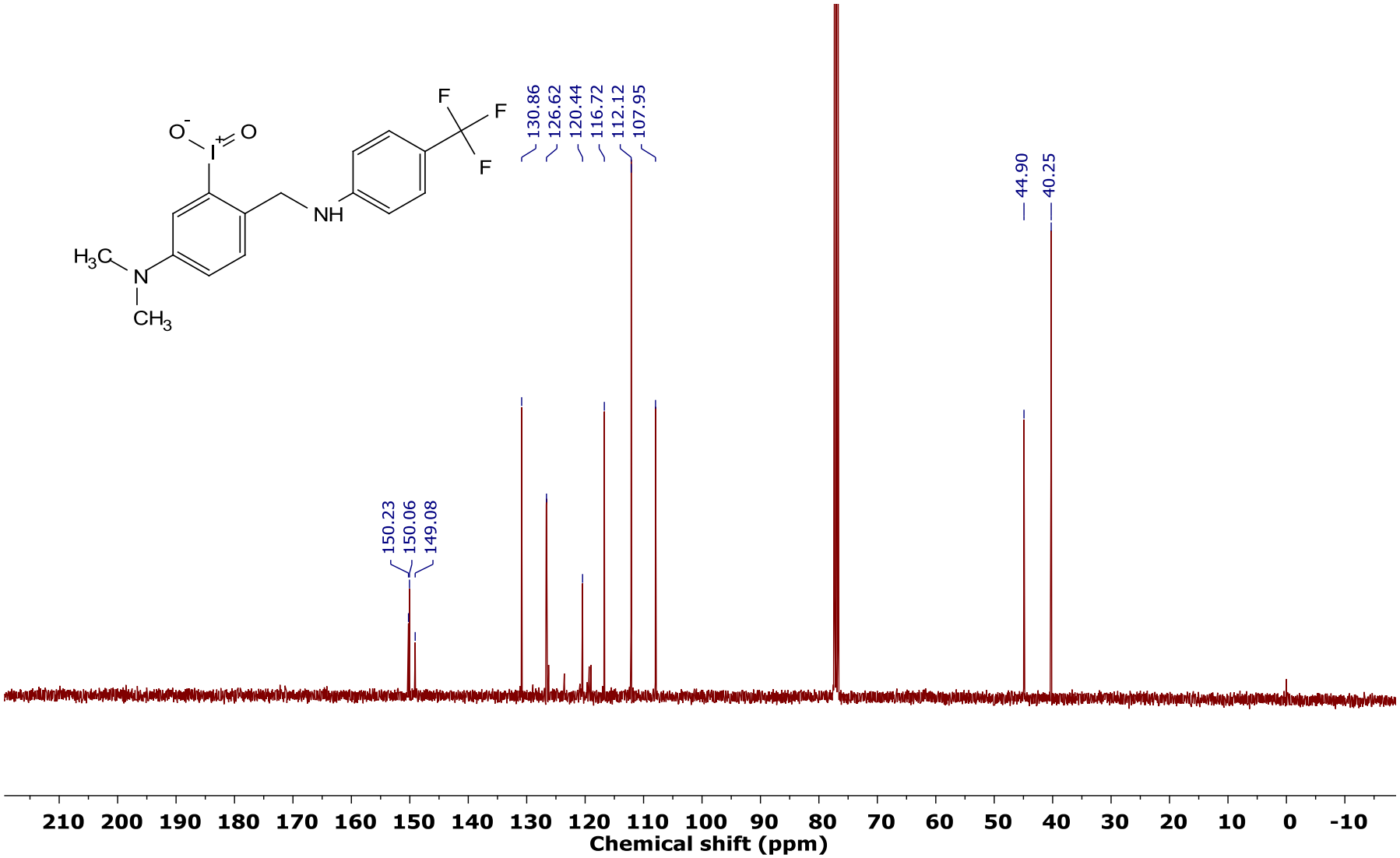

Fig. S65 ^{13}C NMR spectrum (101 MHz) of **6c** in $CDCl_3$ at room temperature.

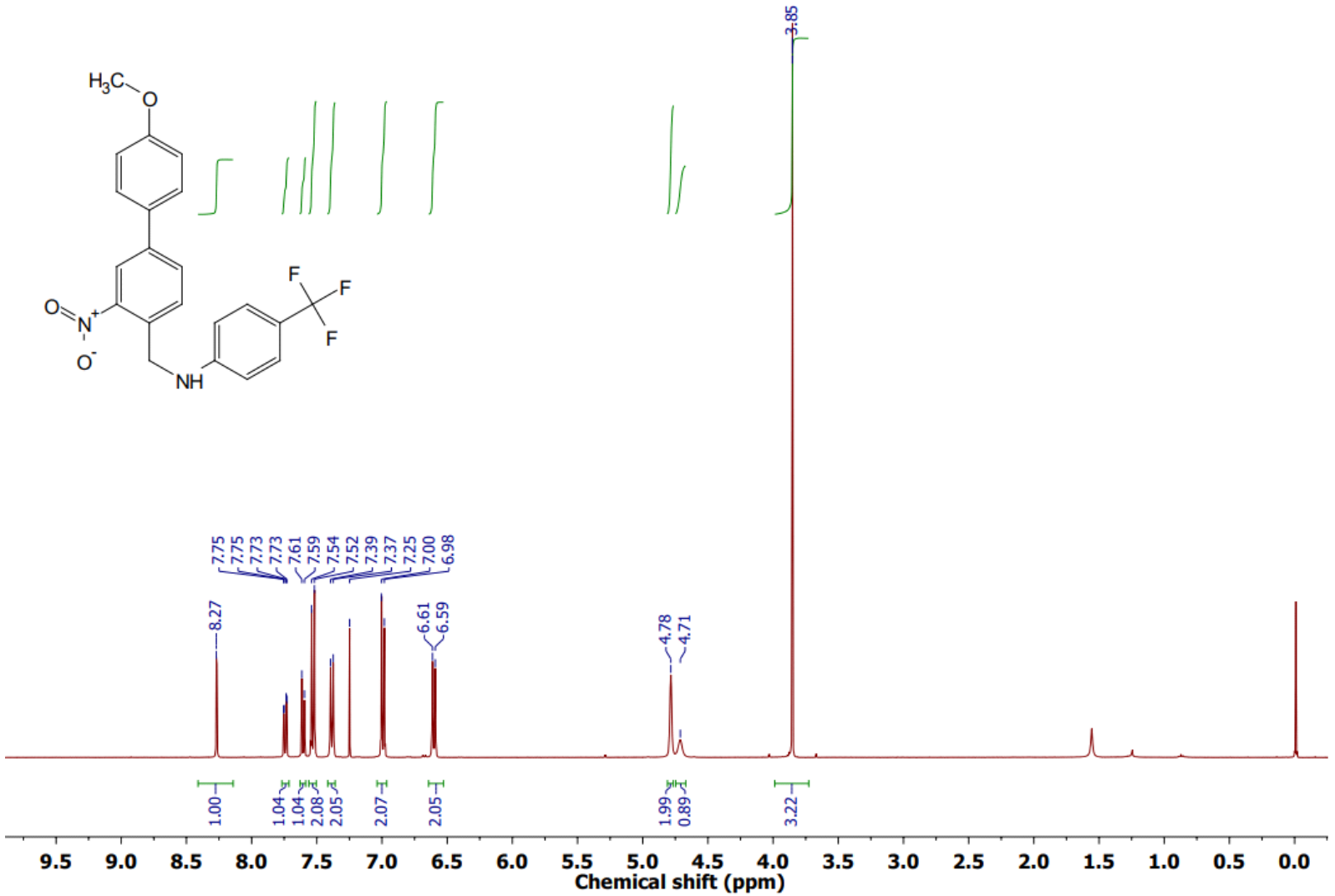

Fig. S66 ^{1}H NMR spectrum (400 MHz) of **6d** in $CDCl_3$ at room temperature.

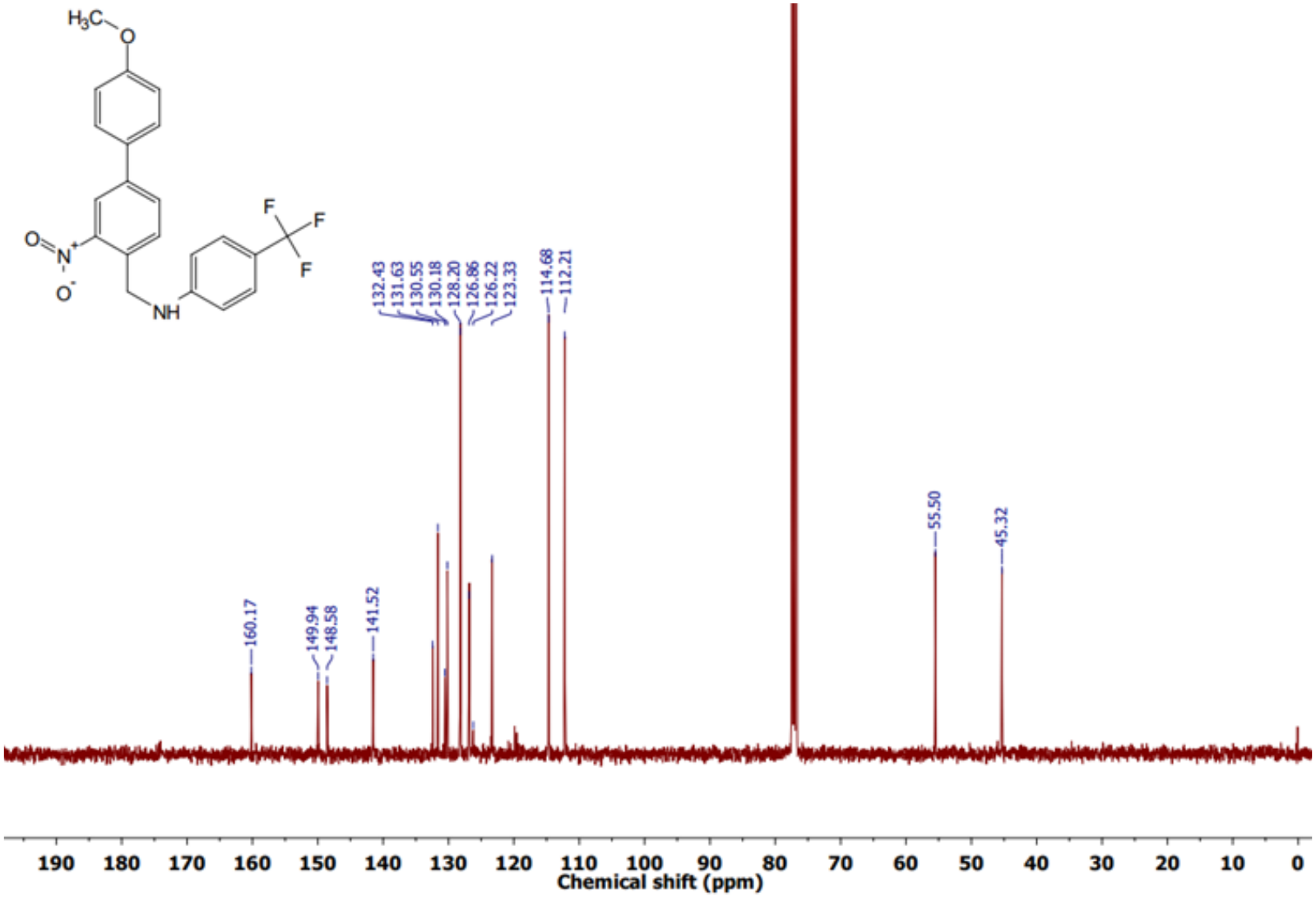

Fig. S67 ^{13}C NMR spectrum (101 MHz) of **6d** in $CDCl_3$ at room temperature.

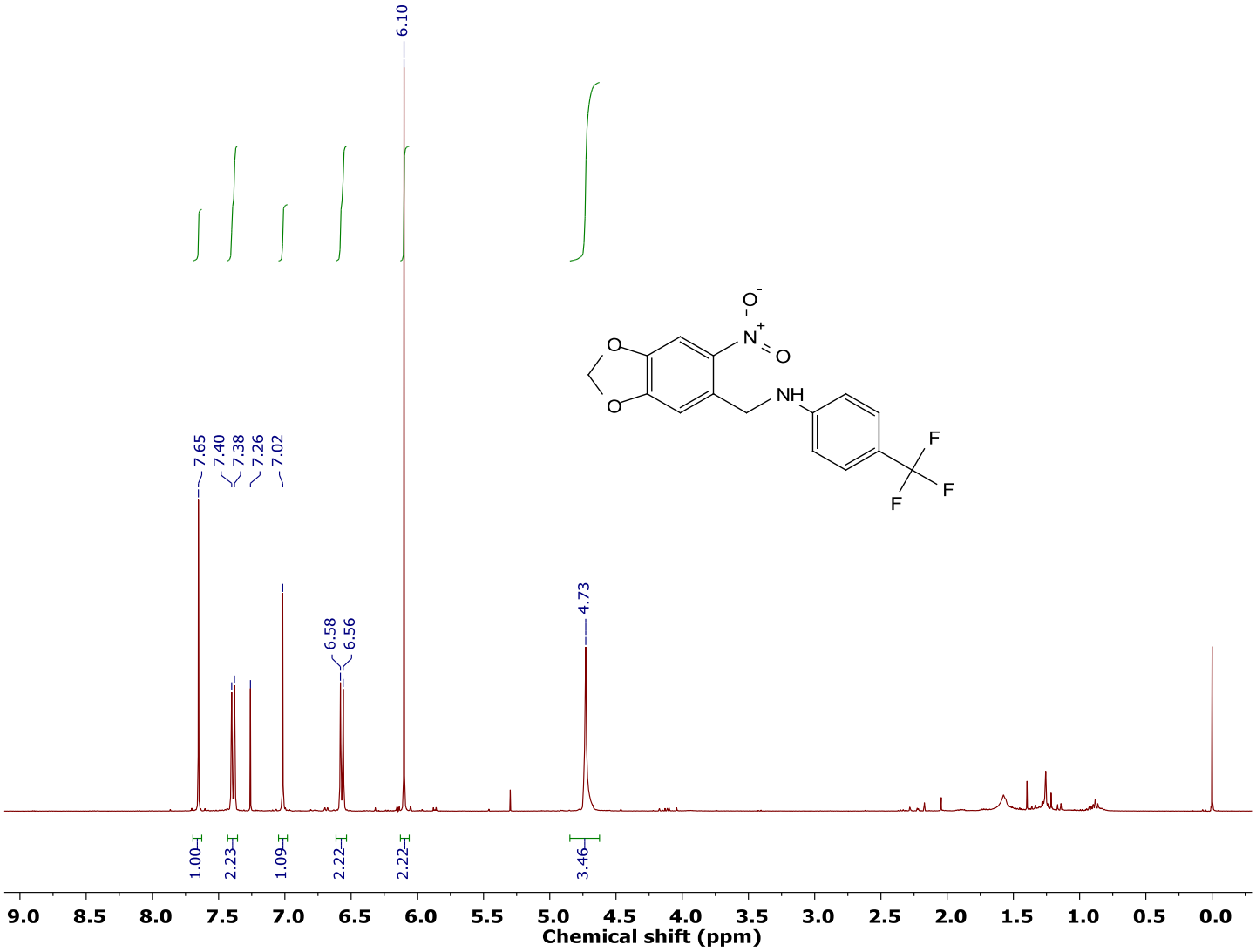

Fig. S68 ^{1}H NMR spectrum (400 MHz) of **6e** in $CDCl_3$ at room temperature.

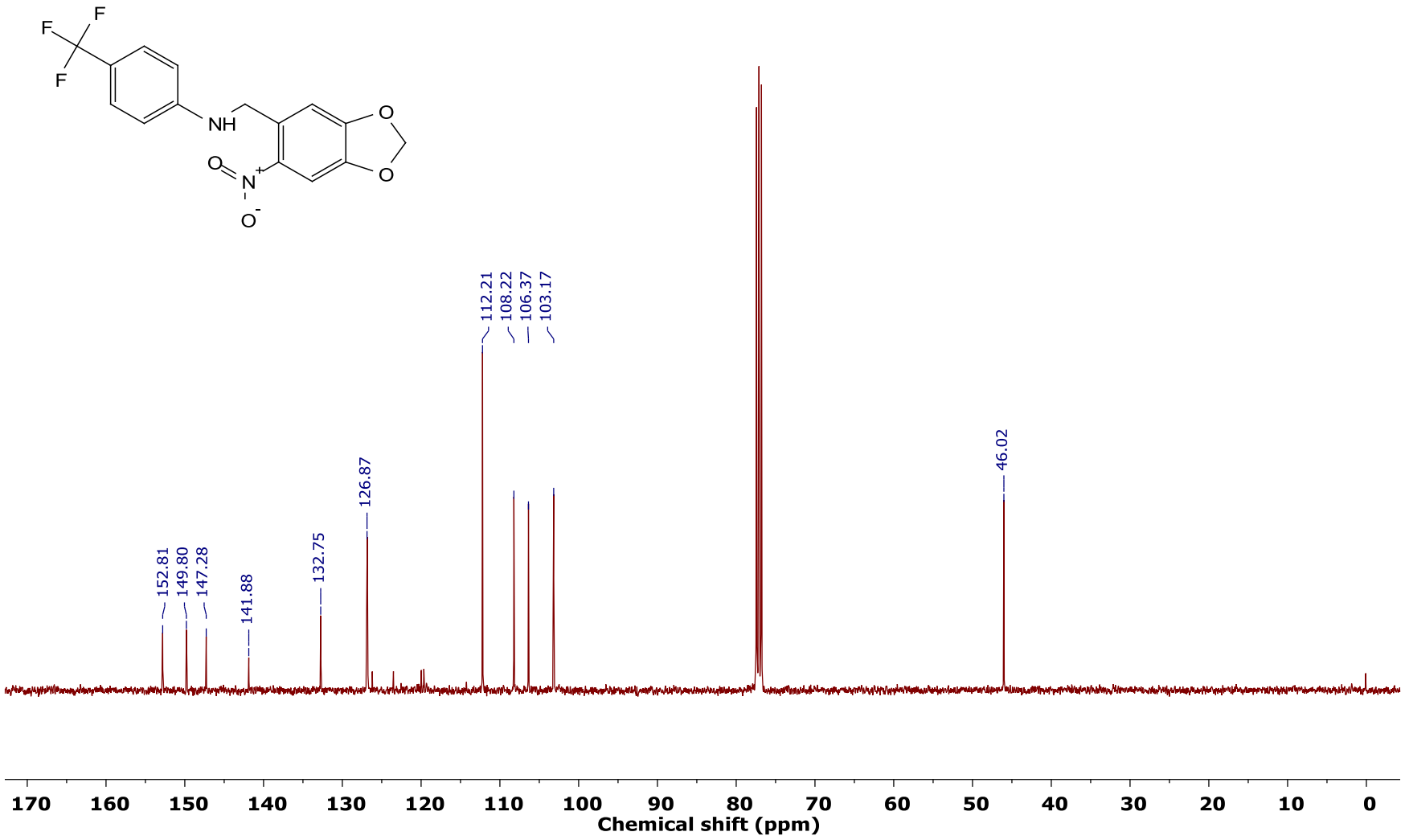

Fig. S69 ^{13}C NMR spectrum (101 MHz) of **6e** in $CDCl_3$ at room temperature.

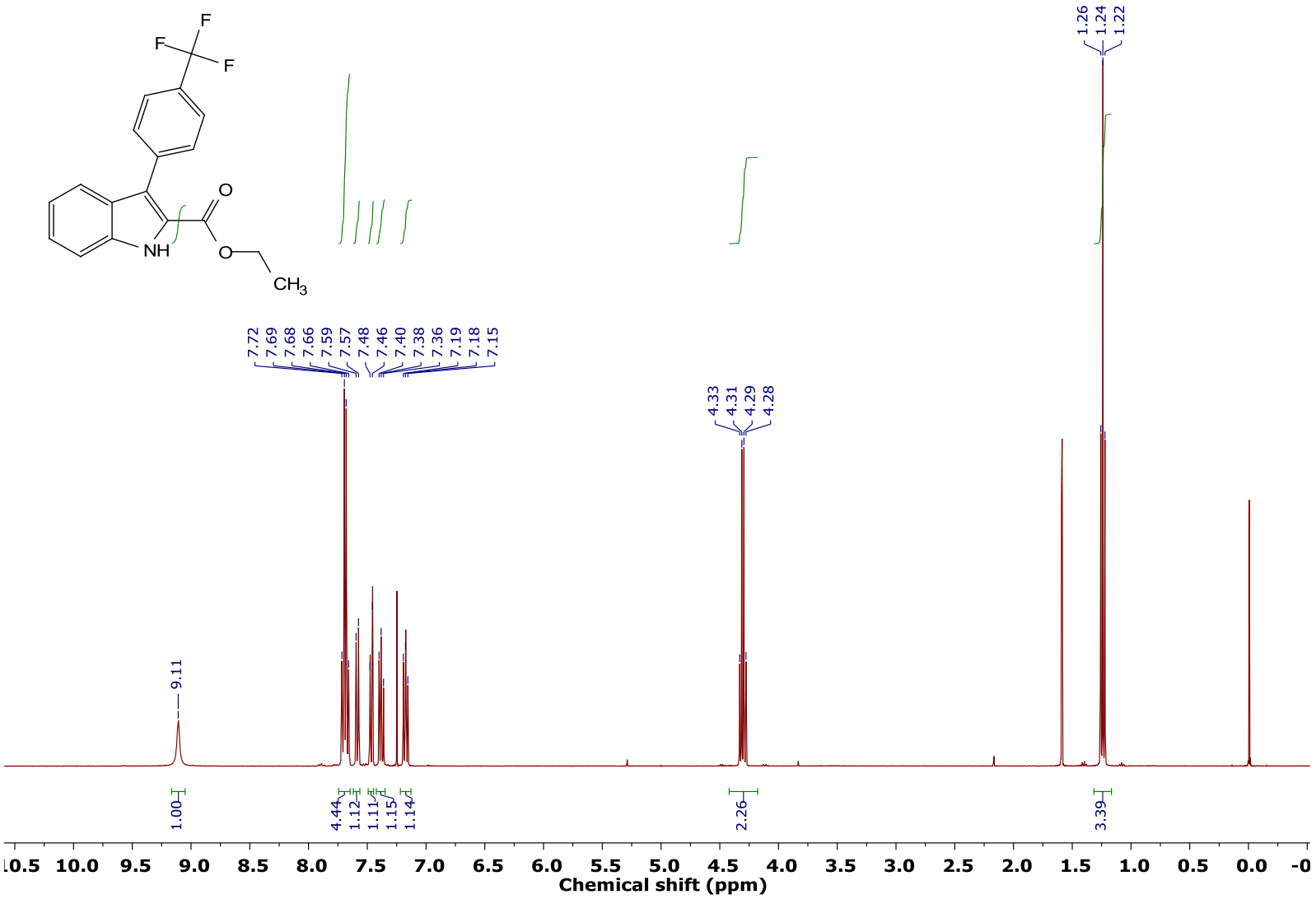

Fig. S70 ^{1}H NMR spectrum (400 MHz) of **14** in $CDCl_3$ at room temperature.

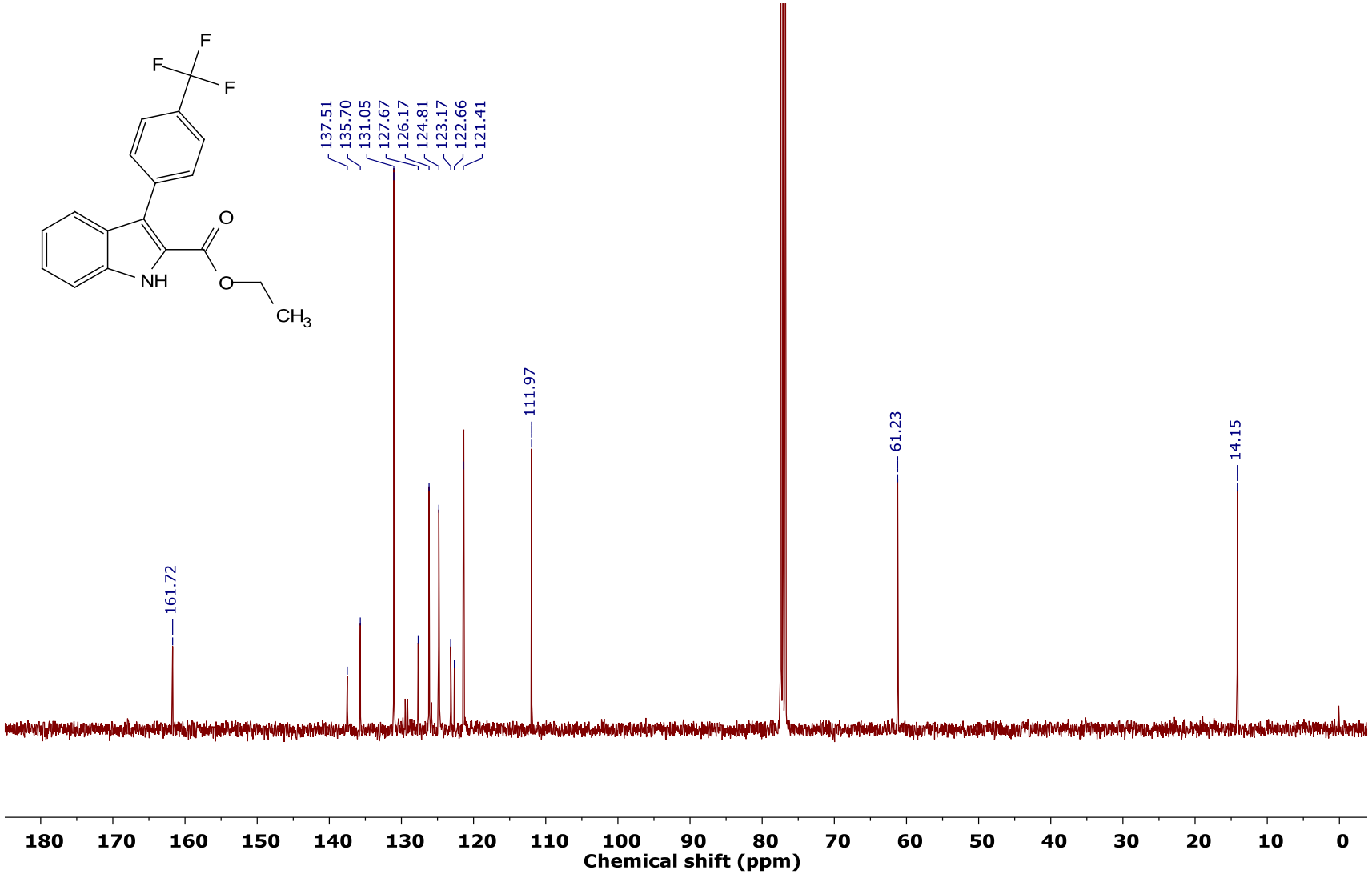

Fig. S71 ^{13}C NMR spectrum (101 MHz) of **14** in $CDCl_3$ at room temperature.

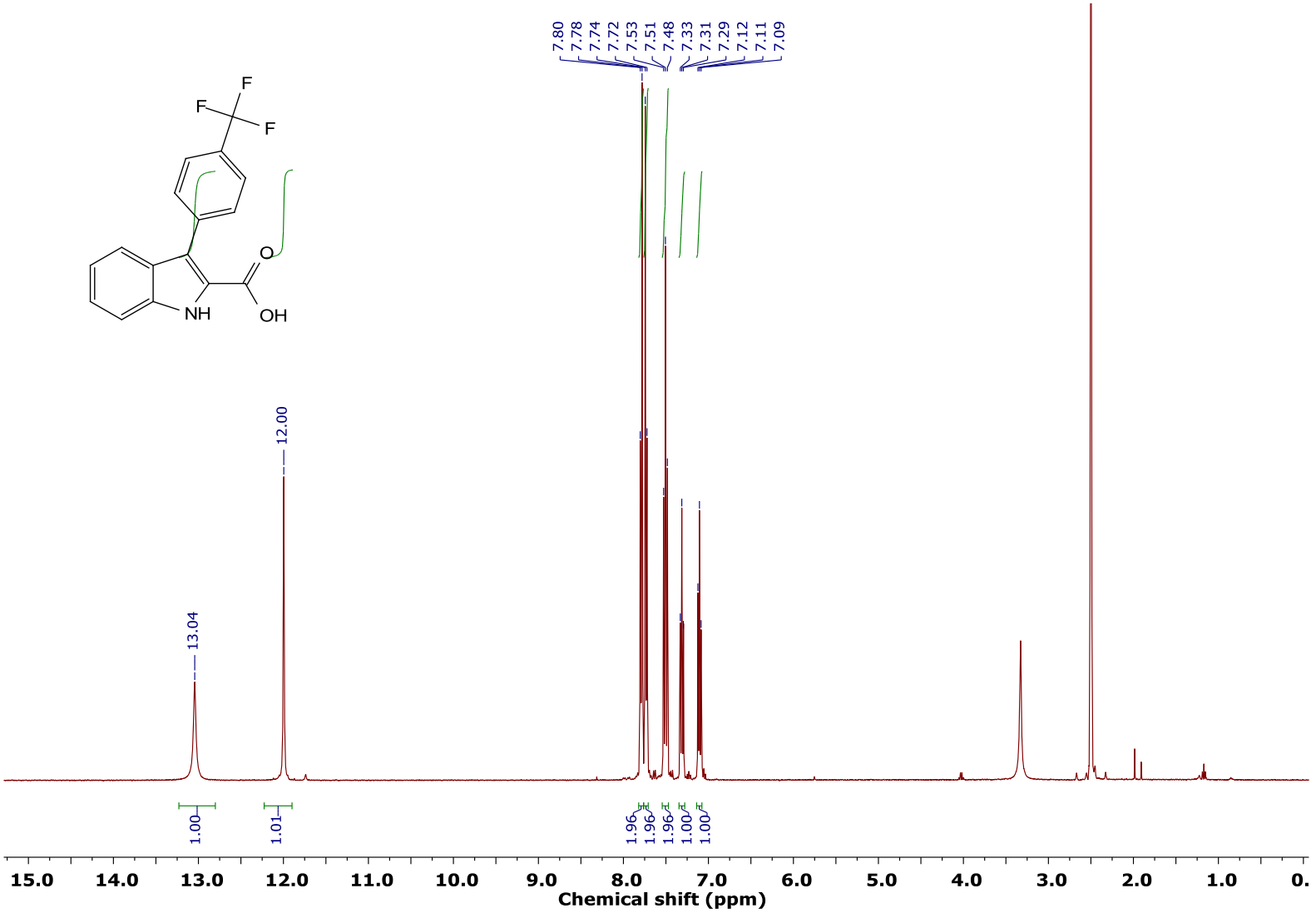

Fig. S72 ^{1}H NMR spectrum (400 MHz) of **15** in DMSO-d_6 at room temperature.

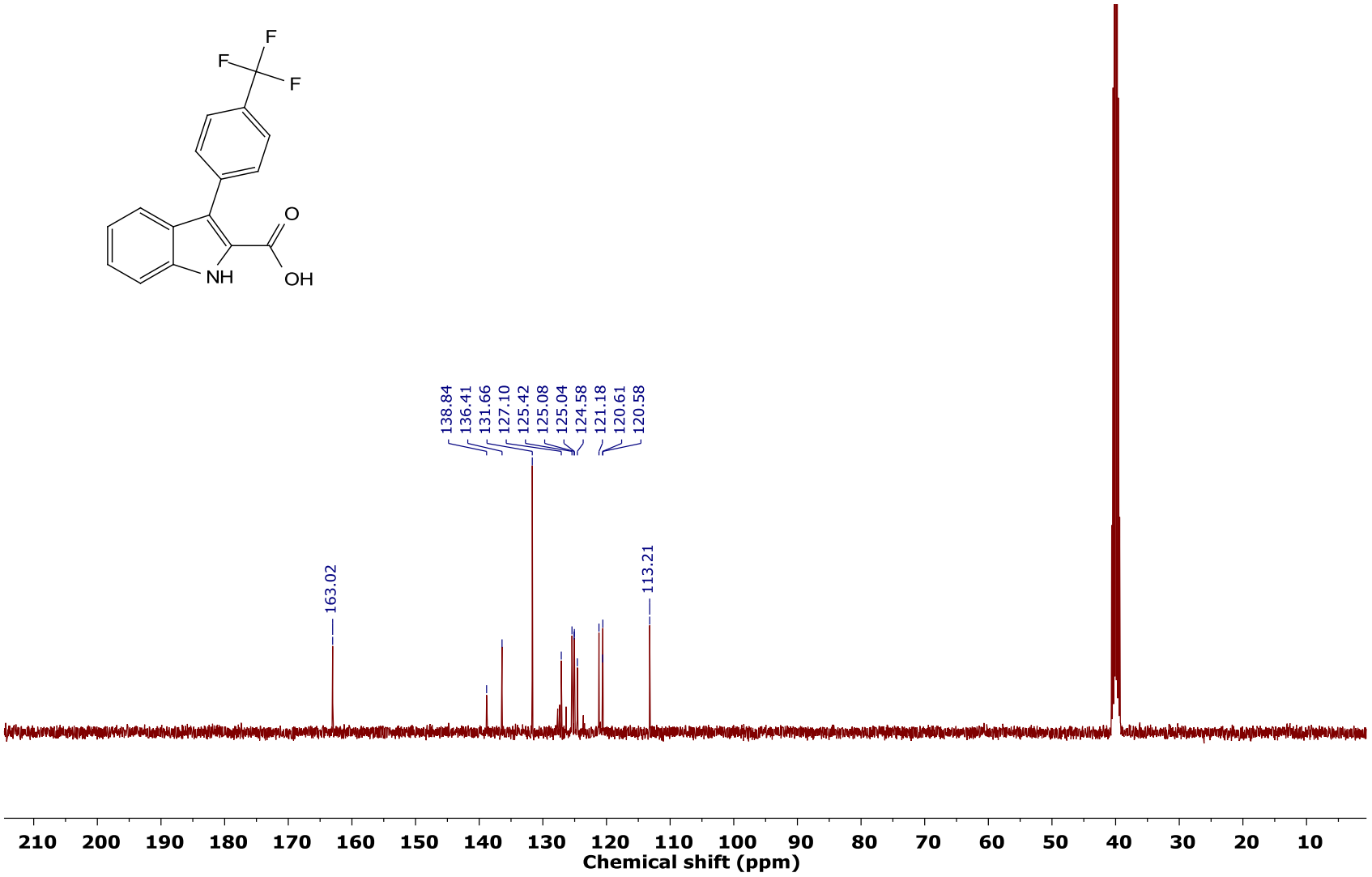

Fig. S73 ^{13}C NMR spectrum (101 MHz) of **15** in DMSO-d_6 at room temperature.

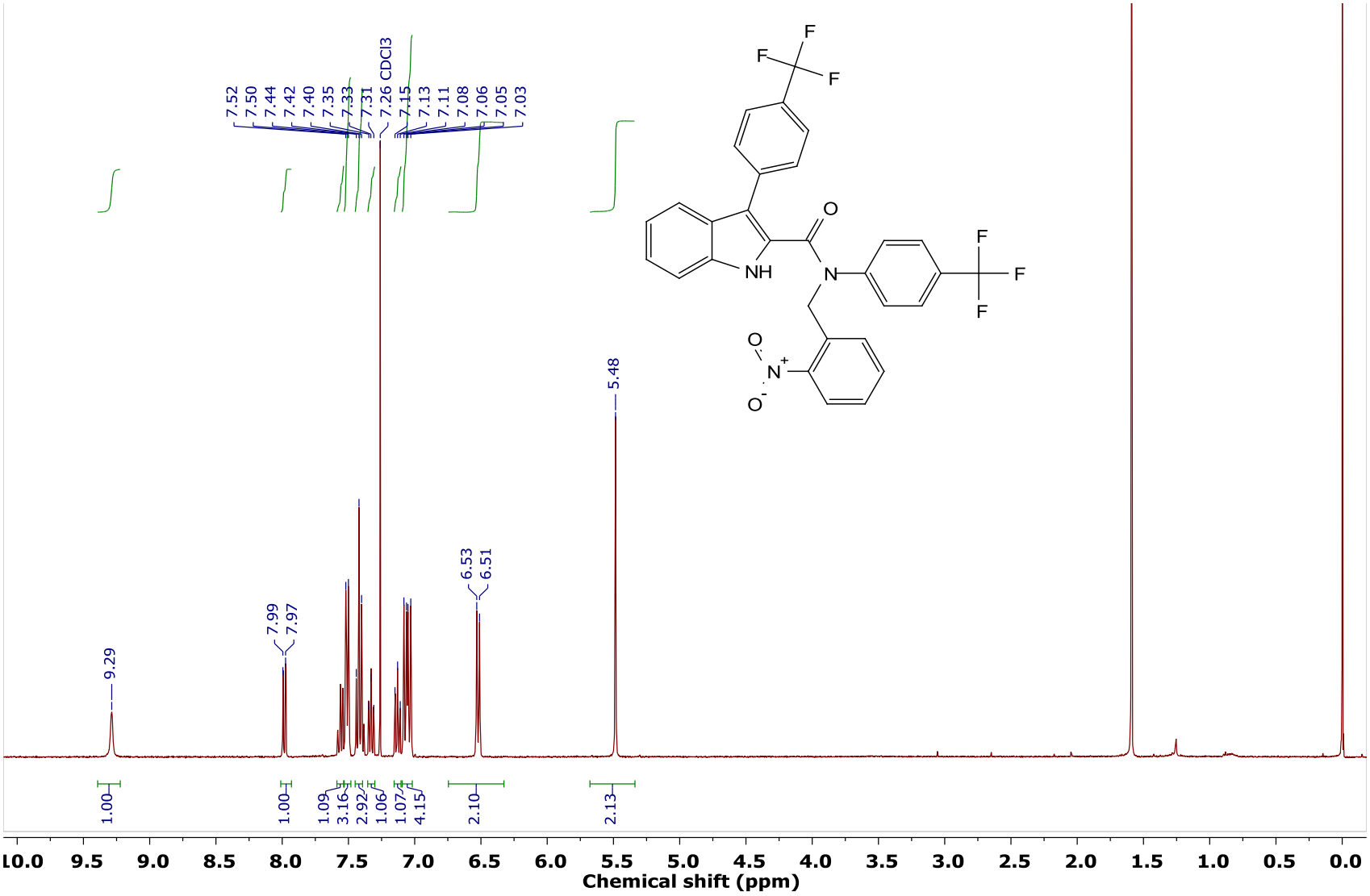

Fig. S74 ^{1}H NMR spectrum (400 MHz) of **5a** in $CDCl_3$ at room temperature.

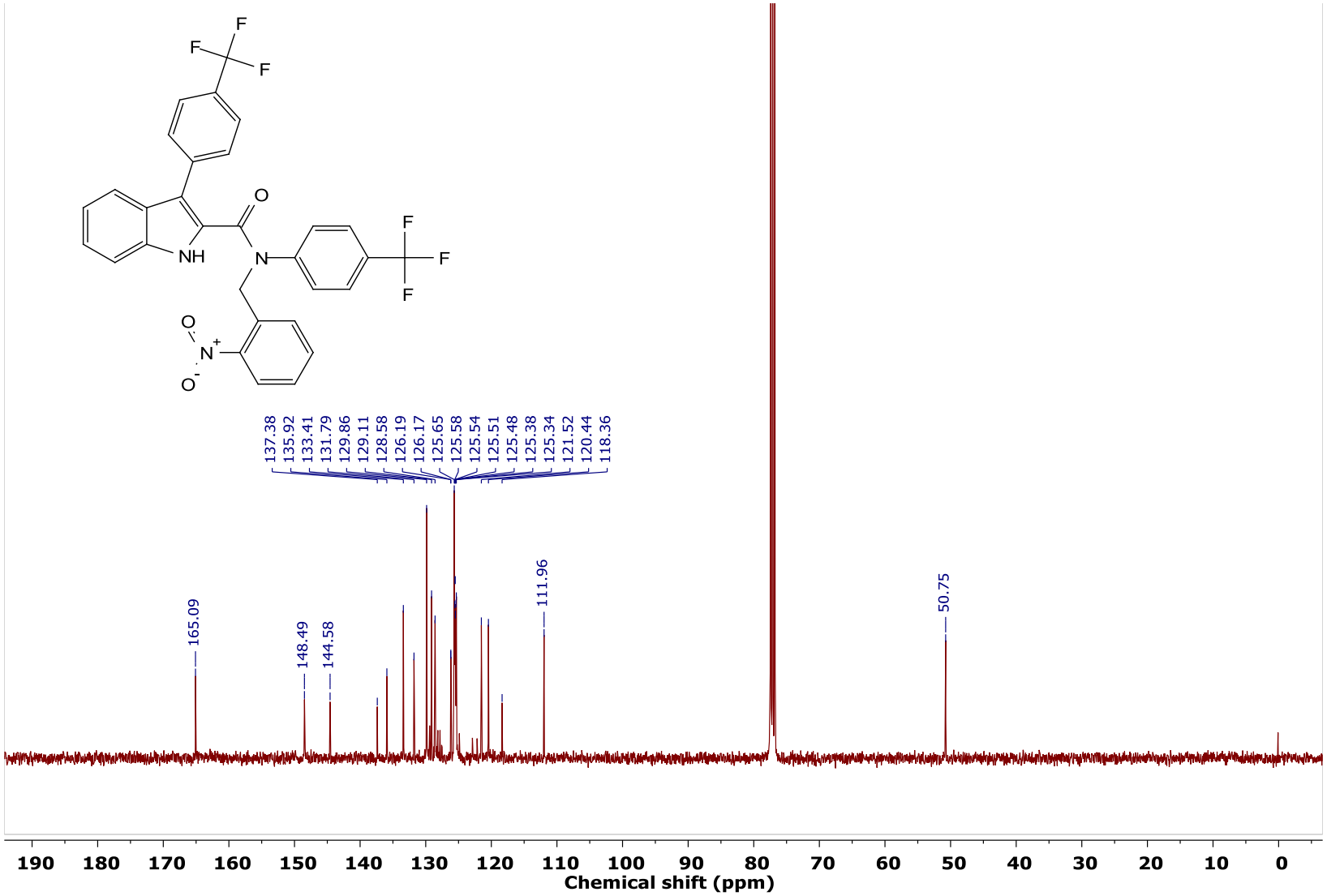

Fig. S75 ^{13}C NMR spectrum (101 MHz) of **5a** in $CDCl_3$ at room temperature.

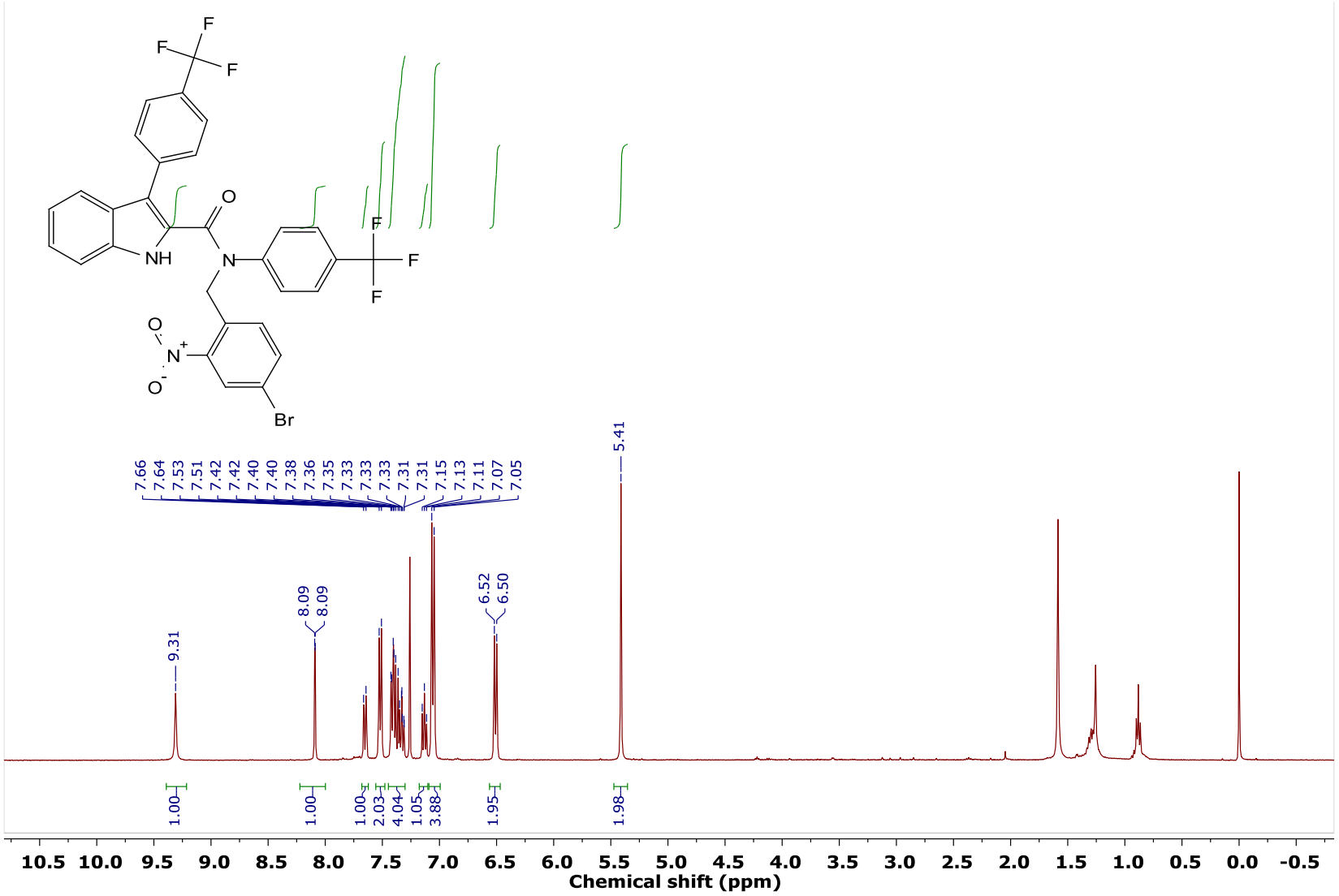

Fig. S76 ^{1}H NMR spectrum (400 MHz) of **5b** in $CDCl_3$ at room temperature.

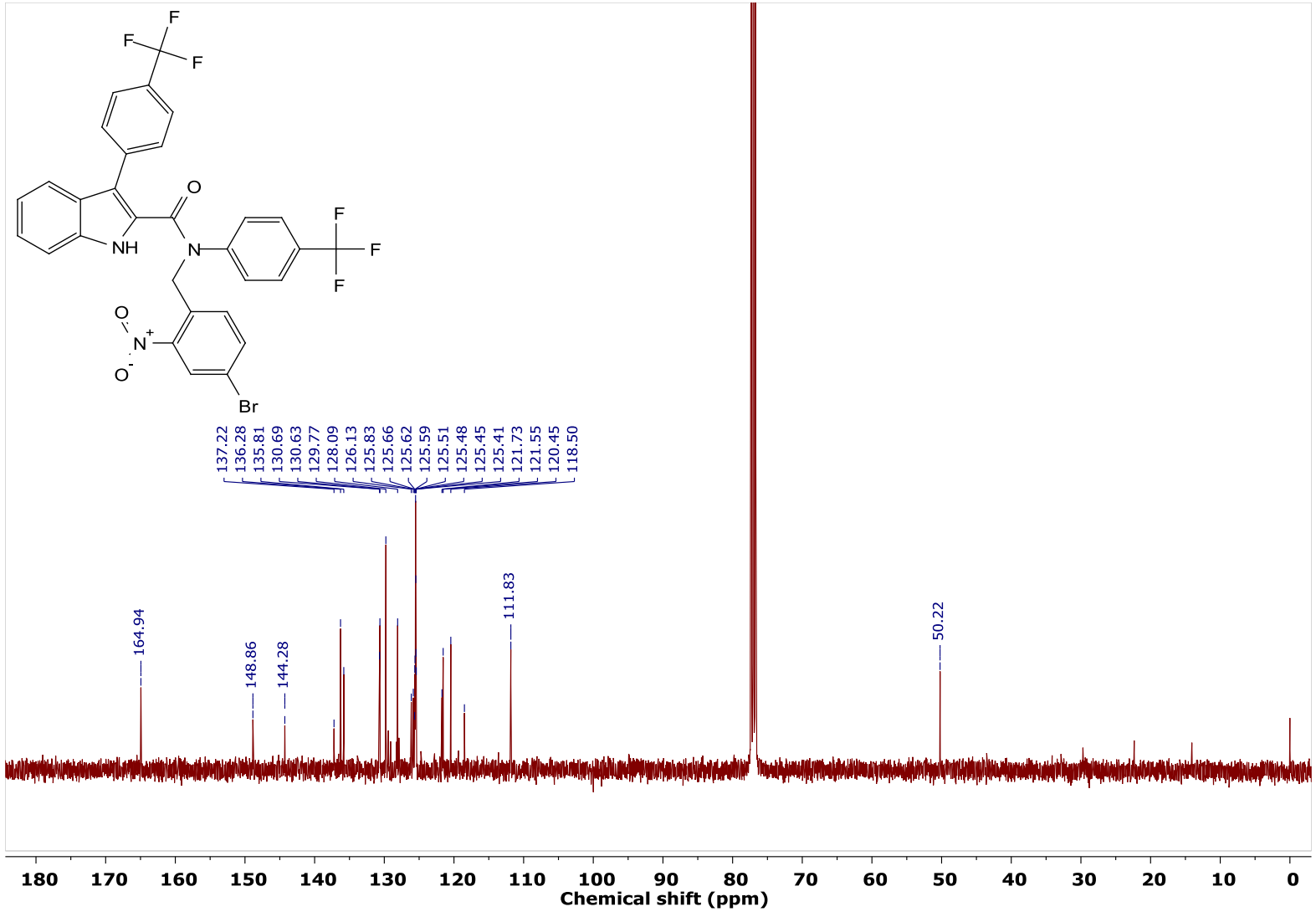

Fig. S77 ^{13}C NMR spectrum (101 MHz) of **5b** in $CDCl_3$ at room temperature.

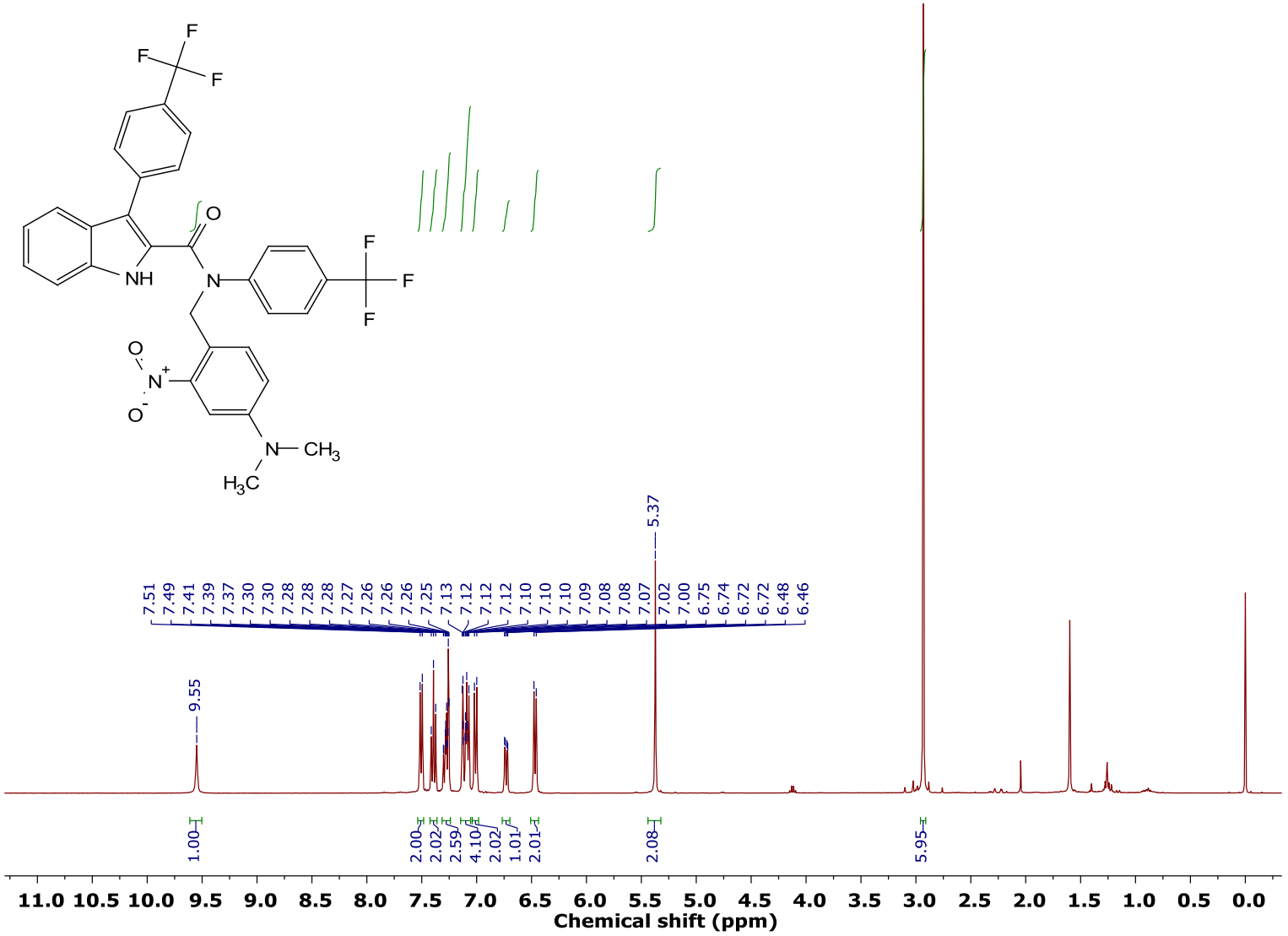

Fig. S78 ^{1}H NMR spectrum (400 MHz) of **5c** in $CDCl_3$ at room temperature.

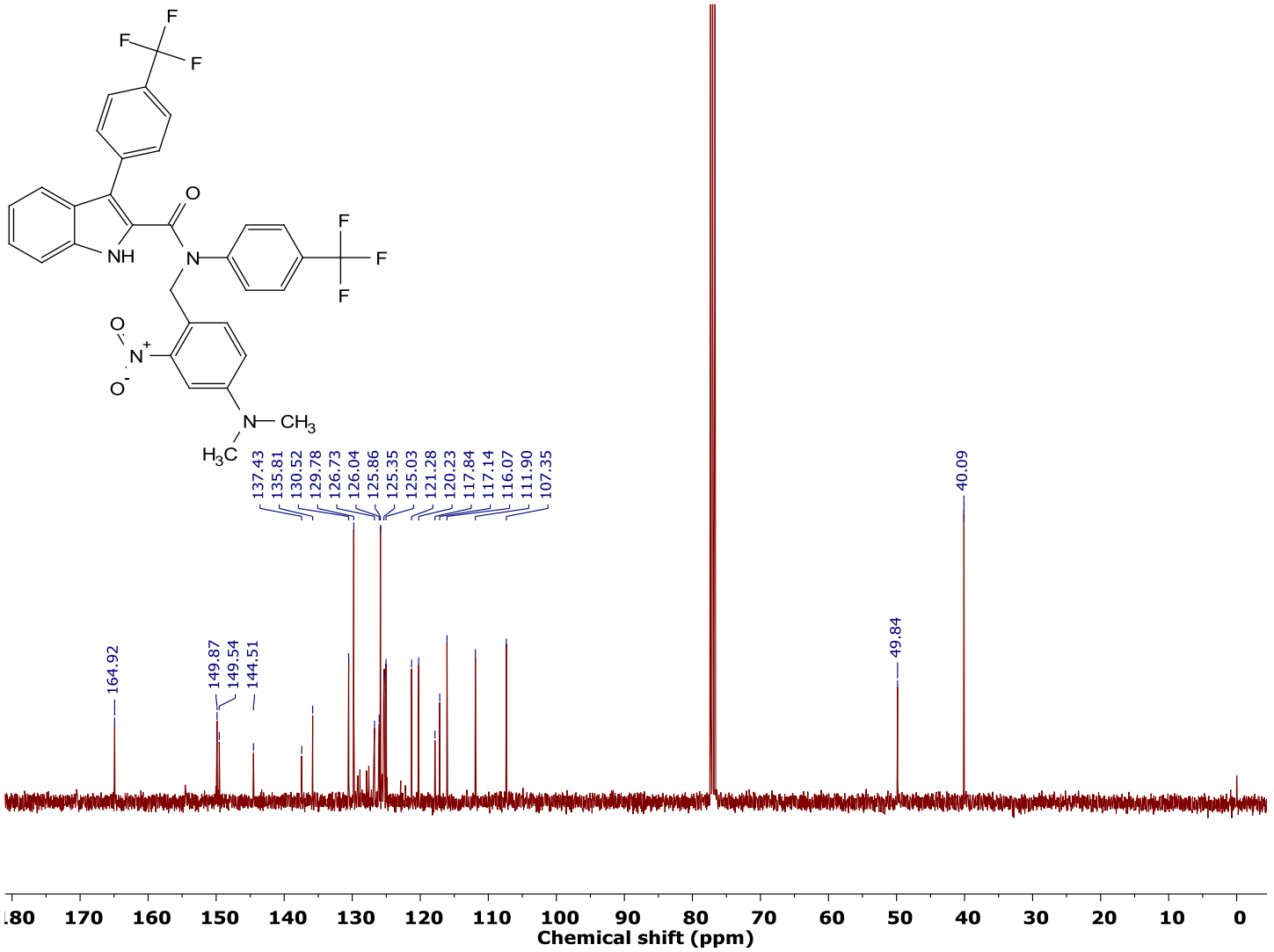

Fig. S79 ^{13}C NMR spectrum (101 MHz) of **5c** in $CDCl_3$ at room temperature.

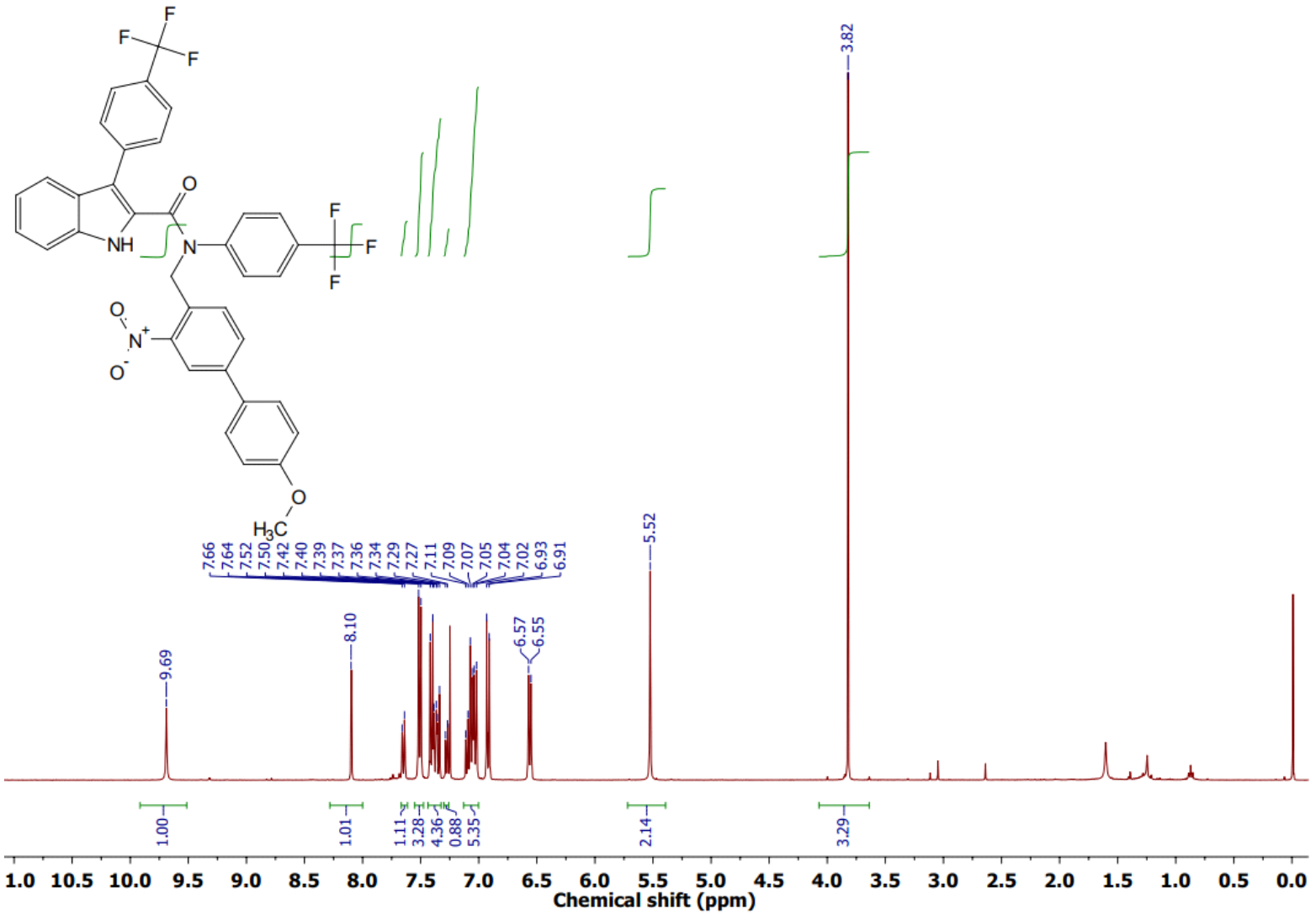

Fig. S80 ^{1}H NMR spectrum (400 MHz) of **5d** in $CDCl_3$ at room temperature.

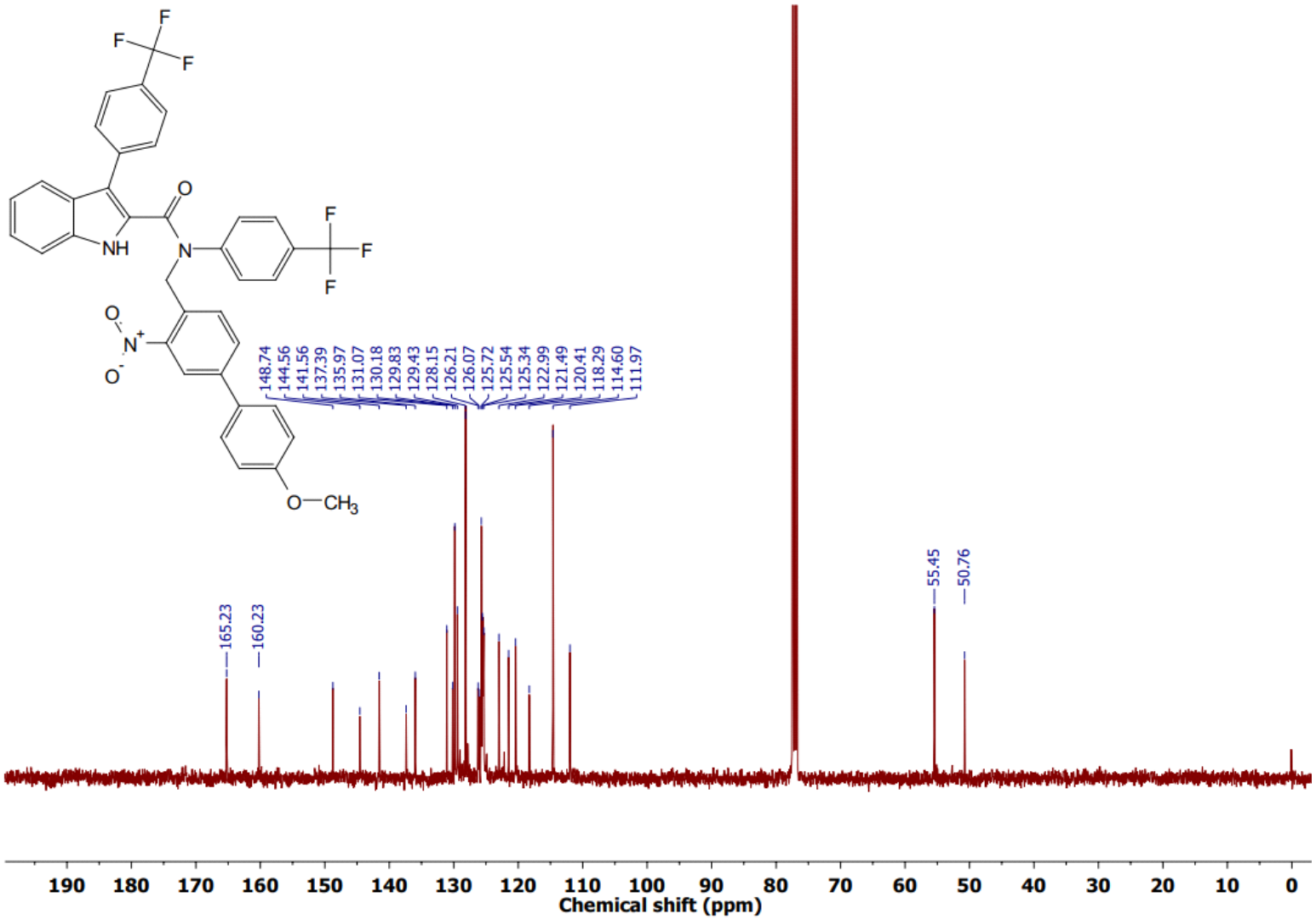

Fig. S81 ^{13}C NMR spectrum (101 MHz) of **5d** in $CDCl_3$ at room temperature.

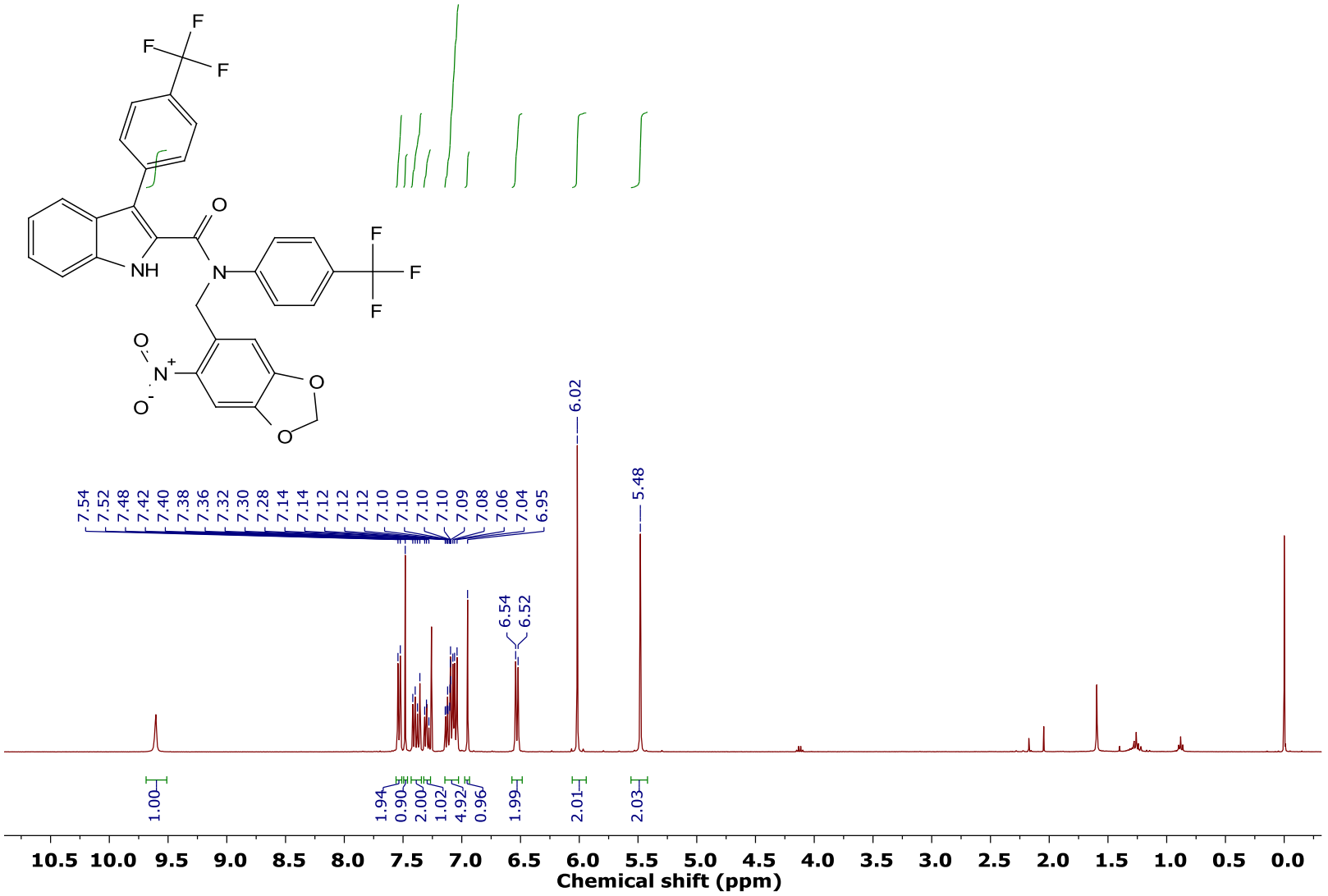

Fig. S82 ^{1}H NMR spectrum (400 MHz) of **5e** in $CDCl_3$ at room temperature.

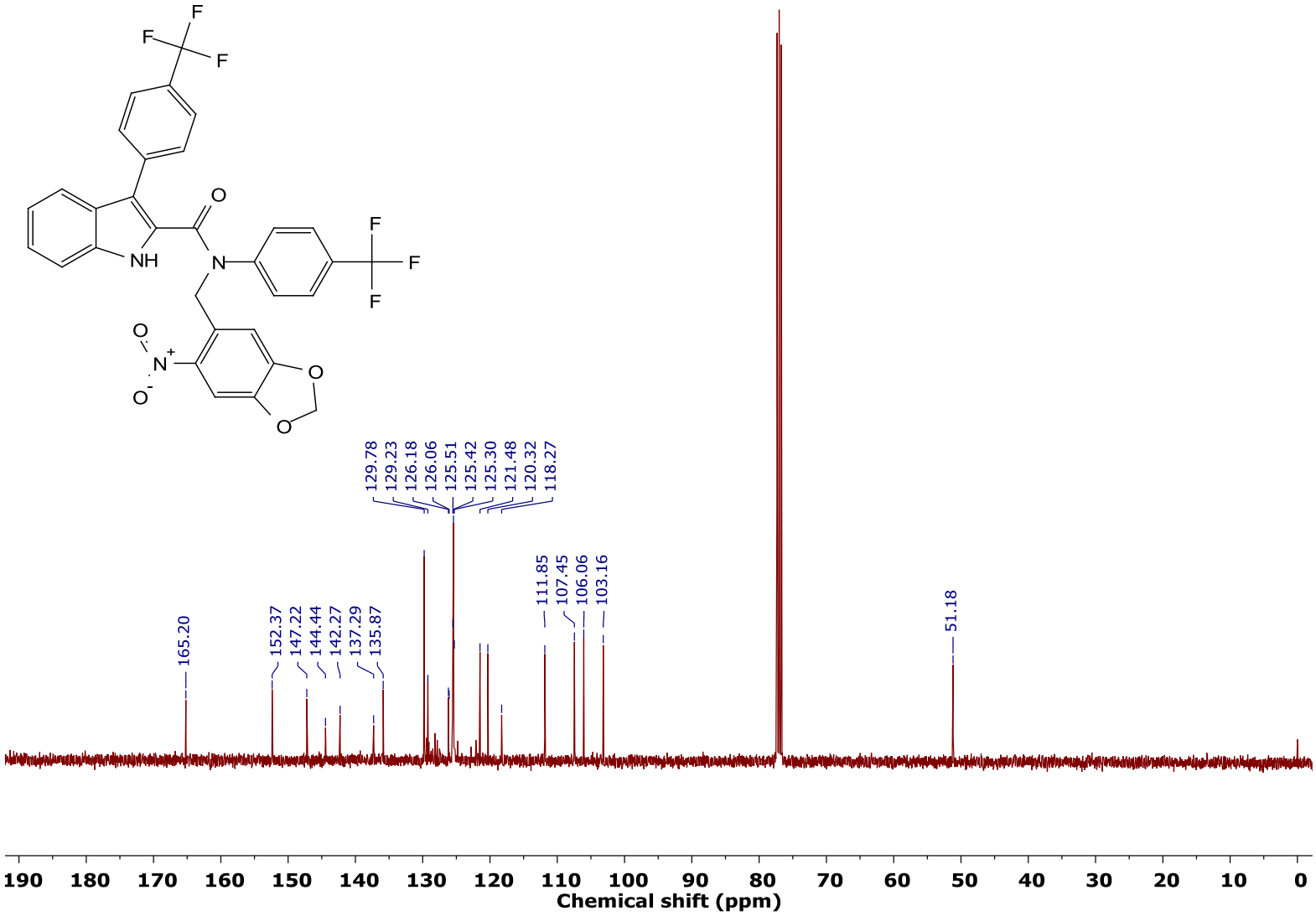

Fig. S83 ^{13}C NMR spectrum (101 MHz) of **5e** in $CDCl_3$ at room temperature.

XII. References

S1 S. B. Salunke, J. A. Malla, P. Talukdar, *Angew. Chem. Int. Ed.*, 2019, **58**, 5354-5358.

S2 http://app.supramolecular.org/bindfit/.

S3 (a) T. Saha, S. Dasari, D. Tewari, A. Prathap, K. M. Sureshan, A. K. Bera, A. Mukherjee, P. Talukdar, *J. Am. Chem. Soc.*, 2014, **136**, 14128-14135; (b) T. Saha, A. Gautam, A. Mukherjee, M. Lahiri, P. Talukdar, *J. Am. Chem. Soc.*, 2016, **138,** 16443-16451; (c) V. Gorteau, G. Bollot, J. Mareda, A. Perez-Velasco, S. Matile, *J. Am. Chem. Soc.*, 2006, **128**, 14788-14789.

S4 A. Vargas Jentzsch, D. Emery, J. Mareda, P. Metrangolo, G. Resnati, S. Matile, *Angew. Chem. Int. Ed.*, 2011, **50**, 11675-11678.

S5 S. Bhosale, S. Matile, *Chirality* 2006, **18**, 849-856.

S6 G. Sheldrick, *Acta Crystallogr.*, 2008, **64**, 112-122.

S7 A. Spek, *Acta Crystallogr.*, 2009, **65**, 148-155.

S8 S. O. H. Goto, N. Nakayama, K. Ohta, *CONFLEX 8*, CONFLEX Corporation, Tokyo,Japan,2012.

S9 M. J. Frisch, H. B. Schlegel, G. E. Scuseria, M. A. Robb, J. R. Cheeseman, G. Scalmani, V. Barone, B. Mennucci, G. A. Petersson, H. Nakatsuji, M. Caricato, X. Li, H. P. Hratchian, A. F. Izmaylov, J. Bloino, G. Zheng, J. L. Sonnenberg, M. Hada, M. Ehara, K. Toyota, R. Fukuda, J. Hasegawa, M. Ishida, T. Nakajima, Y. Honda, O. Kitao, H. Nakai, T. Vreven, J. A. Montgomery, J. E. Peralta, F. Ogliaro, M. Bearpark, J. J. Heyd, E. Brothers, K. N. Kudin, V. N. Staroverov, T. Keith, R. Kobayashi, J. Normand, K. Raghavachari, A. Rendell, J. C. Burant, S. S. Iyengar, J. Tomasi, M. Cossi, N. Rega, J. M. Millam, M. Klene, J. E. Knox, J. B. Cross, V. Bakken, C. Adamo, J. Jaramillo, R. Gomperts, R. E. Stratmann, O. Yazyev, A. J. Austin, R. Cammi, C. Pomelli, J. W. Ochterski, R. L. Martin, K. Morokuma, V. G. Zakrzewski, G. A. Voth, P. Salvador, J. J. Dannenberg, S. Dapprich, A. D. Daniels, O. Farkas, J. B. Foresman, J. V. Ortiz, J. Cioslowski, D. J. Fox, *Gaussian 09*, *Revision B.01*, Gaussian, Inc., Wallingford, CT, 2010.